AD-A045 346 TEXAS UNIV AT AUSTIN APPLIED RESEARCH LABS F/G 20/1
AN EXTENSION OF LANGER'S ASYMTOTIC SOLUTION WITH APPLICATIONS T--ETC(U)
MAR 77 S K MITCHELL N00014-75-C-0429
UNCLASSIFIED ARL-TR-77-13 NL

1 OF 2
AD A045346

APPLIED RESEARCH LABORATORIES
THE UNIVERSITY OF TEXAS AT AUSTIN

ARL-TR-77-13
1 March 1977

Copy No. 46

AN EXTENSION OF LANGER'S ASYMTOTIC SOLUTION WITH APPLICATIONS TO OCEAN ACOUSTICS

Stephen K. Mitchell

NAVAL OCEAN RESEARCH AND DEVELOPMENT ACTIVITY
Contract N00014-75-C-0429

UNCLASSIFIED

SECURITY CLASSIFICATION OF THIS PAGE (When Data Entered)

REPORT DOCUMENTATION PAGE

READ INSTRUCTIONS BEFORE COMPLETING FORM

1. REPORT NUMBER

2. GOVT ACCESSION NO.

3. RECIPIENT'S CATALOG NUMBER

4. TITLE (and Subtitle)

AN EXTENSION OF LANGER'S ASYMTOTIC SOLUTION WITH APPLICATIONS TO OCEAN ACOUSTICS.

5. TYPE OF REPORT & PERIOD COVERED

technical report

6. PERFORMING ORG. REPORT NUMBER

ARL-TR-77-13

7. AUTHOR(s)

Stephen K. Mitchell

8. CONTRACT OR GRANT NUMBER(s)

N00014-75-C-0429

9. PERFORMING ORGANIZATION NAME AND ADDRESS

Applied Research Laboratories
The University of Texas at Austin
Austin, Texas 78712

10. PROGRAM ELEMENT, PROJECT, TASK AREA & WORK UNIT NUMBERS

Doctoral thesis

11. CONTROLLING OFFICE NAME AND ADDRESS

Naval Ocean Research and Development Activity
NSTL Station MS 39529

12. REPORT DATE

1 March 1977

13. NUMBER OF PAGES

141

14. MONITORING AGENCY NAME & ADDRESS (if different from Controlling Office)

151p.

15. SECURITY CLASS. (of this report)

UNCLASSIFIED

15a. DECLASSIFICATION/DOWNGRADING SCHEDULE

16. DISTRIBUTION STATEMENT (of this Report)

Approved for public release; distribution unlimited.

17. DISTRIBUTION STATEMENT (of the abstract entered in Block 20, if different from Report)

18. SUPPLEMENTARY NOTES

19. KEY WORDS (Continue on reverse side if necessary and identify by block number)

ocean acoustics
normal mode theory
asymptotic expansions
Langer's solution
ray-mode equivalency

20. ABSTRACT (Continue on reverse side if necessary and identify by block number)

In this dissertation, Langer's asymptotic solution for second order differential equations is applied to the problem of acoustical propagation in the ocean. Langer's solution is analogous to the WKB solution, but is developed in terms of the Airy functions, Ai(•) and Bi(•), and is valid at the turning points of the equation

→ next page

DD FORM 1 JAN 73 1473 EDITION OF 1 NOV 65 IS OBSOLETE

SECURITY CLASSIFICATION OF THIS PAGE (When Data Entered)

$$d^2u_n/dz^2 + (\omega^2/c^2(z) - k_n^2)u_n = 0 \quad ;$$

$$n = 0, 1, 2, \ldots$$

which arises in normal mode analysis of acoustic propagation in the ocean. Here, $c(z)$ is the function of sound velocity versus depth. The solution is extended to take into account the boundaries of the ocean waveguide in the determination of the normal modes of propagation. It is shown that the eigenvalue equation for the normal modes may be given in the form

$$\int_{z_U}^{z_L} \left(\omega^2/c^2(z) - k_n^2\right)^{1/2} dz = (n + 1/2)\pi + \epsilon_n(\omega) \quad .$$

The quantities $\epsilon_n(\omega)$ depend upon boundary values and upon the distances from turning points to the depth of minimum velocity. From the eigenvalue equation, the formulae for the normal mode quantities of group velocity and mode cycle distance are derived. These are expressed in terms of a characteristic distance, $\hat{D}_n(\omega)$, and period $\hat{T}_n(\omega)$. It is shown that

$$\hat{D}_n(\omega) = \tilde{D}(z_U, z_L; \omega/k_n) + \Delta_n(\omega) \quad ,$$

and

$$\hat{T}_n(\omega) = \tilde{T}(z_U, z_L; \omega/k_n) + \tau_n(\omega) \quad .$$

The terms $\tilde{D}$ and $\tilde{T}$ are the ray theory horizontal distance and travel time between the turning points, z_U and z_L, of a ray with turning point velocity equal to the phase velocity of mode n. The additional terms, Δ_n and τ_n, depend upon the boundary values and upon $c(z)$ between the turning points and the boundaries, and $c(z)$ between turning points and the depth of minimum velocity.

(sound velocity vs. depth)

For illustrative $c(z)$ functions typical of the deep ocean, the normal mode quantities of group velocity and mode cycle distance are computed using the formulae developed in this report. These are presented in the form of plots of, for example, group velocity versus phase velocity for frequencies in the range 10 Hz to 150 Hz. These plots illustrate the effects of the ocean surface and of anomalous segments of $c(z)$ upon the mode quantities; the most prominent frequency dependent effects occur for modes whose phase velocities are close to the sound velocity at a boundary. (U)

ARL-TR-77-13
1 March 1977

AN EXTENSION OF LANGER'S ASYMTOTIC SOLUTION WITH APPLICATIONS TO OCEAN ACOUSTICS

Stephen K. Mitchell

NAVAL OCEAN RESEARCH AND
DEVELOPMENT ACTIVITY
Contract N00014-75-C-0429

APPLIED RESEARCH LABORATORIES
THE UNIVERSITY OF TEXAS AT AUSTIN
AUSTIN, TEXAS 78712

AN EXTENSION OF LANGER'S ASYMPTOTIC SOLUTION WITH APPLICATIONS TO OCEAN ACOUSTICS

by

STEPHEN KEITH MITCHELL, B.S., M.A.

DISSERTATION

Presented to the Faculty of the Graduate School of

The University of Texas at Austin

in Partial Fulfillment

of the Requirements

for the Degree of

DOCTOR OF PHILOSOPHY

THE UNIVERSITY OF TEXAS AT AUSTIN

May 1976

ABSTRACT

In this dissertation, Langer's asymptotic solution for second order differential equations is applied to the problem of acoustical propagation in the ocean. Langer's solution is analogous to the WKB solution, but is developed in terms of the Airy functions Ai(•) and Bi(•), and is valid at the turning points of the equation

$$d^2u_n/dz^2 + (\omega^2/c^2(z) - k_n^2)\, u_n = 0 \quad ;$$

$$n = 0, 1, 2, \ldots$$

which arises in normal mode analysis of acoustic propagation in the ocean. Here, c(z) is the function of sound velocity versus depth. The solution is extended to take into account the boundaries of the ocean waveguide in the determination of the normal modes of propagation. It is shown that the eigenvalue equation for the normal modes may be given in the form

$$\int_{z_U}^{z_L} (\omega^2/c^2(z) - k_n^2)^{1/2} dz = (n + 1/2)\, \pi + \varepsilon_n(\omega) \quad .$$

The quantities $\varepsilon_n(\omega)$ depend upon boundary values and upon the distances from turning points to the depth of minimum velocity. From the eigenvalue equation, the formulae for the normal mode quantities of group velocity and mode cycle distance are derived. These are expressed in terms of a characteristic distance, $\hat{D}_n(\omega)$, and period $\hat{T}_n(\omega)$. It is shown that

$$\hat{D}_n(\omega) = \tilde{D}(z_U,\ z_L;\ \omega/k_n) + \Delta_n(\omega) \quad ,$$

and

$$\hat{T}_n(\omega) = \tilde{T}(z_U,\ z_L;\ \omega/k_n) + \tau_n(\omega) \quad .$$

The terms $\tilde{D}$ and $\tilde{T}$ are the ray theory horizontal distance and travel time between the turning points, z_U and z_L, of a ray with turning point velocity equal to the phase velocity of mode n. The additional terms, Δ_n and τ_n, depend upon the boundary values and upon c(z) between the turning points and the boundaries, and c(z) between turning points and the depth of minimum velocity.

For illustrative c(z) functions typical of the deep ocean, the normal mode quantities of group velocity and mode cycle distance are computed using the formulae developed in this dissertation. These are presented in the form of plots of, for example, group velocity versus phase velocity for frequencies in the range 10 Hz to 150 Hz. These plots illustrate the effects of the ocean surface and of anomalous segments of c(z) upon the mode quantities; the most prominent frequency dependent effects occur for modes whose phase velocities are close to the sound velocity at a boundary.

TABLE OF CONTENTS

ABBREVIATIONS AND NOTATIONS

SVP - Sound Velocity Profile. The function of sound velocity versus depth in the ocean.

TP - Turning Point. The depth at which a ray becomes horizontal; or, the depth at which the phase velocity of a normal mode equals the sound velocity.

LHS - Left Hand Side (of an equation).

RHS - Right Hand Side.

~ - Tilde. Used to denote a ray theory quantity or a WKB approximation to a normal mode quantity.

^ - Caret. Used to denote a Langer approximation to a normal mode quantity.

U - As a subscript or superscript, denoting the upper TP.

L - As a subscript or superscript, denoting the lower TP.

t - As a subscript or superscript, denoting either TP.

z - Depth.

(It is customary in ocean acoustics to measure depth downward from the surface, or z=0 at the surface. Therefore, since the upper TP is above the lower TP, $z_U < z_L$).

I. INTRODUCTION

In the deep ocean, the variations with depth of temperature, pressure, and salinity combine to produce a sound velocity which is also a function of depth. Typically, the sound velocity varies with depth a few percent about the nominal value of 1500 m/sec, with local maximae at the surface and bottom, and a minimum at a depth of, say, 100 m to 1000 m. In many areas, the sound velocity function is approximately unchanging across distances of hundreds of kilometers. Under such conditions, acoustic signals in the frequency range from a few hertz to a few hundred hertz are guided along a deep ocean waveguide, or SOFAR channel, to distances of several thousand kilometers. The most important factor in determining the acoustical impulse response of the ocean waveguide is the sound velocity function. The theoretical models which describe the impulse response may be divided into the categories of geometrical acoustics, or ray theory, and wave theory, or normal mode theory.

The principal topic of this dissertation, the Langer solution, which has not been applied to ocean acoustics before, provides approximate solutions to differential equations which arise in normal mode theory. Two features make the Langer solution well suited for application to ocean acoustics. First, the sound velocity function over much of the ocean depth has an approximately linear form, for which the Langer solution is nearly exact. Second, the Langer solution is valid at and near turning points; as shown in Chapter V, a normal mode

solution is needed when modes with turning points close to boundaries enter into a propagation problem. An additional feature of the Langer solution is that, in order to apply the solution, little in the way of computation, beyond what is necessary for a WKB solution or for a ray theory description, is required.

In this work, the Langer solution is extended by the development of an eigenvalue equation for determination of the normal mode functions. This eigenvalue equation for mode number n has the form:

$$\int_{z_U}^{z_L} \left[\omega^2 / c^2 - k_n^2 \right]^{1/2} dz = (n+1/2)\,\pi + \varepsilon_n(\omega) \quad . \qquad 1\text{-}1$$

The quantities of Eq. 1-1 are defined in Chapter IV. However, note that it is of the form of the Bohr-Sommerfeld equation, plus an additional term $\varepsilon_n(\omega)$ on the RHS. Approximation formulae for the term $\varepsilon_n(\omega)$ are derived in Chapter IV. Additionally, from the eigenvalue equation, the normal mode quantities of group velocity and mode cycle distance are derived and related to corresponding ray theory quantities.

The following two chapters are devoted to providing background and bibliographical material. In Chapter II, the basic features of the ocean acoustical parameters are presented. Then, the acoustical wave equation, and the ray theory and normal mode theory formulae which follow from the wave equation, are introduced. The WKB solution to the depth equation of normal mode theory and the relationship between normal mode theory and ray theory are then discussed. In Chapter III,

a brief survey of the ocean acoustical phenomena analyzed in this work is presented. Recently reported measurements show that, at low frequencies (below 100 Hz), quantities such as signal travel time and convergence zone spacings are frequency dependent. In particular, low frequency signals travel from a source to a receiver more slowly than high frequency signals and along "raypaths" which are shorter than those of high frequency signals.

The Langer solution is derived in Chapter IV. Then, the solution is extended by deriving an eigenvalue equation (Eq. 1-1) which takes into account both the boundary values of the problem, and the exact, rather than the asymptotic, form of the solution at the velocity minimum. Finally, the normal mode quantities of group velocity and mode cycle distance in the Langer approximation are derived and expressed in terms of the ray theory quantities of ray distance and ray travel time.

In Chapter V, the formulae of Chapter IV are applied to compute normal mode functions and mode quantities for example experimental sound velocity functions. In Chapter VI, a review of the dissertation is presented, and suggestions are made for future developments. In the Appendix, the properties of the Airy functions relevant to this work are presented.

II. BACKGROUND - THEORETICAL DESCRIPTION OF OCEAN ACOUSTICS

The purpose of this chapter is to provide a description of the salient features of the acoustical parameters of the ocean in Section II-2, and then to review different aspects of the theory used to describe the acoustics of the ocean for reference in Chapter IV.

In Section II-A, the acoustic wave equation to be used in this paper is derived. The ray theory approach to solving the wave equation is discussed in Section II-C; in particular, the formulae (Eqs. 2C-13) which give the horizontal distance $\tilde{D}$ and the acoustic travel time $\tilde{T}$ between two points of a ray are presented. The functions $\tilde{D}$ and $\tilde{T}$ as defined by these formulae will frequently be used in Chapter IV. The computation of the acoustic field in the ray theory approximation will not be considered in this work.

The normal mode solution to the wave equation and the separated depth equation are discussed in Sections II-D and II-E; the Langer solution, the principal topic of this work, provides approximate solutions to the depth equation. In Section II-F, the concepts of group velocity and phase velocity are introduced. In Section II-G, the WKB solution, which may be used to obtain approximate solutions to the depth equation, is discussed. In two important respects, the WKB solution is inferior to the Langer solution, especially for application to ocean acoustics. First, the WKB solution may not be used at the turning points of the mode, whereas the Langer solution may be. In addition to being useless for computing

the mode function near a turning point, the WKB solution may not be modified to take into account boundary conditions if the turning point is near to a boundary. Second, the quantities of group velocity and mode cycle distance (Section II-H) computed in the WKB approximation are identical to their ray theory counterparts, whereas from the Langer Solution as extended in this work, group velocities and mode cycle distances which reflect the wave nature of propagation are obtained. Finally, in Section II-H, the relation between ray theory and mode theory is presented, and the concept of mode cycle distance is introduced.

II-A OCEAN ACOUSTICAL PARAMETERS

The basic features of the acoustic parameters of the deep ocean are discussed by, for example, Tolstoy and Clay [1966], Williams [1970], and Hampton [1974]. In this work, we shall be interested in the acoustic waveguide formed by the ocean's sound velocity structure and the ocean surface, but will not consider the acoustics of the ocean bottom. An emperical equation published by Wilson [1960] gives the sound velocity c in water as a function of temperature T, salinity S, and pressure P. To first order, this equation is

$$c = 1449.14 + 4.57T + .1603P + 1.40(S-35) \quad . \qquad (2A-1)$$

In Eq. 2A-1, c is in units of m/sec, T is in degrees (Celsius), and P is in kg/cm^2, and S is in parts per thousand. In the ocean, pressure increases linearly with at a rate of approximately 100 kg/cm^2 per kilometer of depth. Therefore, if the temperature and salinity are constant, c will increase with depth at a rate of approximately 16 m/sec per kilometer of depth. In equatorial and moderate latitudes, the temperature T nominally decreases with depth until a minimum temperature is reached at a depth of approximately 1000 m, below which the temperature is constant. This dependence of temperature upon depth results in a minimum of sound velocity, the SOFAR (Sound Fixing and Ranging) axis at a depth of approximately 1000 m. Additionally, the mixing by wave action of the water near the surface may cause the temperature to be constant down to a depth of, say, 50 to 100 m so that a local velocity minimum is formed there.

Typical sound velocity versus depth curves from different areas are shown in Fig. 2A-1. Such a curve is known as a sound velocity profile; the abbreviation SVP will usually be used in this work. As may be

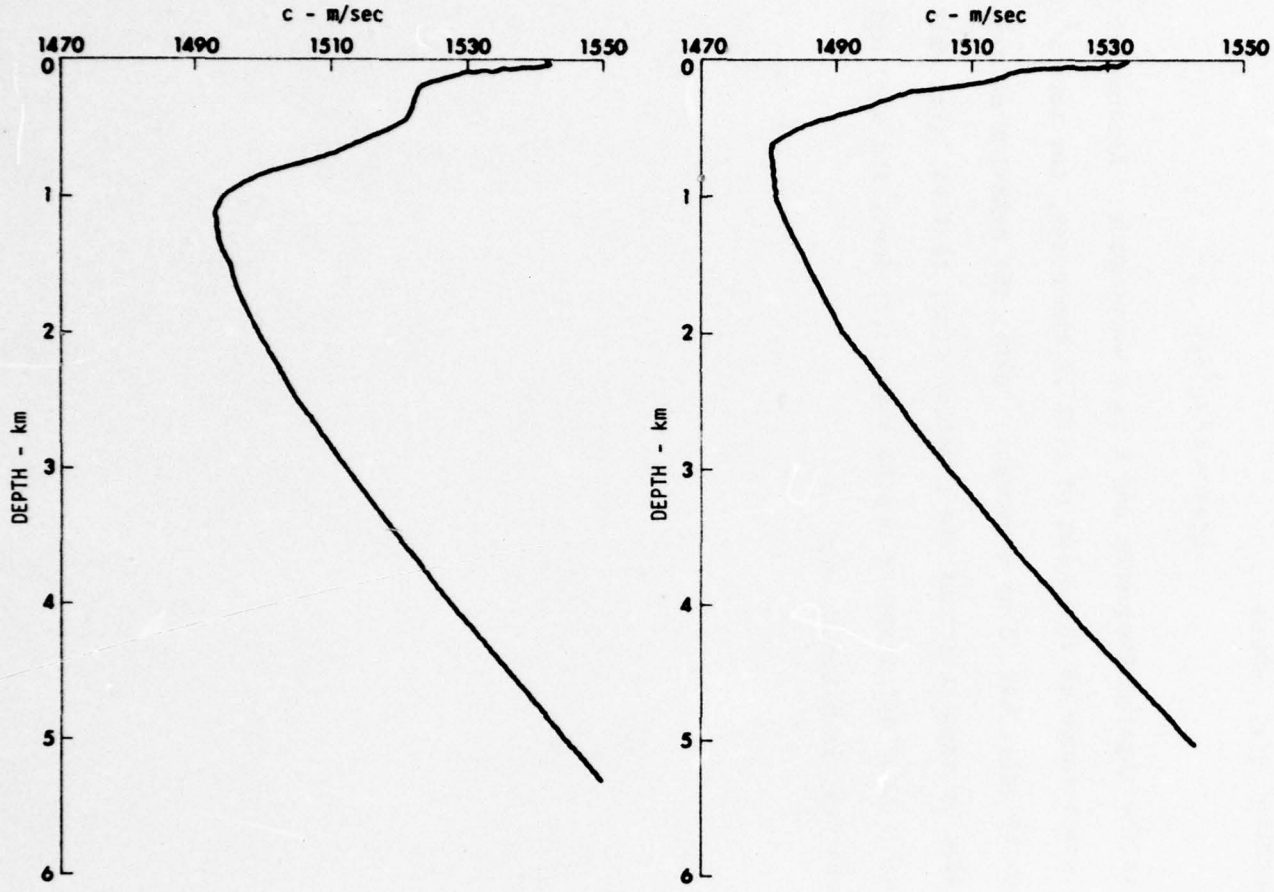

FIGURE 2A-1
EXAMPLE SOUND VELOCITY PROFILES
Left: Western Atlantic, Right: NE Pacific

seen, the sound velocity varies approximately 2 or 3 percent with depth. In the following sections, reference will often be made to the "profile function" q(z), where

$$q(z) = \omega^2/c^2(z) - k^2 \quad ; \qquad (2A\text{-}2)$$

ω is the angular frequency and k is a wavenumber. Because of the relatively small range of variation of c(z) in the ocean, the term $\omega^2/c^2(z)$ will vary by only, say, 5 or 6 percent. Also, the behavior of q(z) may be judged by examination of the function c(z); that is, q(z) will have roughly constant slope at depths where c(z) does, and q(z) has a maximum where c(z) is minimum, etc.

II-B ACOUSTIC WAVE EQUATION

The linearized wave equation for the acoustic pressure, p_a, in a fluid is given by Eq. 2B-8, below. Detailed discussions of the derivation of the acoustic wave equation may be found in Bergmann [1948], Lindsay [1960], and Officer [1958]. Let the pressure p, and density ρ, and fluid velocity at a point by given by

$$\begin{aligned} p &= p_o + p_a \\ \rho &= \rho_o + \rho_a \\ \vec{U} &= \vec{U}_a \end{aligned} \qquad \text{(2B-1)}$$

Here, the subscript "o" refers to the quantity in the absence of acoustic disturbance while the subscript "a" denotes the increment due to the acoustic wave. Newton's law of motion for a fluid element is given by

$$\begin{aligned} \rho\, D\vec{U}/Dt &\equiv \rho(\partial\vec{U}/\partial t + \vec{U} \cdot \nabla U) \\ &= -\nabla p_a + \vec{S} \quad , \end{aligned} \qquad \text{(2B-2)}$$

where the term $\vec{S}$ gives the force density of sources. The equation of continuity for the fluid is given by

$$\frac{D\rho}{Dt} = \partial\rho/\partial t + \nabla \cdot (\rho\vec{U}) = 0 \quad . \qquad \text{(2B-3)}$$

Next, Eqs. 2B-2 and 2B-3 are linearized; that is, terms such as $\rho_a\vec{U}_a$, which involve products of incremental quantities, are ignored. Thus, Eq. 2B-2 becomes

$$-\rho_o \, \partial\vec{U}/\partial t = \vec{\nabla} P_a - \vec{S} \quad , \tag{2B-4}$$

and Eq. 2B-3 becomes

$$\partial\rho_a/\partial t = -\nabla\rho_o \cdot \vec{U} - \rho_o \vec{\nabla} \cdot \vec{U} \quad . \tag{2B-5}$$

Hook's law for fluids is

$$P_a = (B/\rho)\, \rho_a \quad , \tag{2B-6}$$

where B is the adiabatic bulk modulus. Then, take the derivative with respect to t of p_a of Eq. 2B-6, and substitute the result into Eq. 2B-5 (again retaining only first order terms) to get

$$\frac{B}{\rho_o} \, \partial P_a/\partial t = -\vec{U} \cdot \nabla\rho_o \cdot \vec{\nabla} - \vec{U} \quad . \tag{2B-7}$$

Finally, taking the divergence of Eq. 2B-4, the time derivative of Eq. 2B-7, and adding the results to eliminate terms in $\vec{U}$, one obtains

$$\nabla^2 P_a - c^{-2}(\vec{r})\, \partial^2 P_a/\partial t^2 = -\nabla \cdot \vec{S} \quad , \tag{2B-8}$$

where the sound velocity c is given by

$$c(\vec{r}) = (B/\rho)^{1/2} \quad . \tag{2B-9}$$

If the source S has a single frequency ω, so that

$$\vec{S} = \vec{\sigma}\, e^{-i\omega t} \quad , \tag{2B-10}$$

then the acoustic pressure p_a may be expressed as

$$P_a = \Phi(\vec{r})\, e^{-i\omega t} \quad , \tag{2B-11}$$

and the wave equation becomes

$$\nabla^2\Phi + \frac{\omega^2}{c^2(r)}\, \Phi = -\vec{\nabla} \cdot \vec{\sigma} \quad . \tag{2B-12}$$

II-C RAY TRACING EQUATIONS[1]

Assume that a point source of frequency ω is located at $\vec{r}_o$, and that away from $\vec{r}_o$, Φ is expressed as

$$\Phi(\vec{r}) = A(\vec{r})\ e^{i\psi(r)} \quad ; \tag{2C-1}$$

the functions $A(\vec{r})$ and $\psi(\vec{r})$ are real. A surface defined by ψ = constant is a surface of constant phase for the wave. Along the path s which is normal to a constant phase surface,

$$\begin{aligned} \partial\psi/\partial x &= dx/ds\ K(\vec{r}) \quad , \\ \partial\psi/\partial y &= dy/ds\ K(\vec{r}) \quad , \\ d\psi/dz &= dz/ds\ K(\vec{r}) \quad , \end{aligned} \tag{2C-2}$$

Now if Eq. 2C-1 is substituted into Eq. 2B-12, then Eq. 2C-3 is obtained by equating the real parts of the resulting equation

$$\left(\frac{\partial\psi}{\partial x}\right)^2 + \left(\frac{\partial\psi}{\partial y}\right)^2 + \left(\frac{\partial\psi}{\partial z}\right)^2 = \frac{\omega^2}{c^2} - \frac{\nabla^2 A}{A} \quad , \tag{2C-3}$$

The ray theory approximation is that the second term on the RHS of Eq. 2C-2 is zero; this is equivalent to assuming

$$|A''/A| << \omega^2/c^2 \quad , \tag{2C-4}$$

where primes denote a general spatial derivative. Under the ray theory approximation Eq. 2C-3 becomes

$$\left(\frac{\partial\psi}{\partial x}\right)^2 + \left(\frac{\partial\psi}{\partial y}\right)^2 + \left(\frac{\partial\psi}{\partial z}\right)^2 = \frac{\omega^2}{c^2} \quad , \tag{2C-5}$$

Substitute Eqs. 2C-2 into 2C-5, and then use the property of the direction cosines,

$$\left(\frac{dx}{ds}\right)^2 + \left(\frac{dy}{ds}\right)^2 + \left(\frac{dz}{ds}\right)^2 = 1 \quad , \tag{2C-6}$$

[1] Brekhovskikh [1960], Officer [1958], Tolstoy and Clay [1966]

and the factor $K(\vec{r})$ may be shown to be $\omega/c(\vec{r})$, so that Eq. 2C-2 becomes

$$\text{a)} \quad \frac{\partial \psi}{\partial x} = \frac{\omega}{c} \frac{dx}{ds} \quad ,$$

$$\text{b)} \quad \frac{\partial \psi}{\partial y} = \frac{\omega}{c} \frac{dy}{ds} \quad , \qquad \text{(2C-7)}$$

$$\text{c)} \quad \frac{\partial \psi}{\partial z} = \frac{\omega}{c} \frac{dz}{ds} \quad ,$$

Finally, take the derivatives of each of Eq. 2C-7 along the normal (ray path) to obtain the ray equations. For example, the derivative of Eq. 2C-7a is

$$\omega \frac{d}{ds}\left(\frac{1}{c} \frac{dx}{ds}\right) = \frac{\partial}{\partial x} \frac{d\psi}{ds}$$

$$= \frac{\partial}{\partial x}\left(\frac{\partial \psi}{\partial x} \frac{dx}{ds} + \frac{\partial \psi}{\partial y} \frac{dy}{ds} + \frac{\partial \psi}{dz} \frac{dz}{ds}\right)$$

$$= \omega \frac{\partial}{\partial x}\left\{ \frac{1}{c}\left(\left(\frac{dx}{ds}\right)^2 + \left(\frac{dy}{ds}\right)^2 + \left(\frac{dz}{ds}\right)^2\right)\right\} \qquad \text{(2C-8)}$$

The ray path equations are thus

$$\frac{d}{ds}\left(\frac{1}{c} \frac{dx}{ds}\right) = \frac{\partial}{\partial x}\left(\frac{1}{c}\right) \quad ,$$

$$\frac{d}{ds}\left(\frac{1}{c} \frac{dy}{ds}\right) = \frac{\partial}{\partial y}\left(\frac{1}{c}\right) \quad ,$$

$$\frac{d}{ds}\left(\frac{1}{c} \frac{dz}{ds}\right) = \frac{\partial}{\partial z}\left(\frac{1}{c}\right) \quad , \qquad \text{(2C-9)}$$

These equations may also be derived from Fermat's principle.

Restricting $c(\vec{r})$ to be a function of the depth z only simplifies the ray equations. In particular, the ratio of the x and y direction cosines is then constant, so that a ray which starts at the z-axis of a coordinate system remains in one plane which contains the z-axis. Thus, there is no loss of generality by considering a ray to

be in the x-z plane only, and Eq. 2C-9 becomes

$$\text{a)} \quad \frac{dx}{ds} = \frac{c(z)}{c_t}$$

$$\text{b)} \quad \frac{d}{ds}\left(\frac{1}{c(z)}\frac{dz}{ds}\right) = \frac{d}{dz}\left(\frac{1}{c(z)}\right) \quad , \qquad \text{(2C-10)}$$

From Fig. 2C-1, it may be seen that the constant c_t in Eq. 2C-10a is the sound velocity c(z) at a turning point of the ray, where the ray is horizontal (dx/ds = 1). Equation 2C-10a is the form of Snell's law for a continuously variable index of refraction.

By tracing a ray from the point (x_o, z_o), we mean the determination of the curve (x, z) which passes through (x_o, y_o) and satisfies Eq. 2C-10a. The ray is characterized by the turning point velocity, c_t. We also include in the ray tracing operation the determination of the acoustic travel time between two points of the ray, defining an element of time dT among the ray path element ds by

$$dT = ds/c(z) \quad , \qquad \text{(2C-11)}$$

The relation between ds and dz given in Eq. 2C-12 follows from Eqs. 2C-6 and 2C-10b

$$ds = dz \Big/ \left(\left(1-c^2(z)\right) \Big/ c_t^{\,2} \right)^{1/2} \quad . \qquad \text{(2C-12)}$$

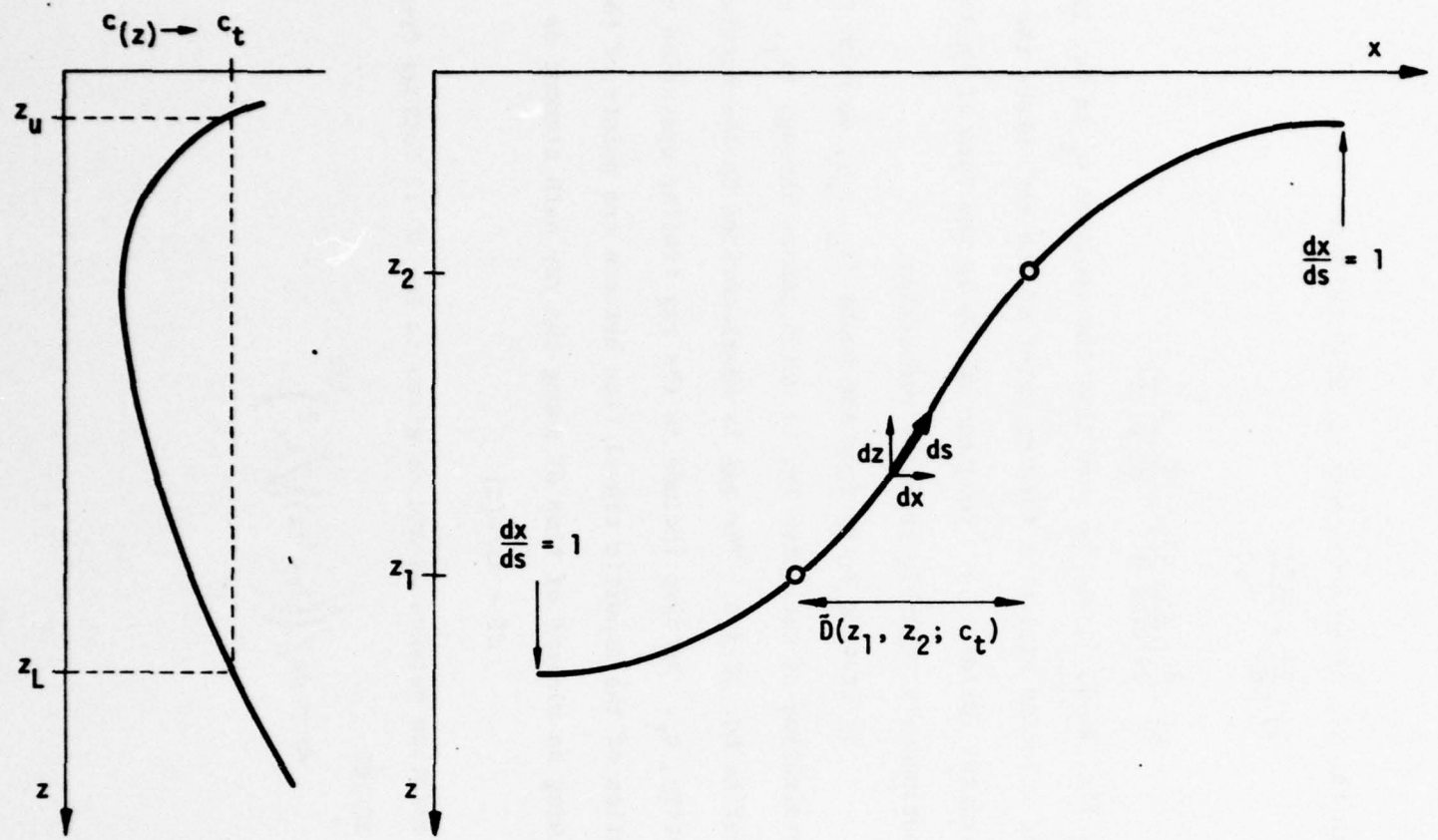

FIGURE 2C-1
RAYPATH FOR REPRESENTATIVE SVP

The turning points of this ray are z_U and z_L.

Combining Eqs. 2C-10a, 2C-11, and 2C-12, the equations for tracing a ray with turning point velocity c_t are given by

$$\tilde{D}(z_1,z_2;c_t) = \int_{z_1}^{z_2} \frac{c\,dz}{c_t(1-c^2/c_t^2)^{1/2}} \quad , \tag{2C-13}$$

$$\tilde{T}(z_1,z_2;c_t) = \int_{z_1}^{z_2} \frac{dz}{c(1-c^2/c_t^2)^{1/2}} \quad ,$$

The horizontal distance $\tilde{D}(z_1,z_2;c_t)$ and travel time $\tilde{T}(z_1,z_2;c_t)$ defined in Eq. 2C-13 are indicated in Fig. 2C-2. When a ray either reaches a turning point (where integrand in Eq. 2C-13 become infinite), or strikes the surface or bottom, it is continued as indicated in Fig. 2C-2. The ray cycle distance and ray cycle time are

$$\tilde{\Lambda}(c_t) = 2D(z_U,z_L;c_t) \quad , \tag{2C-14}$$

and $$\tilde{T}(c_t) = 2T(z_U,z_L;c_t) \quad ,$$

the limits z_U, z_L are turning points if the ray is refracted above or below, respectively, and the corresponding boundaries otherwise.

In general, if the two points (x_o,z_o) and (x,z) are connected by a ray which has the turning point velocity c_t, then

$$x - x_o = N\tilde{\Lambda}(c_t) + \alpha\tilde{D}(z_U,z_o;c_t) + \beta\tilde{D}(z_o,z;c_t) \tag{2C-15}$$

$$\alpha = 0 \text{ or } 2;\ \beta = \pm 1 \quad ,$$

$$N = 0, 1, \ldots \quad ,$$

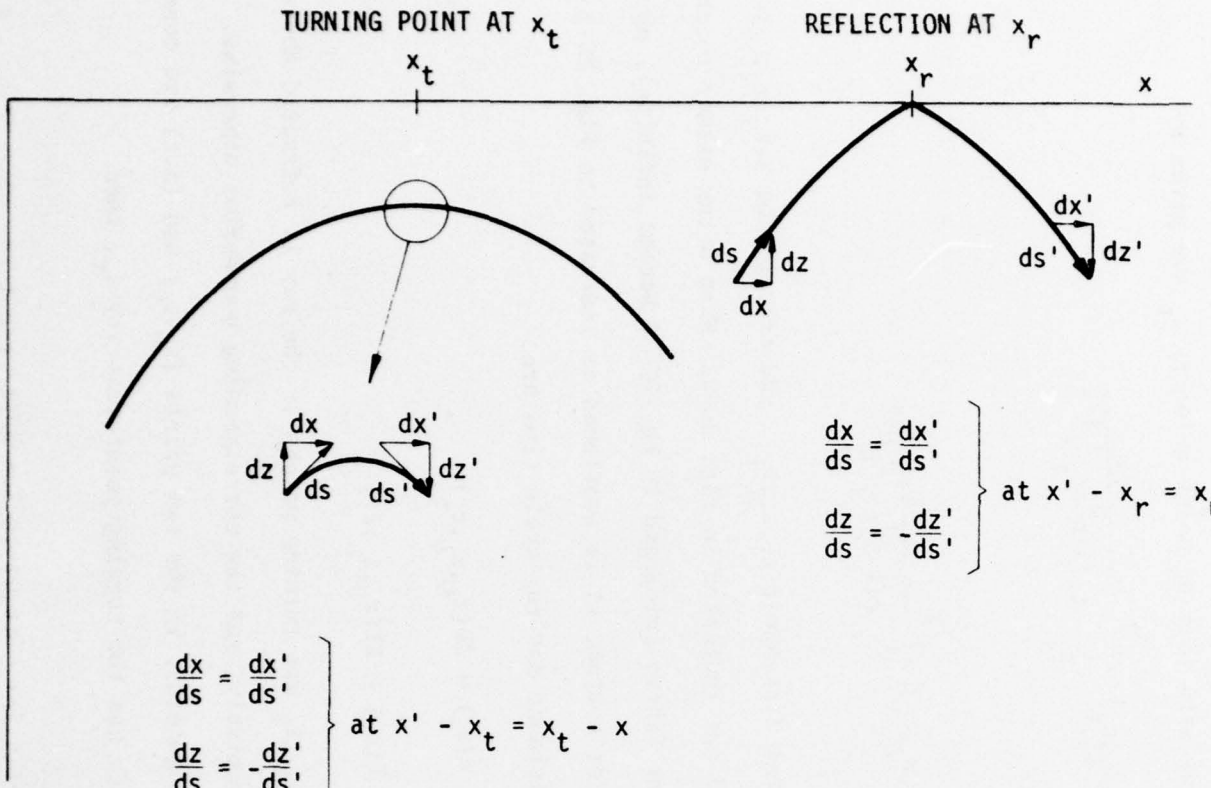

FIGURE 2C-2
CONTINUATION OF A RAY PAST A TURNING POINT OR REFLECTION

must be satisfied for some combination of α, β, and N. Some of the points at depth z connected by a ray to point (x_o, z_o) are shown in Fig. 2C-3. A practical problem in ray tracing is the determination of "eigenrays" which connect two fixed points. There are numerical techniques to find the roots $\{c_t\}$ such that Eq. 2C-15 is satisfied for points (x_o, z_o) and (x,z).

In summary, a ray from a point is a curve which is specified by a simple parameter, the turning velocity c_t. The two basic ray quantities are the ray cycle distance and the ray cycle time. It should be remembered that it follows from Eq. 2C-10a that a point at depth z_s can be connected (at the proper ranges) to another point at depth z by a ray characterized by c_t only if

$$c_t > \max [c(z), c(z_s)] \qquad \text{2C-16}$$

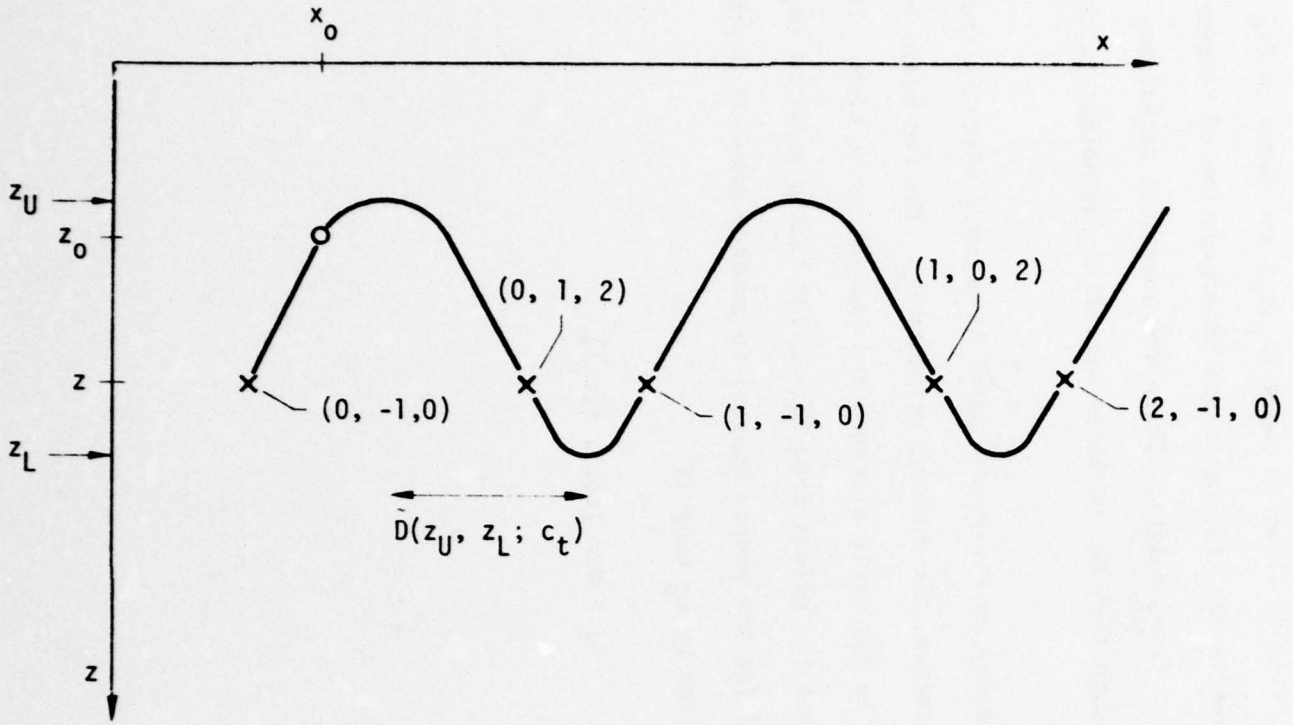

FIGURE 2C-3
RAY WITH TURNING POINTS z_U AND z_L THROUGH (x_o, z_o)

This ray passes through points at depth z (marked x) which are determined by Eq. 2C-15. The numbers beside these points are (N, α, β) of Eq. 2C-15

II-D NORMAL MODE SOLUTION

If the source is a point source of unit strength located at point $\vec{r}_o$, then Eq. 2B-12 becomes

$$\nabla^2\Phi + \frac{\omega^2}{c^2(\vec{r})}\Phi = -4\pi\, e^{i\omega t}\,\delta(\vec{r}-\vec{r}_o) \quad . \tag{2D-1}$$

In this section, $\delta(\cdot)$ is the Dirac delta function; the symbol is used in another sense in Chapter IV (Eq. 4B-6). Then, we express Eq. 2D-1 in a cylindrical coordinate system and assume that the sound velocity is a function of depth z only, and obtain

$$\frac{1}{r}\frac{\partial}{\partial r}\left(r\frac{\partial\Phi}{\partial r}\right) + \frac{\partial^2\Phi}{\partial z^2} + \frac{\omega^2}{c^2(z)}\Phi + \frac{1}{r^2}\frac{\partial^2\Phi}{\partial\psi^2}$$

$$= -4\pi\,\frac{\delta(r-r_o)}{r}\,\delta(z-z_o)\,\delta(\psi-\psi_o) \quad , \tag{2D-2}$$

Next, we eliminate the azimuthal dependence by integrating over ψ from 0 to 2π and then set $r_o = 0$ to obtain

$$\frac{1}{r}\frac{\partial}{\partial r}\left(r\frac{\partial\Phi}{\partial r}\right) + \frac{\partial^2\Phi}{\partial z^2} + \frac{\omega^2}{c^2(z)}\Phi = -\frac{2}{r}\,\delta(r)\,\delta(z-z_o) \quad , \tag{2D-3}$$

Except at $\vec{r} = \vec{r}_o$, Eq. 2D-3 becomes the homogeneous equation

$$\frac{1}{r}\frac{\partial}{\partial r}\left(r\frac{\partial\Phi}{\partial r}\right) + \frac{\partial^2\Phi}{\partial z^2} + \frac{\omega^2}{c^2(z)}\Phi = 0 \quad , \tag{2D-4}$$

which may be separated by substituting

$$\Phi = F(r)\,u(z) \tag{2D-5}$$

into Eq. 2D-4. If this is done, the separated equations 2D-6a and 2D-6b are obtained, where the wave number k is a separation constant.

$$\text{a)} \quad \frac{1}{r}\frac{d}{dr}\left(r\frac{dF}{dr}\right) + k^2 F = 0 \quad ,$$

$$\text{b)} \quad \frac{d^2u}{dz^2} + \left(\frac{\omega^2}{c^2} - k^2\right) u = 0 \quad . \qquad \text{(2D-6)}$$

Equation 2D-6a is Bessel's equation for order zero. In order to satisfy a radiation condition as $r \to \infty$, the solution to Eq. 2D-6a to be chosen must be the Hankel function of the first kind,

$$F(r) = H_o^{(1)}(\kappa r) \quad . \qquad \text{(2D-7)}$$

Equation 2D-6b is known as the depth equation; it is mathematically equivalent to the one-dimensional Schrödinger equation of quantum mechanics. Analyses and solutions of the depth equation, exact, approximate, and/or numerical, are the central part of many papers on underwater acoustics. The principal subject of this paper is a technique for obtaining asymptotic solutions to Eq. 2D-6b.

The spectrum of the depth equation depends upon the nature of $c(z)$ as $z \to \infty$. It will be assumed here that $c(z)$ approaches a limiting value, c_∞, as $z \to \infty$. Both $c(z)$ and the limit c_∞ are real and finite. When the quantities defined in Eq. 2D-8 are substituted into Eq. 2D-6b, Eq. 2D-9

is obtained

$$q(z) = -\left(\frac{\omega^2}{c^2(z)} - \frac{\omega^2}{c_\infty^2}\right) \quad , \tag{2D-8}$$

$$\lambda = \frac{\omega^2}{c_\infty^2} - k^2 \quad ,$$

$$\frac{d^2u}{dz^2} + (\lambda - q(z))\, u = 0 \quad . \tag{2D-9}$$

This equation is discussed in Chapter 5 of Titchmarsh [1962], who shows that the spectrum of u is discrete for $\lambda < 0$ and is continuous for $\lambda > 0$. In terms of the separation constant k, the spectrum is discrete if $|k| > \omega/c_\infty$ and is continuous if $|k| < \omega/c_\infty$.

We will denote the discrete spectrum by $\{k_n\}$, n = 0, 1, 2, ..N, where N is finite or infinite, depending upon the nature of c(z) as $z \to \infty$. The solution of Eq. 2D-6a for the eigenvalue k_n will be denoted by $u_n(z)$; the eigenfunctions u_n are orthogonal, and are defined to form a normalized set

$$\int_0^\infty u_n(z)\, u_m(z)\, dz = \delta_{nm} \quad . \tag{2D-10}$$

These eigenfunctions for the discrete part of the spectrum are the most important part of the solution for long range acoustic propagation in the ocean.

We will denote the continuous spectrum by κ, where $0 < \kappa < \omega/c_\infty$, and denote the corresponding eigenfunctions by $u(\kappa, z)$.

It will be assumed that these eigenfunctions are normalized as

$$\int_0^\infty u(\kappa,z)\ u(\kappa',z)dz = \delta(\kappa-\kappa') \quad . \tag{2D-11a}$$

Also,

$$\int_0^\infty u_n(z)\ u(\kappa,z)dz = 0 \quad . \tag{2D-11b}$$

These eigenfunctions for the continuous spectrum are relatively unimportant for waveguide propagation, as will be shown.

The solutions to the inhomogeneous equation, Eq. 2D-3, may be expressed in terms of the normal modes as

$$\Phi(r,z) = \sum_n H_o^{(1)}(k_n r)\ u_n(z)\ F_n + \int_0^{k_\infty} H_o^{(1)}(\kappa r)\ u(\kappa,z)\ F(\kappa)\,d\kappa \quad . \tag{2D-12}$$

The quantities F_n and $F(k)$ are easily shown to be a constant times the normal mode functions at depth z_o. To do this, substitute Eq. 2D-12 into Eq. 2D-3 and use the fact that the $u_n(z)$ satisfies Eq. 2D-6b to obtain

$$\sum_n \left(\frac{1}{r}\frac{d}{dr}\, r\frac{d}{dr} + k_n^2\right) H_o^{(1)}(k_n r)\ u_n(z)\ F_n$$

$$+\int_0^{k_\infty} \left(\frac{1}{r}\frac{d}{dr}\, r\frac{d}{dr} + \kappa^2\right) H_o(\kappa r)\ u(\kappa,z)\ F(\kappa)\,d\kappa$$

$$= \frac{-2}{r}\,\delta(r)\ \delta(z-z_o) \quad . \tag{2D-13}$$

Next, to obtain F_n, multiply Eq. 2D-13 by $U_n(z)$ and integrate from $z = 0$ to $z = \infty$; from the orthonormality relations, Eqs. 2D-10 and 2D-11, Eq. 2D-14 results:

$$\left(\frac{1}{r}\frac{d}{dr}\left(r\frac{d}{dr}\right) + k_m^2\right) H_o^{(1)}(k_m r)\ F_m = \frac{-2}{r}\ \delta(r)\ u_m(z_o) \quad . \tag{2D-14}$$

Now, the Hankel function of order zero is important as the Green's function for two-dimensional problems; as discussed in Chapter 8 of Morse and Feshbach [1953], it satisfies

$$\left(\frac{1}{r}\frac{d}{dr}\left(r\frac{d}{dr}\right) + k_m^2\right) H_o(k_m r) = \frac{-2i}{\pi}\frac{\delta(r)}{r} \quad . \tag{2D-15}$$

Combining Eqs. 2D-14 and 2D-15, the factor F_n given by

$$F_m = i\pi\, u_m(z_o) \tag{2D-16}$$

is obtained. In a similar fashion, multiply Eq. 2D-13 by $U(\kappa,z)$ and integrate to obtain

$$F(\kappa) = i\pi\, u(\kappa,z_o) \quad , \tag{2D-17}$$

Finally, the normal mode solution to Eq. 2D-13 is given by

$$\Phi(r,z) = \frac{2i}{\pi}\sum_{n=0}^{N} H_o^{(1)}(k_n r)\, u_n(z)\, u_n(z_o) + \Phi_{cont} \, , \tag{2D-18}$$

where

$$\Phi_{cont} = i\pi\int_o^{k_\infty} H_o^{(1)}(\kappa r)\, U(\kappa,z)\, U(\kappa,z_o)\, d\kappa \quad . \tag{2D-19}$$

As mentioned earlier, the continuous portion of the spectrum is relatively unimportant in long range acoustic propagation. To see that this is so, consider only the part of the field at depth z due to the continuous spectrum, defined in Eq. 2D-19. Next, let the interval $[0,k_\infty]$ be divided into segments so that Φ_{cont} is evaluated by summing

the terms $\Phi(n)$

$$\Phi_{cont} = i\pi \sum_{n} \Phi(n) \quad , \tag{2D-20}$$

$$\Phi(n) = i\pi \int_{\kappa_n}^{\kappa_{n+1}} H_o^{(1)}(\kappa r)\, u(\kappa,z)\, u(\kappa,z_o)\, d\kappa \quad .$$

The intervals in Eq. 2D-20 do not depend upon r; they are chosen so that the factor multiplying $H_o^{(1)}(\kappa r)$ vanishes at both ends of each interval and has the same sign over the interval, as indicated by

$$G(\kappa) \equiv u(\kappa,z)\, u(\kappa,z_o) \quad , \tag{2D-21}$$

$$G(\kappa_n) = G(\kappa_{n+1}) = 0 \quad ,$$

$$G(\kappa) \neq 0 \qquad \kappa_n < \kappa < \kappa_{n+1} \quad .$$

Thus, there is an approximation for the magnitude of $\Phi(n)$

$$|\Phi(n)| \lesssim \pi\, \bar{G}_n \left| \int_{\kappa_n}^{\kappa_{n+1}} H_o(\kappa r)\, d\kappa \right| \quad , \tag{2D-22}$$

where

$$\bar{G}_n = \max|G(\kappa)| \qquad \kappa_n < \kappa < \kappa_{n+1} \quad .$$

A simple change of the integration variable then changes Eq. 2D-22 to

$$|\Phi(n)| \lesssim \frac{\pi \bar{G}_n}{r} \left| \int_{r\kappa_n}^{r\kappa_{n+1}} H_o(x)\, dx \right| \quad . \tag{2D-23}$$

The asymptotic form of the integral of Eq. 2D-23 may be directly obtained from Eq. 11.1.11 of Luke [1970]; the modulus of the integrand

approaches a constant times $r^{1/2}$ as r becomes large.

Thus, at large range,

$$|\Phi(n)| \lesssim \text{const} \times r^{-3/2} \qquad \text{(2D-24)}$$

gives an estimate of the magnitude of $\Phi(n)$ and it follows that the sum of the $\Phi(n)$, Φ_{cont}, goes as $r^{-3/2}$ for large r. This is in contrast to the asymptotic behavior of the discrete spectrum portion of the field which, as may be seen from Eq. 2D-18, goes as $r^{-1/2}$ for large r. In the following analysis, the continuous spectrum will be neglected and it will be assumed that the solution to Eq. 2D-1 is given by the normal mode solution

$$\Phi(r,z) = i\pi \sum_{n=0}^{N} H_o^{(1)}(k_n r)\, u_n(z)\, u_n(z_o) \quad . \qquad \text{(2D-25)}$$

II-E THE DEPTH EQUATION

We return now to the major subject of this paper, the depth equation,

$$\frac{d^2 u_n}{dz^2} + q_n u_n = 0 \quad , \tag{2E-1}$$

$$q_n(z) = \frac{\omega^2}{c^2} - k_n^2 \quad ,$$

The wavenumbers which belong to the discrete spectrum of Eq. 2E-1 satisfy

$$k_n > \omega/c_\infty \quad . \tag{2E-2}$$

The normal mode functions $u_n(z)$ are the functions which are solutions to Eq. 2E-1 and also satisfy the appropriate boundary conditions. At the ocean surface, there is such a large mismatch between the density of the atmosphere and the water that the acoustic pressure in the water vanishes. Thus,

$$u_n(0) = 0 \quad . \tag{2E-3}$$

To rigorously specify a second boundary condition, it would be necessary to consider the acoustical properties of the ocean bottom. However, a discussion of the problems involved in ascertaining the acoustical properties of the ocean bottom and then incorporating them into a theory of propagation is beyond the scope of this dissertation. The acoustics of the ocean bottom are discussed in Hampton [1974], Williams [1976], Bucker [1970], and in references therein. In this work, we shall deal only with the modes which do not interact with the bottom. To accomplish this (Tolstoy and Clay [1966]), we model the SVP so that, below the depth

of the bottom z_b, $c(z)$ equals $c(z_b)$; that is, $c_\infty = c(z_b)$. In order for the mode function u_n to be normalizable (Eq. 2D-10), it must vanish at infinity. Thus, the second boundary condition is

$$u_n(z) \underset{z \to \infty}{\longrightarrow} 0 \quad . \tag{2E-4}$$

In Eq. 2E-1, the function $q_n(z)$, which will be called the profile function, has been introduced. In Fig. 2E-1, representative sound velocity profiles, profile functions, and normal modes have been sketched. The points z_U and z_L, where q_n vanishes, are the turning points of Eq. 2E-4. In the regions where q_n is negative (for example, above the point z_U and below the point z_L of Fig. 2E-1), the function u_n has an "exponential behavior" (Morse and Feshbach [1953]), curving away from the z-axis. Because of the boundary conditions, the normal modes are damped above z_U and below z_L. In regions where q_n is positive, the function u_n curves towards the z-axis, with a "sinusoidal behavior", as between the turning points of Fig. 2E-1.

In this paper, the phrase "turning point" usually will be abbreviated as TP. It will be assumed that there are either only two turning points, or a reflection at the surface and a turning point below the axis depth z_o. That is, if q_n is negative at the surface, there is a turning point below the surface, while if q_n is positive at the surface, mode n reflects from the surface.

The wavenumbers k_n may be arranged in a decreasing sequence, as indicated by

$$k_0 > k_1 > k_2 \ . \ . \ . > k_n > \omega/c_\infty \quad . \tag{2E-5}$$

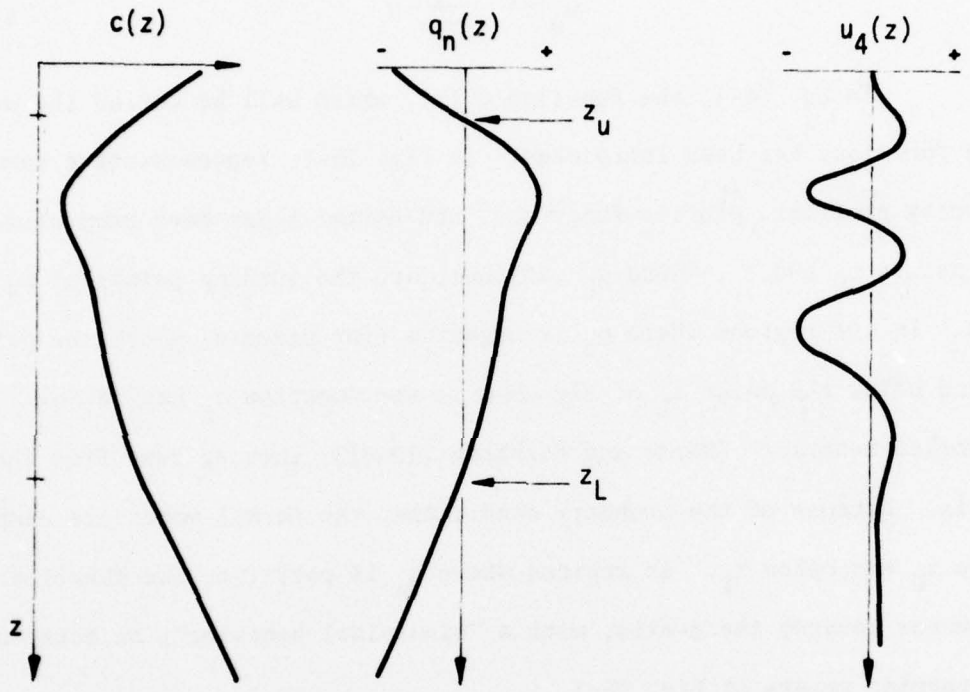

FIGURE 2E-1
SKETCH OF SVP, PROFILE FUNCTION, AND NORMAL MODE FUNCTION
$q_n(z)$ vanishes at the turning points of the mode

When this is done, the upper and lower turning points of the corresponding modes will be ordered as

$$z_o > z_U^0 > z_U^1 \ldots > 0 \quad , \tag{2E-6}$$

$$z_o < z_L^0 < z_L^1 \ldots < z_b \quad ,$$

$$c(z_U^n) = c(z_L^n) = \omega/k_n \quad .$$

More importantly, when the wavenumbers are ordered as in Eq. 2E-5, it may be shown (Titchmarsh [1962]) that u_n has n zeros between z_U^n and z_L^n. It will often be convenient to express u_n in terms of an amplitude, $A_n(z)$, and a phase function, $\phi_n(z)$,

$$U_n(z) = A_n(z) \cos(\phi_n - \pi/4) \quad , \tag{2E-7}$$

$$A_n > 0 \quad ,$$

$$d\phi_n/dz > 0 \quad ,$$

$$0 < \phi_n(z) < (n + 1/2)\pi \quad .$$

Sketches of the amplitude and phase factors are shown in Fig. 2E-2; at the zeros of u_n, $\phi_n(z) = (n - 1/4)\pi$. The amplitude and phase factors may not be uniquely specified from the function $u_n(z)$ alone. However, let $\bar{u}_n(z)$ denote the linearly independent normalized solution to Eq. 2E-1; the function $\bar{u}_n$ will not satisfy the boundary conditions. Then, the functions $A_n(z)$ and $\phi_n(z)$ may be given by

$$A_n(z) = (U_n^2(z) + \bar{u}_n^2(z))^{1/2} \tag{2E-8}$$

$$\phi_n(z) = \arctan(\bar{u}_n/u_n) + \pi/4$$

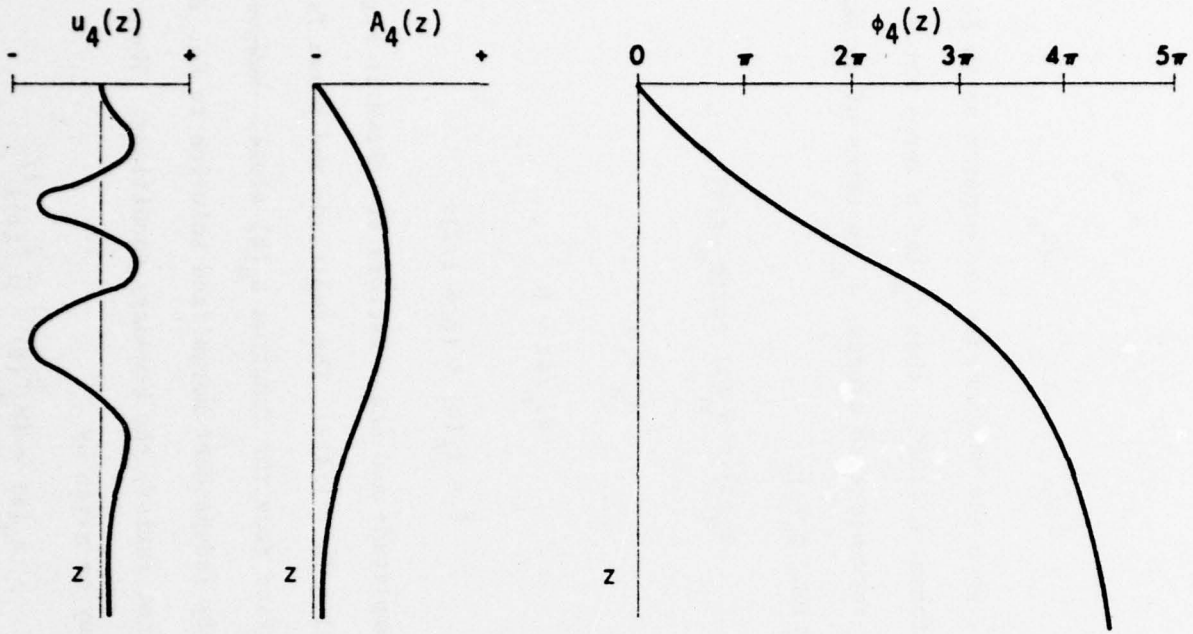

FIGURE 2E-2
SKETCH OF NORMAL MODE FUNCTION, AMPLITUDE MODULATION, AND PHASE FACTOR (Eq. 2E-7)

where $u_4(z) = 0$, $\phi_4(z) = (n - 1/4)\pi$

$(n = 1, 2, 3, 4)$

The representation of Eq. 2E-7 is useful, for example, in discussing the relation between normal mode and ray theory descriptions of sound propagation, as in Section II-H. The WKB solution, discussed in Section II-G, provides approximations for the functions A_n and ϕ_n. In Section IV-B of this paper, an improved approximation (Eq. 4B-3) based upon the Langer solution is used.

II-F BROADBAND SOURCES; PHASE AND GROUP VELOCITY

The normal mode solution developed in section II-D was for a harmonic source of frequency ω. However, by the principal of superposition, the field generated by a broadband source may be given by Eq. 2F-3, below. Analysis of the integral in Eq. 2F-3 leads to the concept of group velocity. Consider that a point is source located at $r = 0$, $z = z_o$, and has the time dependence $S(t)$. The Fourier transform of $S(t)$, $\hat{S}(\omega)$, is given by Eq. 2F-1a; the inverse Fourier transform gives $S(t)$, as shown in Eq. 2F-1b

$$\text{a)} \quad \hat{S}(\omega) = \frac{1}{\sqrt{2\pi}} \int_{-\infty}^{\infty} e^{i\omega t} S(\omega)\, dt \quad ,$$

$$\text{b)} \quad S(t) = \frac{1}{\sqrt{2\pi}} \int_{-\infty}^{\infty} e^{-i\omega t} \hat{S}(\omega)\, d\omega \quad . \qquad \text{(2F-1)}$$

Then, the field generated by the source is

$$\Phi(r,z,t) = e^{-i\pi/4} \sum_n \Phi_n(r,z,t) \quad , \qquad \text{(2F-2)}$$

where the terms $\Phi_n(r,z,t)$ are given by

$$\Phi_n(r,z,t) = \int_{-\infty}^{\infty} d\omega \frac{\hat{S}(\omega)}{\sqrt{2\pi}} \frac{u_n(z_o)\, u_n(z)}{\sqrt{k_n r}} e^{i(k_n r - \omega t)} \quad . \qquad \text{(2F-3)}$$

In Eq. 2F-3, the wavenumber k_n is a function of the frequency ω. The u_n are again the normal modes, solutions of the depth equation 2E-1, and so also depend upon the frequency. The asymptotic form of the Hankel function has been used in Eq. 2F-3.

Assuming that the normal modes have been obtained, and that the functions $k_n(\omega)$ are known, the problem is the evaluation of the integral, Eq. 2F-3. For most problems, the method of stationary phase (Copson [1967], Erdelyi [1956], Pekeris [1948], Tolstoy [1973]), which assumes that the terms in the integrand of Eq. 2F-3 are slowly varying with respect to the oscillations of the complex exponential, is adequate. Because of the cancellation which results from integration over several oscillations, only near points where $k_n r - \omega t$ varies slowly is there significant contribution to the integral. That is, the important frequency is ω_o, defined by

$$\frac{d}{d\omega}(k_n r - \omega t)\Big|_{\omega_o} = 0 \quad , \tag{2F-4}$$

near which the phase of the integrand changes slowly.

Let the group velocity, v_n, be defined by

$$v_n(\omega) \equiv (dk_n/d\omega)^{-1} \quad , \tag{2F-5}$$

so that Eq. 2F-4 may be rewritten as

$$r/t = v_n(\omega_o) \quad . \tag{2F-6}$$

Now, Eq. 2F-6 is a prescription for the frequency ω_o; for mode n, it is expected that the signal arriving near time t will be predominantly made up of components with frequencies near ω_o of Eq. 2F-6. If the factor in the exponential of Eq. 2F-3, $k_n r - \omega t$, is expanded (to second order) in a power series about ω_o and integrated, then $\Phi_n(r,z,t)$ is

given by

$$\Phi_n = \hat{S}(\omega_o)\, v_n(\omega_o)\, \frac{u_n(z_o)\, u_n(z)}{\sqrt{r k_n(\omega_o)\,|\dot{v}_n(\omega_o)|}}\, e^{\pm i\pi/4} \quad . \tag{2F-7}$$

Here, the plus sign in the exponential is to be used if $\dot{v}_n$ is positive, and the negative sign is used if $\dot{v}_n$ is negative. (If $\dot{v}_n(\omega_o) = 0$, a higher order term in the power series is needed. See, for example, Copson [1967]). Note that Eq. 2F-7 predicts that the contribution from the n^{th} mode is disregarding the other factors, proportional to $|\dot{v}_n(\omega_o)|^{-1/2}$.

Another important quantity in addition to the group velocity of mode n is the phase velocity, defined by

$$c_n(\omega) \equiv \omega/k_n \quad , \tag{2F-8}$$

From Eq. 2E-1, it may be seen that the phase velocity of a mode at frequency ω is the same as the sound velocity in the water at the turning points of the mode at frequency ω

$$c_n(\omega) = c(z_u^n) = c(z_u^n) \quad . \tag{2F-9}$$

Therefore, it will sometimes be convenient to abbreviate $c_n(\omega)$ by c_t.

The phase velocity $c_n(\omega)$ of mode n at frequency ω is a useful quantity in that it may be used to estimate whether or not mode n is significant in the propagation of sound of frequency ω from a source at depth z_s to a receiver at depth z'. Since the mode decays with distance away from a TP in a region where $q_n(z)$ is negative, or where c(z) is

less than $c_n(\omega)$, $u_n(z)$ will become small at depths such that $c(z) > c_n(\omega)$. That is, the important modes are those that

$$c_n(\omega) \gtrsim \max \left(c(z_s), c(z')\right) \quad . \tag{2F-10}$$

In the limit of high frequency, the inequality is not an approximate one, but becomes the analogous requirement of ray theory, Eq. 2C-16.

II-G THE WKB SOLUTION

An important technique for obtaining approximate solutions to the depth equation, Eq. 2E-1, was (according to Bellman [1964]) discovered by Liouville in the early nineteenth century. It was rediscovered in the early twentieth century by Wentzel, Kramers, Brillouin, as a means of solving the Schrödinger equation of quantum mechanics and was also used by Jeffreys. The WKB solutions are asymptotic, that is, valid in the limit of "short" wavelengths, as is the ray picture. The WKB picture is a convenient framework within which to relate many aspects of normal mode theory and ray theory.

The WKB solution is derived and discussed in detail in several sources, such as Bellman [1964], Kemble [1958], Morse [1953], and Tolstoy [1966]. The purpose of this section is to enumerate several features of the solution. Following the usual practice, if a turning point is not the surface or bottom, it will be assumed that the turning point is infinitely far from the boundaries.

The normal modes were expressed in terms of an amplitude and phase factor in Eq. 2E-7. The WKB approximation approximates the mode functions by

$$u_n(z) \simeq \tilde{u}_n(z) \quad ,$$

$$\tilde{u}_n(z) = \nu_n q_n^{-1/4} \cos(\tilde{\phi}_n - \pi/4) \text{ if } q_n > 0 \quad , \qquad (2G\text{-}1)$$

in the region between turning points, where the function $\tilde{u}_n$ oscillates, and by

$$\tilde{u}_n(z) = \nu_n |q_n|^{-1/4} e^{-\tilde{\phi}_n} \quad \text{if } q_n < 0 \quad , \tag{2G-2}$$

where $\tilde{u}_n$ decays away from the turning points. The factor $\tilde{\phi}_n$ is the phase between TP's

$$\tilde{\phi}_n(z) = \int_{z_U}^{z} q_n^{1/2} dz' \qquad z_U < z < z_L \quad , \tag{2G-3}$$

and the decay factor in the other regions

$$\tilde{\phi}_n(z) = \int_{z}^{z_U} |q_n|^{1/2} dz' \qquad 0 < z < z_U \quad ,$$

$$\tilde{\phi}_n(z) = \int_{z_L}^{z} |q_n|^{1/2} dz' \qquad z_L < z \quad . \tag{2G-4}$$

The quantity ν_n is a normalization factor, chosen to ensure that Eq. 2D-10 is satisfied. The eigenvalue equation from which the wavenumbers k_n are determined is the Bohr-Sommerfeld equation,

$$\int_{z_U}^{z_L} q_n^{1/2} \, dz = (n + 1/2)\pi \quad . \tag{2G-5}$$

In deriving the WBK solution, it is assumed that the second derivative of the mode amplitude, divided by the mode amplitude, is much less than the profile function. It may be shown that this is equivalent, making reasonable assumptions, to

$$\frac{d|q|}{dz} << |q|^{3/2} \quad , \tag{2G-6}$$

which in terms of the sound velocity c(z) is

$$\frac{\omega^2}{c^2}\frac{1}{c}\frac{dc}{dz} << \left(\frac{\omega^2}{c^2} - k_n^2\right)^{3/2} \quad . \tag{2G-7}$$

There are two situations for which Eq. 2G-7 may not be satisfied. First, if the slope of the sound velocity at some depth is too great, the LHS of Eq. 2G-7 becomes large; second, near a turning point, the RHS of Eq. 2G-7 vanishes.

To estimate the restrictions upon the slope of c(z) imposed by the first type of problem, express k_n in terms of the phase velocity so that Eq. 2G-7 becomes

$$\frac{\omega^2}{c^2}\frac{1}{c}\frac{dc}{dz} << \frac{\omega^3}{c^3}\left(\frac{c_t - c}{c}\right)^3 \quad . \tag{2G-8}$$

Multiply both sides of Eq. 2G-8 by c^3/ω^2 to get

$$\left|\frac{dc}{dz}\right| << \omega\left(\frac{c_t - c}{c}\right)^3 \quad , \tag{2G-9}$$

which says that the slope of c(z) should be much less than the frequency times the cube of the fractional difference between the phase velocity and c(t). In practice, the fractional difference is usually a few percent, so that the WKB solutions are useful only at high frequencies or in regions of slowly varying c(z).

The second type of problem, the failure of the WKB solution at turning points, does not depend upon frequency or details of the SVP. In applying the WKB technique to many problems in underwater acoustics, the difficulty near turning points is a serious one since a source and/or receiver may be near the depths of turning points of many of the modes connecting the source and receiver.

It is interesting to consider the normalization of the WKB solutions. From Eqs. 2G-1 and 2D-10, we obtain

$$1 = \nu_n^2 \int_{z_U}^{z_L} q_n^{-1/2} \cos^2(\phi_n - \pi/4)\,dz$$

$$+ \nu_n^2 \left(\int_0^{z_U} + \int_{z_L}^{\infty} \right) |q_n|^{-1/2} e^{-\tilde{\phi}_n}\,dz \quad . \qquad (2G\text{-}10)$$

Next, assume that the contribution to Eq. 2G-10 from the regions outside of the TP's is negligible and that $q_n(z)$ is slowly varying over each oscillation of the cosine term in the region between the TP's so that the $\cos^2(\phi-\pi/4)$ term may be approximated by 1/2, so that

$$1 = \frac{\nu_n^2}{2} \int_{z_U}^{z_L} q_n^{-1/2}\,dz$$

$$= \frac{\nu_n^2}{2} \int_{z_U}^{z_L} \left(\frac{\omega^2}{c^2} - k_n^2 \right)^{-1/2} dz \quad . \qquad (2G\text{-}11)$$

Both of these assumptions are better the larger the mode number. Next, replacing the wavenumber k_n in Eq. 2G-10 by ω divided by the phase velocity, or turning point velocity, one obtains

$$\nu_n^{-2} = \frac{\omega^2}{2} \int_{z_U}^{z_L} \left(\frac{1}{c^2} - \frac{1}{c_t^2} \right)^{-1/2} dz$$

$$= \frac{c_t \omega^2}{2}\, \tilde{D}(z_U, z_L; c_t) \quad . \qquad (2G\text{-}12)$$

Here, function D is the ray tracing quantity, the ray cycle distance, which is defined in Eq. 2C-13. Thus, the normalization factor for the WKB normal mode functions is approximated as

$$\nu_n = \left(\omega^2 c_t D(z_U, z_c; c_t)/2\right)^{-1/2} \quad . \tag{2G-13}$$

A second connection between the WKB theory and ray theory is seen by considering the group velocity of the WKB modes. The group velocity may be obtained from the Bohr-Sommerfeld condition, Eq. 2G-5, which is

$$(n + 1/2)\pi = \int_{z_U}^{z_L} \left(\frac{\omega^2}{c^2} - k_n^2\right)^{1/2} dz \quad . \tag{2G-14}$$

Taking the derivative with respect to ω of Eq. 2G-14, one obtains

$$0 = \int_{z_U}^{z_L} \left(\frac{\omega^2}{c^2} - k_n^2\right)^{-1/2} \left(\frac{\omega}{c^2} - k_n \frac{dk_n}{d\omega}\right) dz \quad , \tag{2G-15}$$

from which the group velocity, defined by Eq. 2F-5 may be obtained. This gives

$$\tilde{v}_n(\omega) = \frac{k_n \int_{z_U}^{z_L} \left(\frac{\omega^2}{c^2} - k_n^2\right)^{-1/2} dz}{\omega \int_{z_U}^{z_L} c^{-2} \left(\frac{\omega^2}{c^2} - k_n^2\right)^{-1/2} dz} \quad . \tag{2G-16}$$

Then, if the wavenumber is expressed in terms of frequency and phase velocity, then the frequency factors out of the expression, and the group velocity is expressed in terms of the ray theory cycle distance and cycle time (see Eqs. 2C-13 and 2C-14) as

$$\tilde{v}_n(\omega) = \frac{\tilde{D}(z_U, z_L; \omega/k_n)}{\tilde{T}(z_U, z_L; \omega/k_n)} \quad . \tag{2G-17}$$

That is, if two different modes (at different frequencies) have the same phase velocity, then, under the WKB approximation, they will have the same group velocity.

Finally, consider the quantity $\Lambda_n(\omega)$ defined in Eq. 2G-18

$$\tilde{\Lambda}_n(\omega) \equiv \frac{2\pi}{k_{n+1} - k_n} \simeq 2\pi(\partial k_n/\partial n)^{-1} \quad . \tag{2G-18}$$

It will be shown in the next section that Λ_n is the mode-interference spacing, or mode cycle distance, which is analogous to the cycle distance of ray theory. To obtain Λ_n in the WKB approximation, take the derivative of Eq. 2G-14 with respect to n to obtain

$$\pi = -\int_{z_U}^{z_L} \left(\frac{\omega^2}{c^2} - k_n^2\right)^{-1/2} k_n \frac{dk_n}{dn}\, dz \quad . \tag{2G-19}$$

Then, substitute ω/c_n for k_n in Eq. 2G-14 and solve for $\tilde{\Lambda}_n$:

$$\tilde{\Lambda}_n(\omega) = 2\tilde{D}(z_U, z_L; \omega/k_n) \quad . \tag{2G-20}$$

Thus, in the WKB approximation, the mode interference spacings for two different modes with the same phase velocity (again at different frequencies) are equal.

II-H MODE INTERFERENCE, RAY-MODE RELATIONS, AND NORMAL MODE QUANTITIES

A final topic in this chapter is the matter of mode interference in situations where there are a large number of modes. As will be shown, the peaks of mode interference occur along paths which are, in the WKB approximation, identical to the ray paths of a ray theory picture of the problem. Experimental demonstration of the overlap between ray theory and mode theory for a simple situation (isovelocity water overlying glass or rubber) has been given by Wood [1963] and discussed by Weston [1968] and Tolstoy and Clay [1966]. The connection between mode interference and ray paths for the WKB solution was given by Tindle and Guthrie [1974].

The normal mode $u_n(z)$ was expressed in Eq. 2E-7 in terms of amplitude and phase factors. The normal mode solution, Eq. 2D-25, is rewritten here as

$$p(r,z) = r^{-1/2} \sum_n e^{i(k_n r - \pi/4)} B_n \cos(\phi_n(z_s) - \pi/4) \cos(\phi_n(z) - \pi/4) \quad , \qquad (2H\text{-}1)$$

in terms of these factors. The terms B_n depend upon the source and receiver depth and include the normalizing factors; the asymptotic form of the Hankel function $H_o^{(1)}(\cdot)$ has been used. Equation 2H-1 is then written in terms of complex exponentials as

$$p(r,z) = r^{-1/2} \sum_n B_n \{ e^{i\psi_n^{++}} + e^{i\psi_n^{+-}} + e^{i\psi_n^{-+}} + e^{i\psi_n^{--}} \} \quad ; \quad (2H\text{-}2)$$

the phase terms are defined by

$$\psi_n^{++} = k_n r + \phi_n(z_s) + \phi_n(z) - \pi/2 \quad ,$$

$$\psi_n^{+-} = k_n r + \phi_n(z_s) - \phi_n(z) \quad ,$$

$$\psi_n^{-+} = k_n r - \phi_n(z_s) + \phi_n(z) \quad ,$$

$$\psi_n^{--} = k_n r - \phi_n(z_s) - \phi_n(z) + \pi/2 \quad . \tag{2H-3}$$

With substitutions such as

$$p^{+-} = r^{-1/2} \sum B_n e^{i\psi_n^{+-}} \quad , \tag{2H-4}$$

Eq. 2H-2 is rewritten as

$$p(r,z) = P^{++} + P^{+-} + P^{-+} + P^{--} \quad , \tag{2H-5}$$

and we consider, as an example, the function p^{+-}. If the number of modes is large, the contributions from the individual terms in the sum of Eq. 2H-5 will tend to cancel after summing a few adjacent modes except for those modes such that

$$\Delta\psi_n^{+-} = \psi_{n+1}^{+-} - \psi_n^{+-} = 2M\pi, \; M = 0, 1, 2, \ldots \quad . \tag{2H-6}$$

When Eq. 2H-6 is satisfied, successive modes will be in phase and a large contribution to the sum in Eq. 2H-5 will result. In terms of the range, wavenumbers, and mode phases, the interference condition is given by

$$r\,\Delta k_n + \Delta\phi_n(z_s) - \Delta\phi_n(z) = 2M\pi \quad . \tag{2H-7}$$

Mode reinforcement will occur at the ranges given by

$$r = \frac{2M\pi}{\Delta k_n} - \frac{\Delta\phi_n(z_s) - \Delta\phi_n(z)}{\Delta k_n} \quad ; \tag{2H-8}$$

in terms of the mode-cycle distance defined by Eq. 2G-18, these ranges are given by

$$r = M\Lambda_n - \frac{\Delta(\phi_n(z_s) - \phi_n(z))}{\Delta k_n} \quad . \tag{2H-9}$$

In Eq. 2H-9, the mode cycle distance is independent of source and receiver depth. The second term, involving differences between the mode phases at the two depths, is zero when $z = z_s$ and increases as the difference between source and receiver depth increases.

In the WKB approximation, the mode cycle distance $\tilde{\Lambda}_n$ has been given by Eq. 2G-20. The WKB expression for the difference in the phase is given by

$$\tilde{\phi}_n(z_s) - \tilde{\phi}_n(z) = \int_z^{z_s} \left(\frac{\omega^2}{c^2} - k_n^2\right)^{1/2} dz' \quad . \qquad (2H\text{-}10)$$

The derivative of this difference with respect to k_n is

$$\frac{d}{dk_n}\left(\tilde{\phi}_n(z_s) - \tilde{\phi}_n(z)\right) = -\int_z^{z_s} k_n \left(\frac{\omega^2}{c^2} - k_n^2\right)^{-1/2} dz' \quad . \qquad (2H\text{-}11)$$

If k_n in Eq. 2H-11 is replaced by ω/c_n, then the frequency ω may be factored from the KHS, so that the integral is of the same form as Eq. 2C-13a for the horizontal distance between depth z_s and depth z along a ray of turning point velocity $c_t = \omega/k_n$:

$$\frac{d}{dk_n}\left(\tilde{\phi}_n(z_s) - \tilde{\phi}_n(z)\right) = \tilde{D}(z, z_s; \omega/k_n) \quad . \qquad (2H\text{-}12)$$

Thus, the ranges at which modes of order close to n constructively interfere for the p^{+-} term are

$$r = 2M\tilde{D}(z_U, z_L; \omega/k_n) - \tilde{D}(z_s, z; \omega/k_n) \quad . \qquad (2H\text{-}13)$$

The relationships between mode number and the ranges at which they are dominant for all of the terms in Eq. 2H-4 may be developed along similar lines and are combined in

$$r = 2M\tilde{D}(z_U, z_L; \omega/k_n) + \alpha\tilde{D}(z_s, z; \omega/k_n) + \beta\tilde{D}(z_U, z_s; \omega/k_n)$$

$$M = 0, 1, 2, \ldots$$

$$\alpha = \pm 1$$

$$\beta = 0 \text{ or } 2 \quad . \tag{2H-14}$$

Again, in the WKB approximation, note that Eq. 2H-14 is identical to Eq. 2C-15.

To generalize Eq. 2H-14, one may regard the WKB expression (Eq. 2G-3) for the phases of the normal modes as a first approximation and add a correction term (to get the exact phase)

$$\phi_n(z) = \int_{z_U}^{z} q_n^{1/2} dz' + e_n(z, \omega) \quad . \tag{2H-15}$$

Correspondingly, the Bohr-Sommerfeld condition is regarded as an approximation for the exact expression

$$\int_{z_U}^{z_L} q_n^{1/2} dz = (n + 1/2)\pi + \varepsilon_n(\omega) \quad . \tag{2H-16}$$

The terms e_n and ε_n of Eqs. 2H-15 and 2H-16 take into account the effect of boundary conditions in addition to errors in the WKB solution to the problem at hand. If the problem at hand involves a SVP whose exact solution is known (a parabolic profile, for example), then the factors e_n and ε_n may be determined exactly. The principal topic of this paper, the Langer solution discussed in Chapter IV, provides approximation formulae for e_n and ε_n.

Now, in the same way that Eq. 2G-20 followed from Eq. 2G-14, when the derivative of Eq. 2H-16 with respect to k_n is taken and the

resulting equation solved for $(dk_n/d\eta)^{-1}$, one obtains

$$\Lambda_n(\omega) \equiv \frac{2\pi}{\Delta k_n} = 2\,\frac{2\pi\tilde{D}(z_U, z_L; \omega/k_n)}{\pi + \Delta\epsilon_n(\omega)} \quad . \tag{2H-17}$$

Similarly, the derivative of the phase difference with respect to wavenumber, which defines a distance L_n is given by

$$\frac{d}{dk_n}\left(\phi_n(z_s) - \phi_n(z)\right) \equiv L_n(z, z_s; \omega)$$

$$= \tilde{D}(z_s, z; \omega/k_n) + \frac{d}{dk_n}\left(e_n(z_s, \omega) - e_n(z, \omega)\right) \quad . \tag{2H-18}$$

Then, substituting Eqs. 2H-17 and 2H-18 into Eq. 2H-9 (and its equivalents), one obtains the mode reinforcement equation

$$r = \frac{2M\pi\tilde{D}(z_U, z_L; \omega/k_n)}{\pi + \Delta\delta_n(\omega)} + \alpha L_m(z, z_s; \omega) + \beta L_n(z_U, z_s, \omega)$$

$$M = 0, 1, 2, \ldots$$

$$\alpha = \pm 1$$

$$\beta = 0 \text{ or } 2 \quad . \tag{2H-19}$$

The interpretation of Eq. 2H-19 is straightforward, that is, the important modes in the propagation of sound from a source to a receiver are those whose phase velocities are close to the turning point velocities of ray paths which also connect the source and receiver. The contribution from other modes is relatively unimportant. The interpretation of the exact Eq. 2H-19 is identical to that of Eq. 2H-14 if Eq. 2H-19 is interpreted as defining frequency dependent "raypaths." In the paper by Tindle and Guthrie [1974], they showed that the maximae (vs depth) of the sum of only a few terms of the normal mode solution (Eq. 2D-25) did

trace out "raypaths" as the range at which the sum was computed changed. The normal modes were exact in the sense that they were obtained by numerical solution of the depth equation for an experimental SVP.

III. BACKGROUND - EXPERIMENTS AND MODELS

The purpose of this chapter is to offer a survey of ocean acoustic phenomena and of the analyses and models to explain them. The measurement of greatest practical interest is that of propagation loss. Propagation loss from a source to a receiver is defined as the ratio of the signal intensity at the receiver to the signal intensity at a reference distance, say, 1 m, from the source. In terms of the normal mode solution, Eq. 2D-25, propagation loss is modeled as

$$PL = 10 \log_{10} \left[\frac{\pi}{4} \left| \sum_n H_o^{(1)} \left(k_n r \right) u_n(z) u_n(z_o) \right|^2 \right] \quad . \qquad (3\text{-}1)$$

In this paper, we shall not be interested in the computation or measurement of propagation loss per se. Instead, we shall be interested in the structure of signals from impulsive sources, and in the structure of propagation loss versus range curves as a function of frequency. Ray theory provides an approximate description of these details in terms of the quantities of ray cycle distance, $2\tilde{D}$, and ray cycle time, $2\tilde{T}$, which were presented in Section II-C. However, some recently published measurements (A. Guthrie [1974], Porter [1973]) show that at frequencies less than, say, 100 Hz, quantities such as signal travel time are frequency dependent, rather than frequency independent as predicted by ray theory or the WKB solution (see Sections II-C and II-G). The formulae to be derived in Section IV-C of this work will give normal mode theory quantities $\tilde{D}_n$ and $\tilde{T}_n$ which differ from the ray

theory quantities at low frequencies, but approach them at high frequencies. These will be applied in Chapter V to compute group velocities and mode cycle distances for representative SVP's.

The basic characteristics of deep ocean acoustic propagation were originally discovered in experiments using explosive sources; these were reported by Ewing and Worzel [1948]. The greatest interest during the period following was in the SOFAR (Sound Fixing and Ranging) propagation situation, whereby the source and receiver are both at the depth z_o of minimum velocity. The SOFAR signal at a range of several hundred miles from an explosive source (of duration of a few msec or less) is of duration of, say, 2 to 10 sec; the arrival consists of a series of impulses perhaps 100 msec apart which increase in amplitude until the end of the signal when, abruptly, there is quiet. The final part of the arrivals, the crescendo, travels at the speed of sound at the axis. That is, the earliest arrivals have traveled away from the axis while the strongest portion traveled directly down the channel. Hirsch and Carter [1965] analyzed the ray quantities for the SVP modeled by

$$c^2(z) = c_o^2\left(1-a|z-z|^b\right)^{-1} \quad . \tag{3-2}$$

Some of the profiles of this model are shown in Fig. 3-1. Hirsch showed (using analytical forms for $\tilde{D}$ and $\tilde{T}$) that only for profiles such that $b<2$ did the slowest arrival travel along the axis; that is, where the SOFAR signal shape is observed, the SVP must be "sharper"

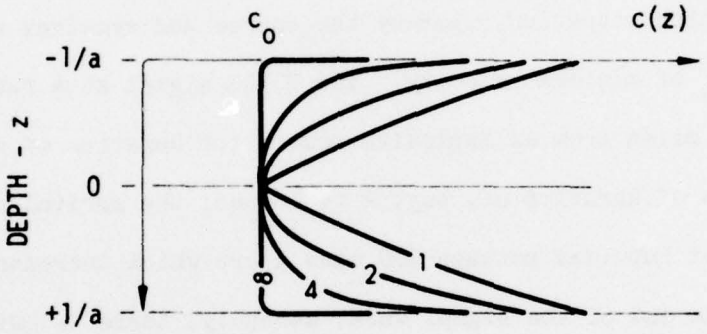

FIGURE 3-1
HIRSCH PROFILES (Eq. 3-2)

The number labeling each curve
is the parameter b of Eq. 3-2.

than that represented by a parabola. Propagation to ranges up to 4000 nm across the Atlantic, Pacific, Arctic, and Indian Oceans has been reported (Urick [1963], [1966]; Kibblewhite [1965], [1974]). Models of the SOFAR signal structure using normal mode theory have been published by Hirsh [1965], using a parabolic fit to the SVP, by Normandy and Uberall [1975], who used an Epstein profile, and K. M. Guthrie [1974b], using a numerical solution for experimental profiles.

In the SOFAR configuration, with both source and receiver at z_o on the SVP axis, the received signal is dominated by refracted arrivals; that is, energy which was not reflected from the surface or bottom. However, when the source and/or the receiver are not close to the axis, those modes or rays which have TP velocities less than the sound velocity at the source or receiver are not significant to the propagation between that source and receiver. This effect is illustrated by the ray diagrams of Fig. 3-2. With the shallow source and, say, a receiver at the same depth, Fig. 3-2b shows the field at the receiver depth to be separated into relatively narrow bands of high intensity, known as the convergence zones, and the region between them where there appear no rays, called the shadow zones. Depending upon the reflectivity of the bottom, and upon the range from source to receiver, there may be signals propagating into the shadow zones which have reflected from the bottom; however, in this work, the contribution of bottom reflected components is not considered. The convergence zone phenomenon is apparent in both theoretical and experimental plots of propagation loss versus range (see, for example, A. Guthrie [1974]) as a

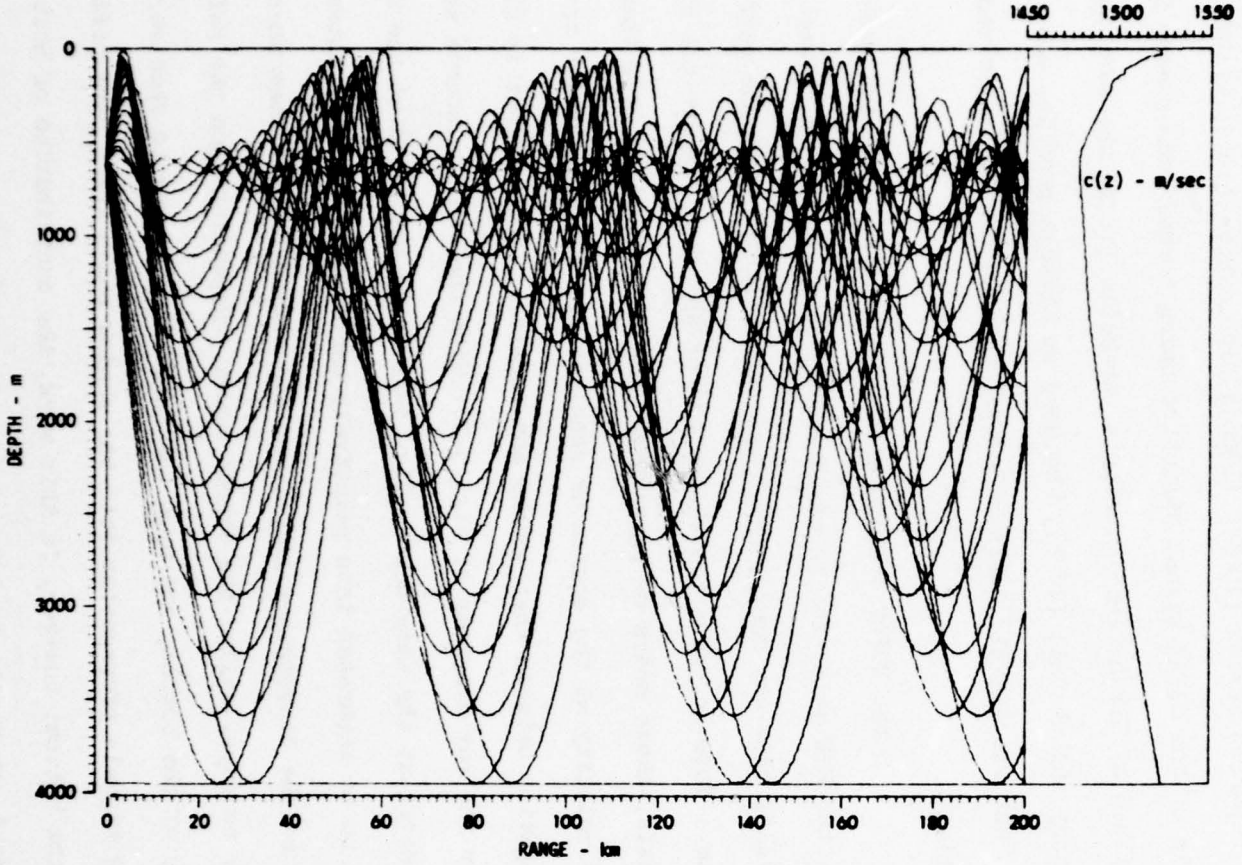

FIGURE 3-2(a)
RAY DIAGRAM FOR NE PACIFIC SVP - 600 m SOURCE

The profile is shown to the right;
600 m is the velocity minimum.

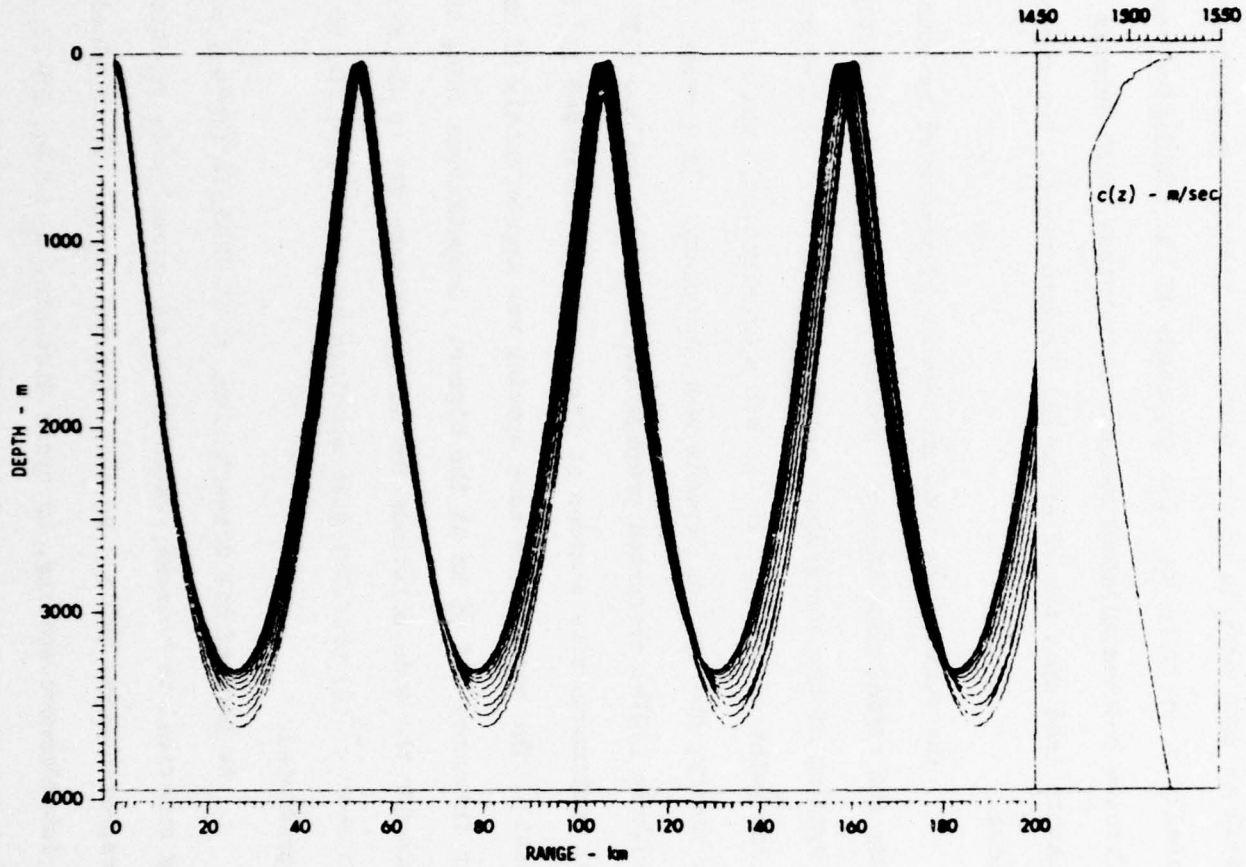

FIGURE 3-2(b)
RAY DIAGRAM FOR NE PACIFIC SVP - 60 m SOURCE

The profile is shown to the right. Most of the water mass is shadowed by refraction.

scalloped modulation of the propagation loss curve which otherwise is decaying with range. The period of the modulation depends upon the SVP as well as upon details of the source and receiver geometry, but is nominally 60 km to 65 km. The amplitude of the modulation, or the difference between adjacent maximae and minimae, also depends upon the situation (and upon the experimental dynamic range), but may be 10 dB or more.

The convergence zone phenomenon is predicted by both ray theory and normal mode theory. However, as discussed in Section II-H, the spacing of the convergence zones is independent of frequency from the ray point of view (or in the WKB approximation), while in normal mode theory, the spacing depends upon frequency. In a recent paper, A. Guthrie [1974] presented propagation loss from shallow (150 m or less) continuous tone sources at frequencies of 14 Hz and 111 Hz in the Atlantic. The convergence zone spacing was approximately 62 km at the lower frequency and 65 km at the higher. Computations using the eigenvalues for the mode solutions for an approximate fit to the SVP (using a bilinear $c^{-2}(z)$ profile) gave spacings near to these; the 5% spread was predicted.

As part of his dissertation, K. M. Guthrie [1974a] computed, using numerical techniques, wavenumbers and normal mode functions for a few representative SVP's. He then computed $\Delta k_n(\omega)$ and obtained the mode interference spacing, or cycle distance, Λ_n of Eq. 2H-17, and plotted Λ_n versus "ray angle" $\left(\text{Arc cos}(c(z_o)/c_n(\omega))\right)$ for different frequencies. He showed that, depending upon details of the SVP, the mode cycle distance can vary by 5% or more (2 km to 5 km out of 60 km) with

frequency at those phase velocities which are approximately equal to the sound velocity at the surface, c(0).

Examples of the envelopes of signals received from explosive sources are shown in Fig. 3-3. The time-pressure waveforms of such signals may be analyzed to determine the travel time of the individual arrivals, and to determine the spreading of the arrivals caused by slightly different travel velocities of different frequency components. There are several reports of detailed analysis of the arrival times of such signals. These show an agreement between predictions from ray theory and measurements which indicate that, in spite of the variability of the ocean environment, detailed phenomena predicted by ray theory may be observed.

Porter [1973] has analyzed a series of signals obtained in the Mediterranean at ranges out to 600 km; both the source and receiver were near the axis. Each signal consisted of a series of 4 to 5 arrivals spaced 200 msec to 500 msec apart. The measured travel times of arrivals, relative to the slowest (axial) arrival, were within 50 msec of the predictions of ray theory using only an approximate fit to the SVP (bilinear form for c(z)).

Fitzgerald [1974] analyzed the multiple arrivals from explosive sources in the Atlantic. He showed that the arrival structure was in accordance with the predictions of ray theory. Also, the evolution of the signal structure with changing range out to 2000 km formed a regular pattern, showing that the ocean acoustical parameters were reasonably stable during the experiment. The time of signal travel

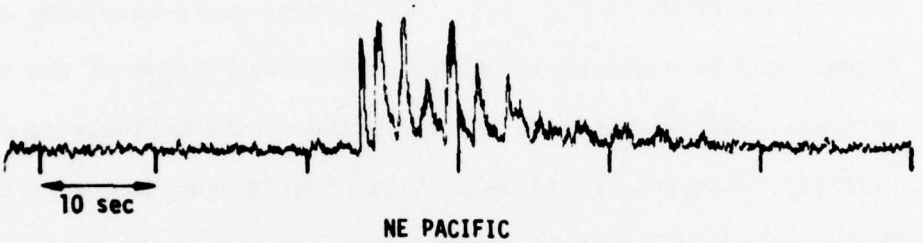

NE PACIFIC
18 m SOURCE, 3925 m RECEIVER
185 km SOURCE TO RECEIVER RANGE

NE ATLANTIC
91 m SOURCE, 2000 m RECEIVER
780 km SOURCE TO RECEIVER RANGE

FIGURE 3-3
EXAMPLES OF ENVELOPES OF SIGNALS FROM EXPLOSIVE SOURCES

In both signals, the arrivals later than approximately 2 sec after the initial arrival have reflected from the bottom. The signal at the top has an unusual amount of bottom reflected energy.

from detonation at long range of the earliest arrival of signals was studied by Mitchell and Hampton [1975]. We compared the speed of the earliest detectable arrival (along the time minimizing ray path) from source to receivers at different ranges, and showed that the signal speed has a periodic structure. The signal travel times were the by-product of propagation loss measurements in which explosive sources were used. Signal arrivals were decided by an automatic computer algorithm, using a threshold based upon the background noise level. Only the time of the earliest detectable arrival was measured.

A typical situation is shown in Fig. 3-4. The sound velocity profile is from the Northeast Pacific during summertime. The two earliest distinguishable rays from the sources at 91 m depth to a deep receiver at the different ranges is shown along with the travel time and corresponding signal velocity along each ray. Between 85 nm and 92 nm, the leading path has become deeper and the signal speed increases because of the travel in the higher velocity portion of the water column. Then, at 93 nm, there is no ray path which does not reflect from the bottom. Because of the steeper angles involved, the signal speed suddenly drops 18 m/sec within 1 nm. The most dramatic jumps in signal speed occur when an increase with range causes the path of the earliest arrival to strike the bottom.

Several features are illustrated by Fig. 3-5, which shows the ray theory signal speed versus range for the geometry and SVP of Fig. 3-4. The number of deep turning points, direction, and type of path (bottom reflected or not) are indicated to help understand the

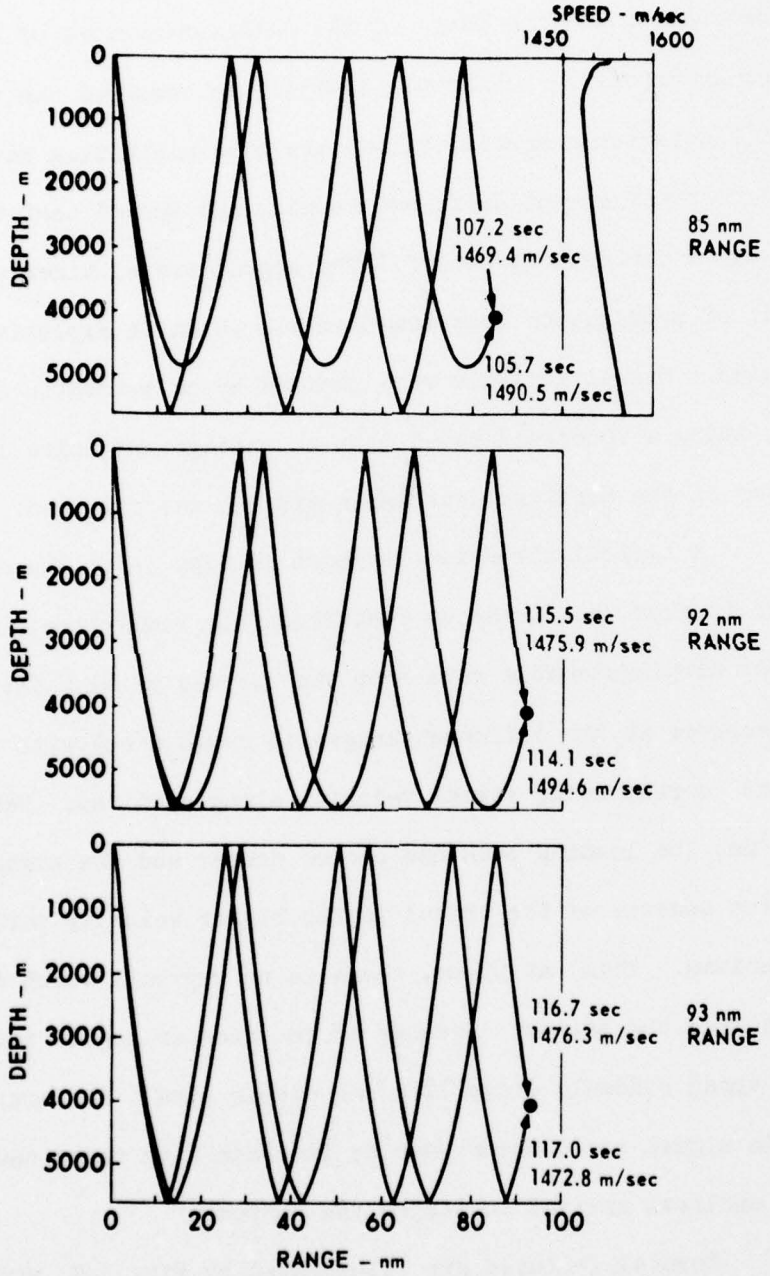

FIGURE 3-4
EIGENRAY PATHS, TRAVEL TIMES, AND SIGNAL SPEEDS FOR FIRST TWO DETECTABLE ARRIVALS NE PACIFIC PROFILE
91 m SOURCE
4055 m RECEIVER

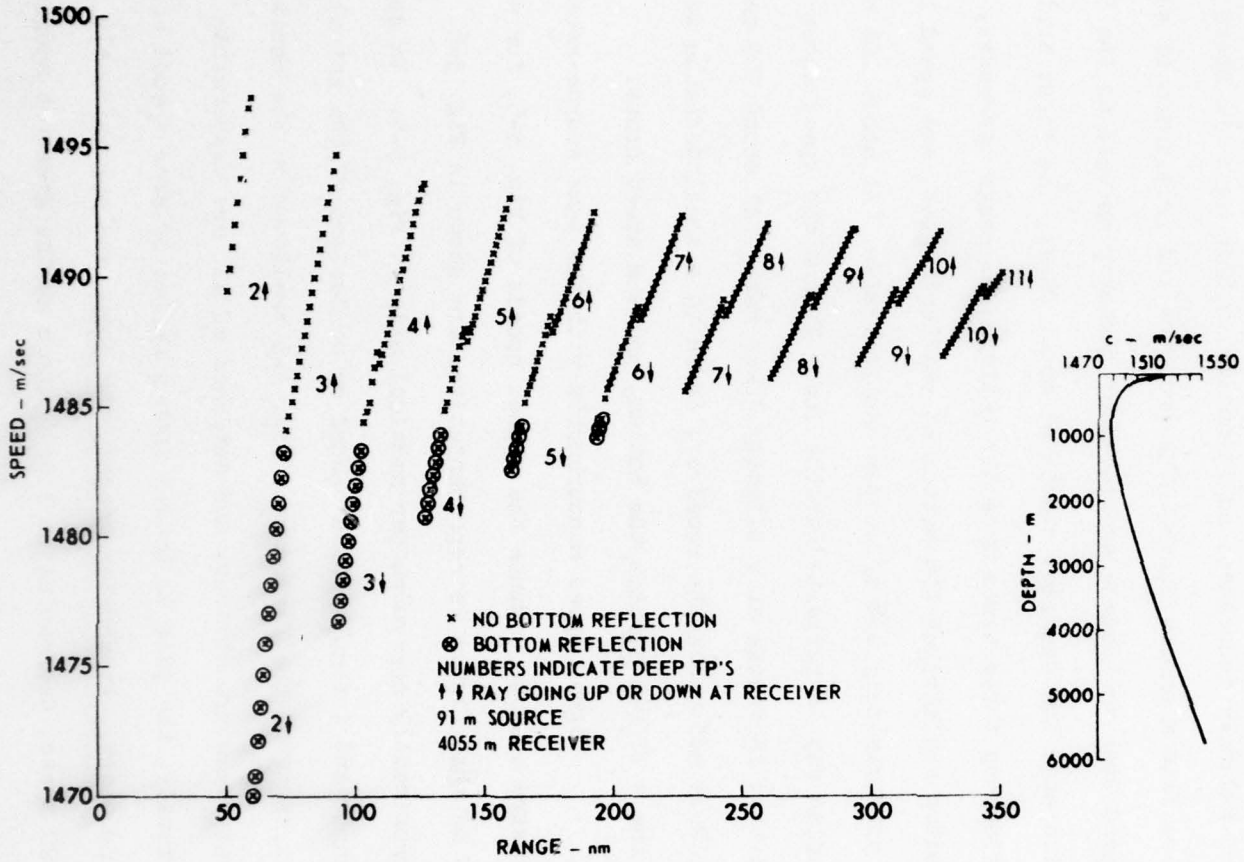

FIGURE 3-5
SIGNAL SPEED VERSUS RANGE
NE PACIFIC PROFILE

changes. The most obvious feature is the separation of the plot into arcs along which the signal speed generally increases with range, and then suddenly decreases; additionally, within each arc there are departures from a smooth curve. The presence and prominence of such features depend upon the source and receiver geometry as well as the SVP. The third arc, for example, starts at about 94 nm, the first arrival reflecting three times from the bottom. As range increases, the leading ray strikes the bottom at smaller angles, and speed increases at approximately 0.8 m/sec per nautical mile. At about 103 nm, the leading ray is refracted at the lower TP and the speed shows a jump, and then increases at a slightly lower rate. At about 109 nm, the 3 TP ray does not reach the receiver; there is a small decrease with speed as the 4 TP ray strikes the bottom, and the speed drops.

Signal speed measurements with the same source-receiver geometry used to compute the signal speeds of Fig. 3-5, for which the SVP of that figure is representative, are shown in Fig. 3-6. There is approximately one point per nautical mile in Fig. 3-6. In spite of the changes and irregularities caused by variations of the actual environment, some of the features of Fig. 3-5 predicted on the basis of an ideal ocean are obvious, and evidence of all are discernible. Most obviously, the plot is broken into a series of arcs spaced approximately 30 nm apart. At shorter ranges, the jumps are approximately 15 m/sec to 20 m/sec, decreasing to 5 or 6 m/sec at the greatest ranges. On some of the arcs, e.g., near 170 nm, there are discontinuities such as those predicted for the change from a bottom reflected to a bottom refracted first arrival. Also, the bunching of the data, such as

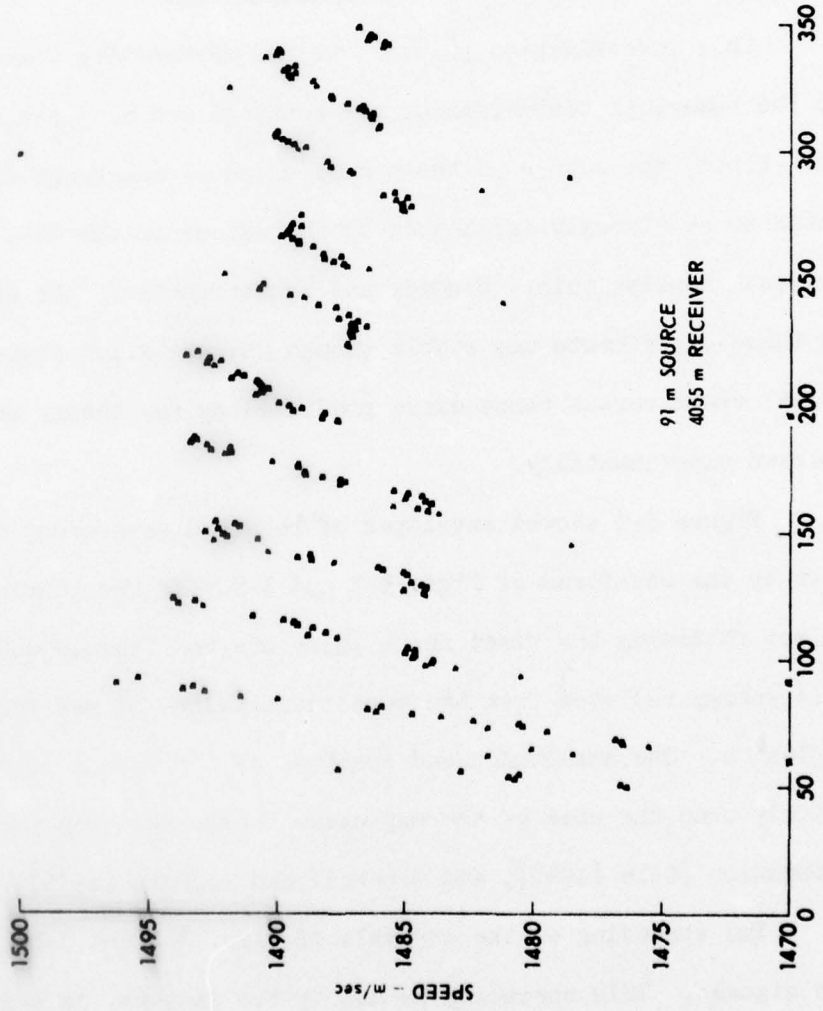

FIGURE 3-6
MEASURED SIGNAL SPEED
NE PACIFIC PROFILE

occurs near 215 nm, is due to a slight decrease in signal speed with increasing range. This behavior was predicted for a change in number of lower turning points, which is from 6 to 7 at 215 nm. Measurements in the North Atlantic, with a SVP different from that of Fig. 3-5, showed a similar agreement between the features of the signal speed predicted by ray theory and seen in the measurements.

This investigation pointed out two interesting features, beyond the numerical comparison of the computed and measured signal speeds. First, the nature of the signal speed versus range curve is predicted to be strongly influenced by the nature of the SVP, and the measurements confirm this. Second, and more important, the environment during these experiments was stable enough that detailed features of the signal speed versus range curve predicted by ray theory may actually be observed experimentally.

Figure 3-3 showed envelopes of received waveforms; more detail is shown by the waveforms of Figs. 3-7 and 3-8. In the source waveforms the pulses following the first shock pulse are the "bubble pulses": acoustic energy radiated from the oscillating globe of gas formed by the explosion. The amplitudes and spacings of the bubble pulses depend sensitively upon the size of the explosive charge and upon the depth of the detonation (Cole [1948], and Mitchell and Bedford [1975]).

The spreading of the arrivals of Figs. 3-7 and 3-8 is typical of such signals. This spreading is due to two factors, in addition to the spread of the bubble pulses of the source. First, there are several ray paths along which the signal may travel to constitute each arrival,

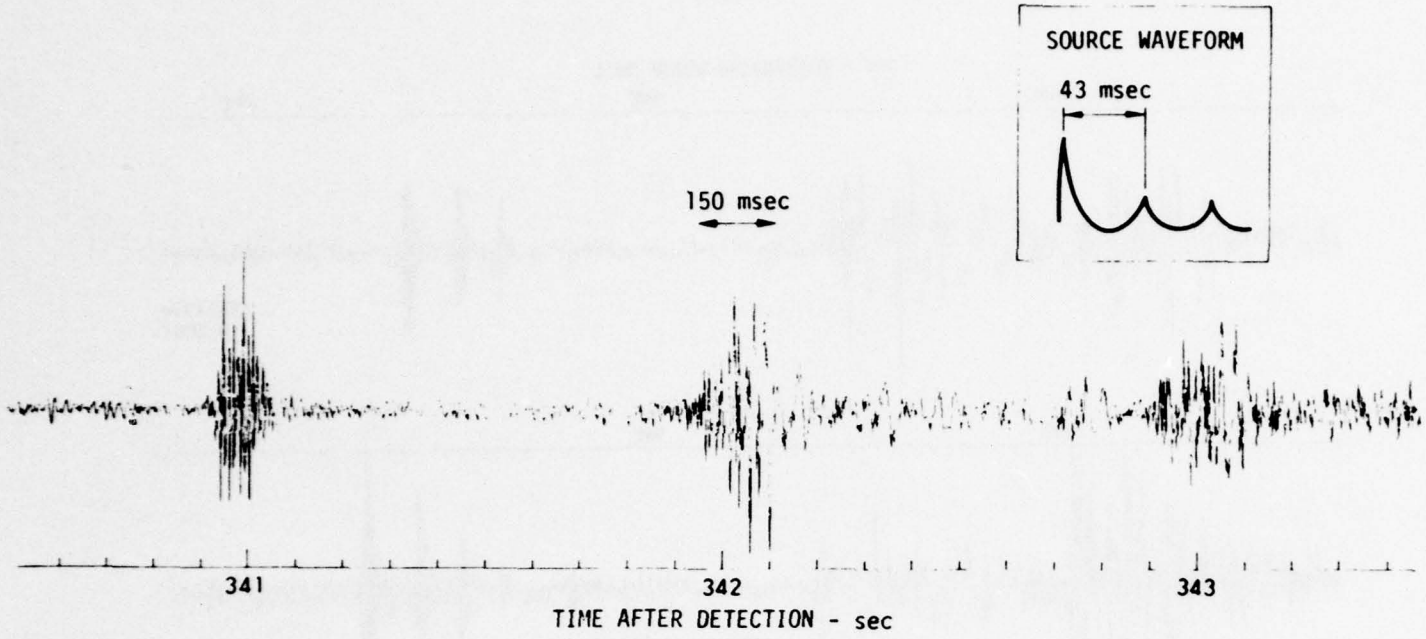

FIGURE 3-7
WAVEFORM FROM 91 m DEEP EXPLOSIVE SOURCE

4053 m receiver in NE Pacific; source to receiver range is approximately 510 km. The spreading of the arrivals attributable to the source waveform and raypath timing differences is 150 msec at most

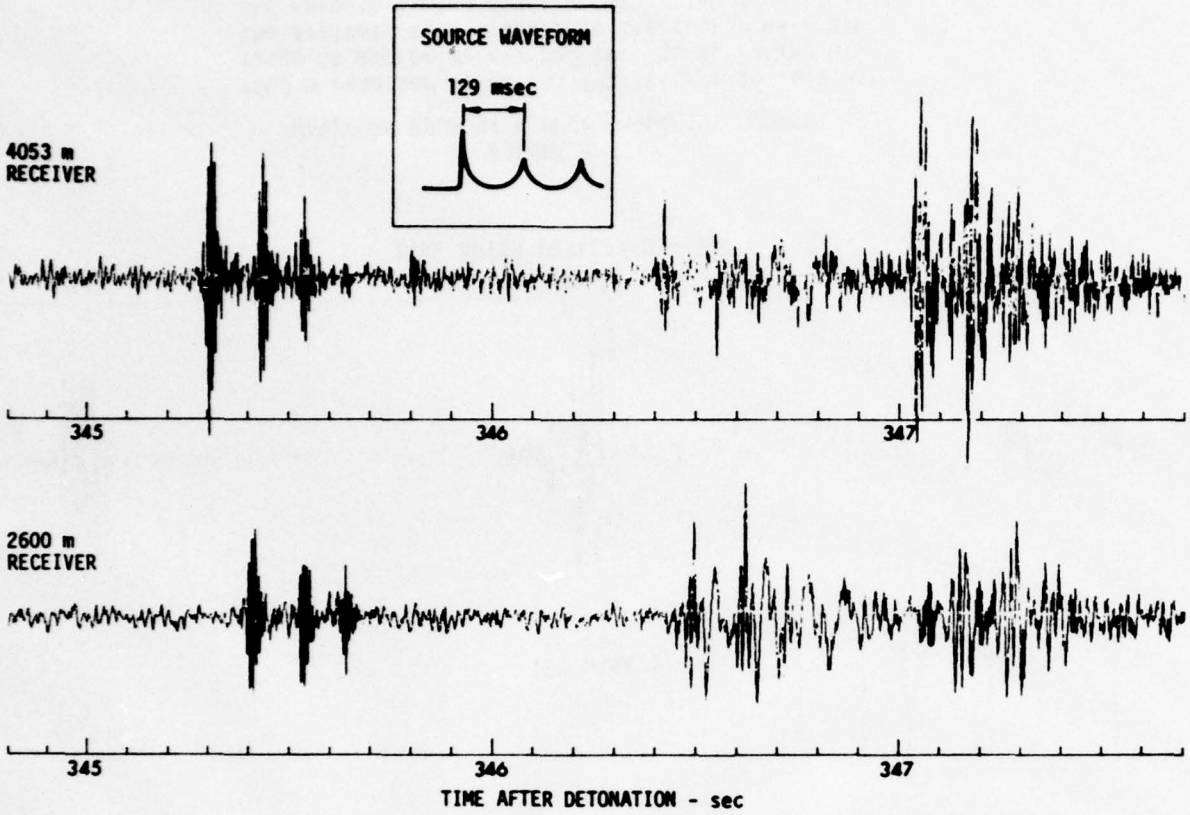

FIGURE 3-8
WAVEFORM FROM 18 m DEEP EXPLOSIVE SOURCE

2600 m and 4053 m receivers in NE Pacific
Source to receiver range is approximately 510 km

and the travel times along the different paths will differ slightly. This spread of ray path travel time for the arrivals of Fig. 3-7 is shown. Second, ray theory is valid only at high enough frequencies; at low frequencies, even signal travel time is frequency dependent. The observed spread in the arrivals of Figs. 3-7 and 3-8 is greater than can be accounted for by the bubble pulse spacing and ray path differences.

Porter [1973] observed that, in signals received in the Mediterranean, individual arrivals were spread approximately 100 to 150 msec while the source bubble pulse characteristic and multiple ray arrivals together could account for only one-half of this spreading. At the ranges involved, 200 to 400 km, a 50 msec difference in travel time corresponded to approximately 0.5 m/sec spread in signal speed. Only the arrivals which reflected from neither the surface nor the bottom were analyzed. In this region, there is a large gradient in $c(z)$ above the depth z_o. Porter presented an analysis, based upon a bilinear model for $c^{-2}(z)$, to explain the observed spreading. His conclusion was that the spreading was caused by the closeness of the ray turning point depths to the SVP minimum z_o, and did not consider any effect of the surface above the upper TP's.

In his numerical investigations, K. M. Guthrie [1974a] also computed, for several SVP's, group velocity versus ray angle $\left(\text{Arc cos}\left|c(z_o)/c_n(\omega)\right|\right)$ at different frequencies. He found that, for some profiles, there could be 1 or 2 m/sec difference between the signal speeds at different frequencies along rays which almost grazed the surface. The magnitude of the effect depended upon the actual SVP but, again, the lowest frequencies (less than 100 Hz) traveled most slowly.

IV. LANGER'S SOLUTION AND EXTENSIONS

In a series of papers published during the 1930's, Rudolph Langer [1931], [1935], [1937] presented an asymptotic solution to what in this paper is called the depth equation, Eq. 2E-1. Langer's solution is formally analogous to the WKB solution, but is expressed in terms of the Airy functions Ai(·) and Bi (·), which are solutions to Stokes' equation. The Langer solution is an asymptotic one, approaching the exact solution as the parameter $k_n \to \infty$. However, if the profile function $q_n(z)$ has a linear or bilinear form, the Langer solution is exact to the extent that the eigenvalues k_n may be determined (just as the WKB solution is exact if $q_n(z)$ is a constant between the boundaries). The asymptotic solutions of differential equations have been discussed by Cherry [1954], Erdelyi [1953], and Olver [1954a] and applied, for example, by Olver [1954b] to analyze Bessel functions. Asymptotic solutions analogous to the WKB and Langer solutions are discussed by Dingle [1956]. Surprisingly, the Langer solution does not seem to have been applied to ocean acoustics, though it is occasionally mentioned in the literature (e.g., Weinberg [1975]).

There are two features which make the Langer solution especially attractive for application to ocean acoustics problems. First, in the deep ocean, at depths below, say, 1500 m, the SVP is

dominated by the effects of increasing hydrostatic pressure (see section II-1), so that the profile function $q_n(z)$ very nearly has a linear form in that region. Therefore, a solution in terms of the Airy functions is a natural one for the lower part of the SVP. Second, and more importantly, the Langer solution (in contrast to the WKB solution) provides a uniform representation at, and on both sides of, the turning points of each mode. This is more than merely a convenient feature, because it allows one to determine solutions which satisfy the boundary conditions even when the boundaries are near to the turning points. As discussed in Chapter III, there is experimental evidence that the modes which have phase velocities nearly equal to the sound velocity at a boundary are the modes which have group velocities and mode cycle distances noticeably different (at low frequencies) from the ray theory predictions. An additional feature, which is shown in this work, is that by extending the Langer solution to take into account the boundary conditions, the turning point depths, and details of the SVP, one obtains an eigenvalue equation of the same form as Eq. 2H-16,

$$\int_{z_U}^{z_L} q_n^{1/2}\, dz = (n+1/2)\pi + \epsilon_n(\omega) \quad .$$

From this eigenvalue equation, expressions for the normal mode quantities of group velocity and mode cycle distance may be derived.

In section IV-A, the Langer solution, Eq. 4A-17, is derived by substituting Eq. 4A-3 into the depth equation and analyzing the

resulting differential equations. The solution is derived by, for example, Olver [1954a], by transforming the independent variable of the depth equation. In section IV-D, an assumption which is made to obtain the Langer solution is analyzed.

In section IV-B, the solution is extended by providing eigenvalue equations from which the k_n may be determined. This is done in a way intended to result in an equation of the form of Eq. 2H-1t Eq. 2H-15 (above). The boundary conditions and the details of the SVP are taken into account via functions whose arguments are the integrals of the square root of the profile function $q_n(z)$ from a TP to either a boundary or to the depth of minimum sound velocity, z_o.

In section IV-C, the normal mode quantities of group velocity, $\hat{v}_n$, and mode cycle distance, $\hat{\Lambda}_n$, are derived. It is shown that these may be expressed as

$$\hat{\Lambda}_n = 2\,\hat{D}_n$$

and

$$\hat{v}_n = \hat{D}_n/\hat{T}_n \quad .$$

The term $\hat{D}_n$ is shown to equal the ray theory cycle distance $\tilde{D}$ (along a ray whose turning point velocity is ω/k_n) plus an additional distance, $\Delta_n(\omega)$. The distance $\Delta_n(\omega)$ arises from the fact that the turning points are within a finite distance of the boundaries and the velocity minimum, z_o. Similarly, the term τ_n is shown to equal the ray theory cycle time $\tilde{T}$ plus a time $\tau_n(\omega)$. Both $\Delta_n(\omega)$ and $\tau_n(\omega)$ vanish at high frequencies and when the TP's are far from the boundaries and the velocity minimum.

IV-A DEVELOPMENT OF THE SOLUTION

The initial task is to obtain a solution to the depth equation,

$$\frac{d^2u}{dz^2} + q(z)\, u = 0 \quad . \tag{4A-1}$$

In Eq. 4A-1, the subscripts denoting mode order have been dropped for convenience. In analogy with Eq. 2E-7, where u(z) is expressed in terms of amplitude and phase factors, let the solution to Eq. 4A-1 be expressed in terms of an amplitude factor W(z) and combination of Airy functions, $\mathcal{A}(\cdot)$, of argument $\gamma(z)$.

$$u(z) = W(z)\, \mathcal{A}(\gamma(z)) \quad . \tag{4A-2}$$

The functions W(z) and $\gamma(z)$ are to be chosen so that Eq. 4A-2 is a solution of Eq. 4A-1. The function $\mathcal{A}(\gamma)$ is defined by

$$\mathcal{A}(\gamma) \equiv \alpha \mathrm{Ai}(-\gamma) + \beta \mathrm{Bi}(-\gamma) \quad ; \tag{4A-3}$$

the constants α and β are arbitrary until boundary conditions are specified. Properties of the Airy functions Ai(x) and Bi(x) which are relevant to this paper are discussed in the Appendix; these functions are discussed in more detail by Antosiewicz [1970], Erdelyi [1956], and Miller [1946]. The sign of γ in Eq. 4A-3 is chosen so that the function $\mathcal{A}(\gamma)$ is an oscillating function for positive γ.

The second derivative of Eq. 4A-2 is

$$\frac{d^2u}{dz^2} = \frac{d^2W}{dz^2}\mathcal{A}(\gamma) + \left(2\frac{dW}{dz}\frac{d\gamma}{dz} + W\frac{d^2\gamma}{dz^2}\right)\dot{\mathcal{A}}(\gamma) - W\gamma\left(\frac{d\gamma}{dz}\right)^2\mathcal{A}(\gamma) \quad . \tag{4A-4}$$

Here, dots denote the derivative of a function with respect to its argument. In Eq. 4A-4, the differential equation (Eq. A-1) which is satisfied by the Airy functions has been used to eliminate the term in $\ddot{a}(\gamma)$. When Eqs. 4A-2 and 4A-4 are substituted into Eq. 4A-1 and the factors of $a(\gamma)$ and $\dot{a}(\gamma)$ are collected, we obtain

$$a(\gamma)\left[-W\gamma\left(\frac{d\gamma}{dz}\right)^2 + q(z)\,W + \frac{d^2W}{dz^2}\right] + \dot{a}(\gamma)\left[2\frac{dW}{dz}\frac{d\gamma}{dz} + W\frac{d^2\gamma}{dz^2}\right] = 0 \quad (4A\text{-}5)$$

This equation will be satisfied if the factors of $a(\gamma)$ and $\dot{a}(\gamma)$ can be individually equated to zero and the resulting equations solved. Within the errors introduced by the approximation of Eq. 4A-11, this may be done.

First, setting the factor of $\dot{a}(\gamma)$ to zero gives

$$2\frac{dW}{dz}\frac{d\gamma}{dz} + W\frac{d^2\gamma}{dz^2} = 0 \quad , \qquad (4A\text{-}6)$$

which may be rewritten as

$$2\frac{d}{dz}\ell n(W) = -\frac{d}{dz}\ell n\left(\frac{d\gamma}{dz}\right) \quad . \qquad (4A\text{-}7)$$

Both sides of Eq. 4A-7 are total derivatives; if both sides are integrated and exponentiated, we get

$$W = \text{constant} \times \left|\frac{d\gamma}{dz}\right|^{-1/2} \quad . \qquad (4A\text{-}8)$$

This is an exact formula for W(z) if an exact expression for $\gamma(z)$ is available.

Next, setting the factor of $\alpha(\gamma)$ to zero gives

$$\gamma \left(\frac{d\gamma}{dz}\right)^2 = \left(q(z) + \frac{1}{W}\frac{d^2W}{dz^2}\right) \quad . \tag{4A-9}$$

If the factor W"/W on the RHS of Eq. 4A-9 were zero, the equation could be integrated to give an expression for $\gamma(z)$. Therefore, it seems profitable to consider the function $\hat{\gamma}$ defined by

$$\hat{\gamma}\left(\frac{d\hat{\gamma}}{dz}\right)^2 = q(z) \tag{4A-10}$$

and to regard $\hat{\gamma}$ as an approximation for γ,

$$\hat{\gamma} \approx \gamma \quad . \tag{4A-11}$$

The conditions upon the profile functions for which the approximation is good are discussed in Section IV-D. Note, though, that the approximation is a good one near enough to a TP, since it follows from Eq. 4A-9 that $d^2W/dz^2=0$ at a TP where $q(z)$ and $\gamma(z)$ are both zero.

Equation 4A-10 may be rewritten as

$$\left[\frac{d}{dz}\left(\frac{2}{3}\hat{\gamma}^{3/2}\right)\right]^2 = q(z) \quad , \tag{4A-12}$$

from which the solution for $\hat{\gamma}(z)$ follows.

$$\hat{\gamma}(z) = \left(\frac{3}{2}\int^z q^{1/2}(z')\,dz'\right)^{2/3} \quad . \tag{4A-13}$$

In order that the solutions $u(z)$ oscillate where $q(z)$ is positive and be damped elsewhere, it is necessary that $\hat{\gamma}(z)$ be zero at at TP and have the same sign as $q(z)$. Accordingly, in the 2TP case, we may define an argument $\hat{\gamma}(z)$ about each turning point

$$\hat{\gamma}^U(z) = \left(\frac{3}{2}\int_{z_U}^{z} q^{1/2}(z')\,dz'\right)^{2/3}$$

$$\hat{\gamma}^L(z) = \left(\frac{3}{2}\int_{z}^{z_L} q^{1/2}(z')\,dz'\right)^{2/3} \quad . \tag{4A-14}$$

Also, the amplitude modulation, W(z), will be approximated as

$$\hat{W} = \text{constant} \times \left|\frac{d\hat{\gamma}}{dz}\right|^{-1/2} \quad . \tag{4A-15}$$

It follows from Eq. 4A-13 that $\hat{W}$ may be written as:

$$\hat{W}(z) = \text{constant} \times \left|\frac{q(z)}{\hat{\gamma}(z)}\right|^{-1/4} \quad . \tag{4A-16}$$

If the square root of q(z) is defined as

$$\begin{aligned} q^{1/2} &= |q|^{1/2}\, e^{i\pi/2} && 0 \leq z \leq z_U \\ q^{1/2} &= q^{1/2} && z_U \leq z \leq z_L \\ q^{1/2} &= |q|^{1/2}\, e^{i\pi/2} && z_L \leq z \leq z_b \quad , \end{aligned} \tag{4A-17}$$

then the signs of $\hat{\gamma}^U$ and $\hat{\gamma}^L$ will be

$$\begin{aligned} &\hat{\gamma}^U(z) < 0 && 0 < z < z_U \\ &\hat{\gamma}^U(z) > 0 \quad \text{and} \quad \hat{\gamma}^L(z) > 0 && z_U < z < z_L \\ &\hat{\gamma}^L(z) < 0 && z_L < z < z_b \quad . \end{aligned} \tag{4A-18}$$

The approximate solution $\hat{u}(z)$ is then defined on two overlapping intervals as

$$\begin{aligned} &(a) \quad \hat{u}^U(z) = \hat{W}(z)\, \mathcal{A}(\hat{\gamma}^U(z)) \qquad 0 \le z \le z_L \\ &(b) \quad \hat{u}^L(z) = \hat{W}(z)\, \mathcal{A}(\hat{\gamma}^L(z)) \qquad z_U \le z \le z_b \end{aligned} \quad . \tag{4A-19}$$

In application, the solution developed about the upper TP, Eq. 4A-19(a), will be used from zero depth down to the depth of velocity minimum, z_o, and the solution developed about the lower TP will be used below the velocity minimum. In Section 4B, the eigenvalue equations are obtained by matching Eq. 4A-19(a) and Eq. 4A-19(b) at z_o.

Finally, the combination of Airy functions used in Eq. 4A-19 needs to be made specific. To do this, rewrite Eq. 4A-19 as

$$\begin{aligned} &(a) \quad \hat{u}_n{}^U(z) = N_n{}^U \left| \frac{d\hat{\gamma}_n{}^U}{dz} \right|^{-1/2} \left[Ai\left(-\hat{\gamma}_n{}^U\right) + \beta^U Bi\left(-\hat{\gamma}_n{}^U\right) \right] \\ &(b) \quad \hat{u}_n{}^L(z) = N_n{}^L \left| \frac{d\hat{\gamma}_n{}^L}{dz} \right|^{-1/2} \left[Ai\left(-\hat{\gamma}_n{}^L\right) + \beta^L Bi\left(-\hat{\gamma}_n{}^L\right) \right] \end{aligned} \quad , \tag{4A-20}$$

where the terms $N_n{}^U$ and $N_n{}^L$ are chosen to ensure that the normal mode functions are normalized.

In general, the boundary quantities depend upon the SVP, the TP depths, and frequency. The boundary condition at the surface is that the pressure vanish there; this is accomplished by specifying β^U by

$$\beta^U = -Ai\left(-\hat{\gamma}_n{}^U(0)\right) \Big/ Bi\left(-\hat{\gamma}_n{}^U(0)\right) \quad . \tag{4A-21}$$

In this work, we do not consider the effects of the ocean bottom. However, if the bottom is described by an impedance condition (Bucker [1970]),

$$\frac{d}{dz} u_n(z) = \kappa\, u_n(z) \quad , \tag{4A-22}$$

where κ depends upon the properties of the bottom, then from Eq. 2A-20 it follows that β^L is given by

$$\beta^L = - \frac{\kappa\, \mathrm{Ai}\left(-\hat{\gamma}^L(z_b)\right) - \dot{\hat{\gamma}}^L(z_b)\, \dot{\mathrm{Ai}}\left(-\hat{\gamma}^L(z_b)\right)}{\kappa\, \mathrm{Bi}\left(-\hat{\gamma}^L(z_b)\right) - \dot{\hat{\gamma}}^L(z_b)\, \dot{\mathrm{Bi}}\left(-\hat{\gamma}^L(z_b)\right)} \quad . \tag{4A-23}$$

To apply the Langer solution, it is necessary to compute the integrals of Eq. 4A-13, with $q^{1/2}$ determined by the problem at hand. The same computations must be made to apply the WKB solution, and similar integrals arise in ray theory. Therefore, to apply the Langer solution, only the capability to compute the functions $\mathrm{Ai}(\cdot)$ and $\mathrm{Bi}(\cdot)$ is needed beyond what is needed to apply the WKB solution.

IV-B EIGENVALUE EQUATION

To complete the analysis, we must require that the solutions developed about different turning points, Eq. 2A-19, match properly at some depth. Above that depth, $\hat{u}_n^U$ will be used to approximate $u_n(z)$, while below that depth $\hat{u}_n^L$ is used. In the next section it will be shown that the approximation errors are greatest at the depths where the change in the slope of $c(z)$ is greatest. Thus, it is proper to match the two solutions at the depth of minimum velocity, z_o, where the greatest change in dc/dz normally occurs, and not continue the solution across depth z_o. To match the solutions, since it is assumed that the density in the medium is a continuous function of depth, it is required that the pressure and the normal derivative of the pressure be continuous. Thus,

$$u_n(z) \approx \hat{u}_n^U(z) \qquad z \leq z_o$$

$$u_n(z) \approx \hat{u}_n^L(z) \qquad z \geq z_o \tag{4B-1}$$

$$\hat{u}_n^U(z_o) = \hat{u}_n^L(z_o) \qquad \text{(a)}$$

$$d\hat{u}_n^U/dz = d\hat{u}_n^L/dz \qquad \text{at } z_o \qquad \text{(b)} \quad .$$

We will find it convenient to replace the second of Eq. 4B-1 by the condition:

$$\frac{d\,\hat{u}_n^U/dz}{\hat{u}_n^U} = \frac{d\,\hat{u}_n^L/dz}{\hat{u}_n^L} \quad . \tag{4B-2}$$

If only the asymptotic form of the phase of the Airy functions (Eq. A-11) were taken into account to match the solutions, then the Bohr-Sommerfeld equation would be obtained. In this section, the exact form of the Airy functions is used. However, in this work, the phase of these functions is expressed in terms of their asymptotic form plus the function $\delta(\cdot)$, defined below. Thus, we obtain an eigenvalue equation which is a generalized form of the Bohr-Sommerfeld eigenvalue equation. In the next section, this generalized eigenvalue equation will be used to compute group velocity and mode interference wavelength equations.

The solutions $\hat{u}_n^U$ and $\hat{u}_n^L$ are defined in Eqs. 4A-20; however, it is convenient for the present task to rewrite the solutions in terms of amplitude and phase factors,

$$\hat{u}_n^U = \hat{W}(z)\, M(\hat{\gamma}_n^U)\, \cos\left(\theta(\hat{\gamma}_n^U) + \sigma^U\right) N_n^U / \cos(\sigma^U)$$
$$\hat{u}_n^L = \hat{W}(z)\, M(\hat{\gamma}_n^L)\, \cos\left(\theta(\hat{\gamma}_n^L) + \sigma^L\right) N_n^L / \cos(\sigma^L) \quad . \tag{4B-3}$$

No approximation is involved in going from Eq. 4A-20 to Eq. 4B-3; the amplitude and phase functions are defined by

$$M(\gamma) = \left(Ai^2(-\gamma) + Bi^2(-\gamma)\right)^{1/2}$$
$$\theta(\gamma) = \arctan\left(Bi(-\gamma)/Ai(-\gamma)\right) \quad , \tag{4B-4}$$

Properties of these amplitude and phase factors are discussed in the appendix. The phase shifts, σ^U and σ^L, which depend upon boundary conditions, are

$$\sigma^U = \arctan(\beta^U)$$

$$\sigma^L = \arctan(\beta^L) \quad . \tag{4B-5}$$

Note that the function $\theta(\gamma)$ is not limited to the principal value interval $(-\pi/2,\pi/2)$. Also, at this point, it is assumed that the TP's are below the surface and above the bottom so that the arguments of the Airy functions at the boundaries are positive ($\gamma_n^U(0)$ negative, for example) so that σ^U and σ^L are small. If the mode reflects from the boundary, the phase there may be large and the analysis needs to be modified as is done at Eqs. 4B-19 through 4B-24, below.

Next, Eq. 4B-6

$$\delta(\gamma) \equiv \pi/4 - 2/3\ \gamma^{3/2} - \theta(\gamma)$$

$$\delta(\gamma) \underset{\gamma\to\infty}{\longrightarrow} 0 \tag{4B-6}$$

defines the function $\delta(\cdot)$ as the difference between the exact expressions for $\theta(\gamma)$, Eq. 4B-4, and the asymptotic form, Eq. A-11. A plot of this function is given in Fig. 4B-1.

In computing the derivatives of Eqs. 4B-2, it will be assumed that the functions determining the magnitudes, that is, $\hat{W}(z)$ and $M(\hat{\gamma}_n)$, are slowly varying with respect to the variations of the cosine terms, as expressed by

$$\left|\frac{d\hat{W}}{dz}\right| \ll \hat{W} \left|\frac{d}{dz}\,\theta(\gamma)\right| \tag{4B-7}$$

and

$$\left|\frac{dM}{dz}\right| \ll \left|M\,\frac{d}{dz}\,\theta(\gamma)\right| \quad . \tag{4B-8}$$

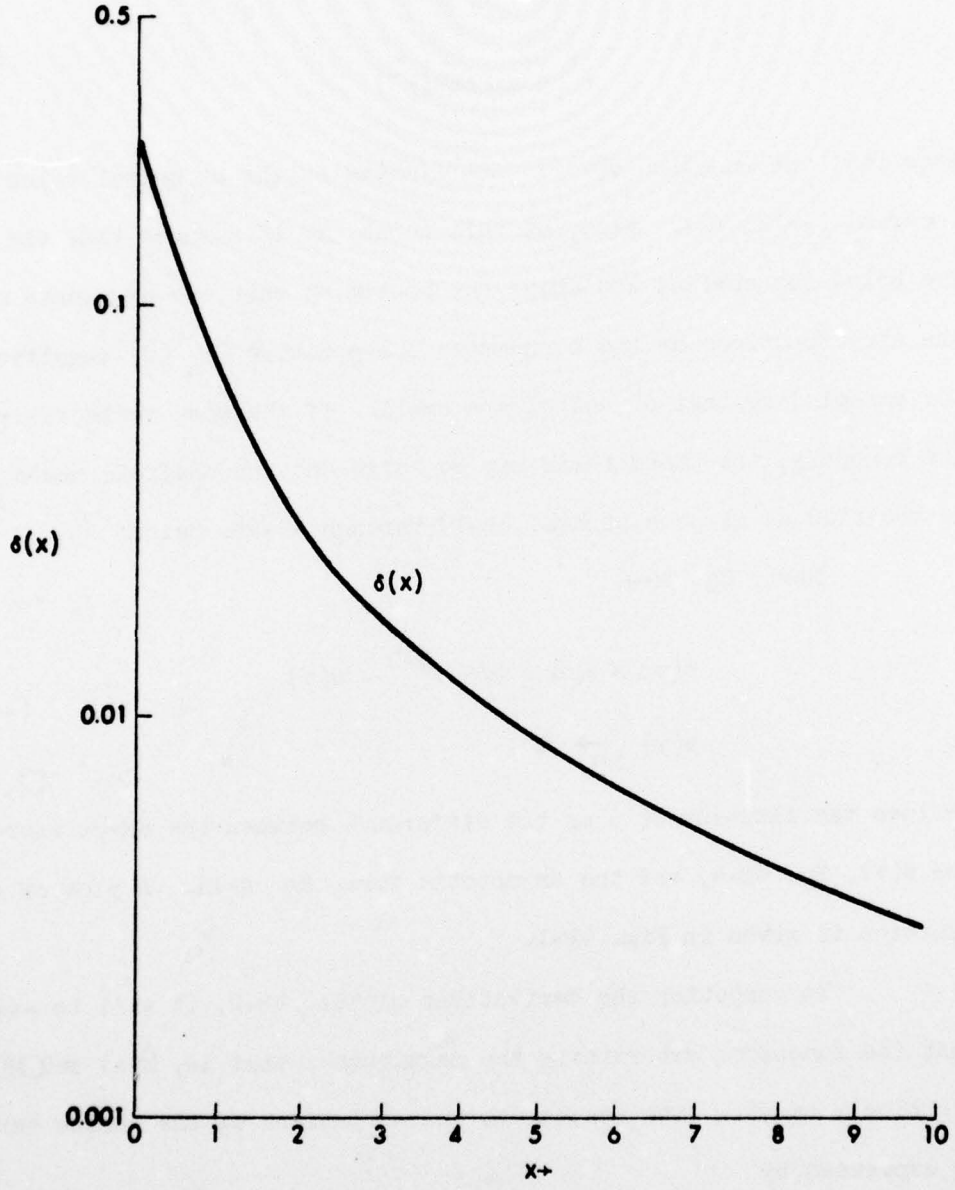

FIGURE 4B-1
THE FUNCTION $\delta(x)$

$$\delta(x) = \frac{\pi}{4} - \frac{2x^{3/2}}{3} - \text{Arctan}\,\frac{Ai(-x)}{Bi(-x)}$$

$$\delta(0) = \frac{\pi}{12}$$

These approximations are discussed more thoroughly in Section 4D. However, note that Eqs. 4B-7 and 4C-8 may be rewritten as

$$\left|\frac{d}{dz}\, \ell n\hat{W}\right| \ll \left|\frac{d}{dz}\, \theta(\gamma)\right| \tag{4B-9}$$

and

$$\left|\frac{d}{dz}\, \ell nM\right| \ll \left|\frac{d}{dz}\, \theta(\gamma)\right| \quad , \tag{4B-10}$$

both of which may be reasonably expected to be satisfied in typical ocean acoustics problems.

If one assumes that Eqs. 4B-7 and 4B-8 hold, the derivatives of the normal mode functions of Eqs. 4B-3 are

$$\begin{aligned}
\frac{d}{dz}\, \hat{u}_n^{\,U} &= -\hat{W}(z)M(\hat{\gamma}_n^{\,U})\, \frac{N_n^{\,U}}{\cos(\sigma^U)}\, \sin\left(\theta(\hat{\gamma}_n^{\,U}) + \sigma^U\right) \frac{d}{dz}\, \theta(\hat{\gamma}_n^{\,U}) \\
\frac{d}{dz}\, \hat{u}_n^{\,L} &= -\hat{W}(z)M(\hat{\gamma}_n^{\,L})\, \frac{N_n^{\,L}}{\cos(\sigma^L)}\, \sin\left(\theta(\hat{\gamma}_n^{\,L}) + \sigma^L\right) \frac{d}{dz}\, \theta(\hat{\gamma}_n^{\,U}) \quad .
\end{aligned} \tag{4B-11}$$

Then, substitute Eq. 4B-3 and Eq. 4B-11 into Eq. 4B-2 to obtain

$$\tan\left(\theta(\hat{\gamma}_n^{\,U}) + \sigma^U\right) \frac{d}{dz}\, \theta(\gamma_n^{\,U}) = \tan\left(\theta(\hat{\gamma}_n^{\,L}) + \sigma^L\right) \frac{d}{dz}\, \theta(\gamma_n^{\,L}) \tag{4B-12}$$

$$\text{at } z = z_o \quad .$$

Now, the derivative of the phase function θ for the solution from the upper TP is given by, from Eq. A-12 and Eq. 4A-8,

$$\frac{d}{dz}\, \theta(\hat{\gamma}_n^{\,U}) = -\frac{1}{\pi M^2(\hat{\gamma}_n^{\,U})}\, \frac{d\hat{\gamma}_n^{\,U}}{dz} = -\frac{1}{\pi M^2(\hat{\gamma}_n^{\,U})\, \hat{W}^2(z)} \quad , \tag{4B-13}$$

and similarly for the derivative of the phase of the solution from the lower TP. Since the magnitudes of the solutions must match at $z=z_o$, as expressed by Eq. 4B-1a, the derivatives of the phase functions θ are opposites,

$$\frac{d}{dz}\,\theta(\hat{\gamma}_n^{U}) = -\frac{d}{dz}\,\theta(\hat{\gamma}_n^{L}) \quad \text{at } z = z_o \quad . \tag{4B-14}$$

Thus, the two solutions are properly matched if

$$\tan\left(\theta(\hat{\gamma}_n^{U}) + \sigma^{U}\right) = -\tan\left(\theta(\hat{\gamma}_n^{L}) + \sigma^{L}\right) \quad . \tag{4B-15}$$

Equation 4B-15 is satisfied if

$$\theta(\hat{\gamma}_n^{U}) + \sigma^{U} = -\theta(\hat{\gamma}_n^{L}) - \sigma^{L} - n\pi \tag{4B-16}$$

$$n = 0, 1, 2, \ldots \quad .$$

Now, use the definition of $\hat{\gamma}$, Eq. 4A-13, and substitute Eq. 4B-6 into Eq. 4B-16 to obtain

$$\begin{aligned} &\frac{\pi}{4} - \int_{z_U}^{z_o} q_n^{1/2} dz - \delta\left(\hat{\gamma}_n^{U}(z_o)\right) + \sigma^{U} = \\ &\qquad -\frac{\pi}{4} + \int_{z_o}^{z_L} q_n^{1/2}\, dz + \delta\left(\hat{\gamma}_n^{L}(z_o)\right) - \sigma^{L} - n\pi \quad . \end{aligned} \tag{4B-17}$$

Finally, combine the two integrals and rearrange terms in Eq. 4B-17 to obtain the eigenvalue equation,

$$\begin{aligned} \int_{z_U}^{z_L} q_n^{1/2}\, dz = &\left(n + \frac{1}{2}\right)\pi - \delta\left(\hat{\gamma}_n^{U}(z_o)\right) + \sigma^{U} \\ &- \delta\left(\hat{\gamma}_n^{L}(z_o)\right) + \sigma^{L} \quad . \end{aligned} \tag{4B-18}$$

If the mode reflects from the surface ($k_n < \omega/c(0)$), the eigenvalue analysis must be modified slightly. As discussed in the next section, it is no longer possible to have $\hat{\gamma}_n^U(z)=0$ at $z=0$ when reflection occurs, so we must have

$$\hat{\gamma}_n^U(z) = \left(\frac{3}{2} g_o + \frac{3}{2} \int_o^z q_n^{1/2}\, dz\right)^{2/3} \qquad (4B\text{-}19)$$

$(g_o > 0)$.

The term g_o accounts for the effects introduced by the fact that the profile function q_n is not zero at the lower limit of the integral of Eq. 4B-19. In the discussion up to now, with the upper TP beneath the surface, the angle σ^U has been small (less than $\pi/6$) and it has been sufficient to define σ^U in terms of an inverse tangent, Eq. 4C-5. When reflection occurs, the function β^U as a function of, say, frequency, oscillates and we must take into account the proper branch of β^U. This is done by using the function $\theta(\gamma)$, defined by Eq. 4B-4, so that Eq. 4A-19 may be rewritten as

$$\beta^U = -\tan\left(\theta(\hat{\gamma}_n^U(0))\right) \quad , \qquad (4B\text{-}20)$$

so that

$$\sigma^U = -\theta\left(\gamma_n^U(0)\right) \quad . \qquad (4B\text{-}21)$$

Finally, express σ^U in terms of the function $\delta(\cdot)$ as

$$\sigma^U = -\pi/4 + g_o + \delta\left(\hat{\gamma}_n^U(0)\right) \quad . \qquad (4B\text{-}22)$$

Then, substitute Eqs. 4B-19 and 4B-22 into Eq. 4B-17, to get

$$\int_o^{z_L} q_n^{1/2}\, dz = (n+1/4)\pi - \delta\left(\hat{\gamma}_n^{U}(z_o)\right) + \delta\left(\hat{\gamma}_n^{U}(o)\right) - \delta\left(\hat{\gamma}_n^{L}(z_o)\right) + \sigma_L \quad . \tag{4B-23}$$

If we consider only the $(n+1/4)\pi$ term to be on the RHS of this equation, it is the same as the Bohr-Sommerfeld equation for the case of a mode reflecting from the surface (Schiff [1955], Tolstoy and Clay [1965]).

Equations 4B-18 and 4B-23 both have the form

$$\int_{z_U}^{z_L} \left(\omega^2/c^2(z) - k_n^2\right)^{1/2} dz = (n+1/2)\pi + \epsilon_n(\omega) \tag{4B-24}$$

which is the same as Eq. 2H-15, which was discussed previously. The function ϵ_n is

$$\epsilon_n(\omega) = \sigma^U - \delta\left(\hat{\gamma}_n^{U}(z_o)\right) + \sigma^L - \delta\left(\hat{\gamma}_n^{L}(z_o)\right) \quad , \tag{4B-25(a)}$$

if $z^U > 0$, and

$$\epsilon_n = \delta\left(\hat{\gamma}_n^{U}(0)\right) - \delta\left(\hat{\gamma}_n^{U}(z_o)\right) + \sigma_L - \delta\left(\hat{\gamma}_n^{L}(z_o)\right) - \frac{\pi}{4} \quad , \tag{4B-25(b)}$$

if the mode reflects from the surface.

Thus, the eigenvalue equation which is obtained by extending the Langer solution to account for the effects of boundaries and of the actual SVP contains important terms in addition to those of the Bohr-Sommerfeld equation. In Section IV-C, the mode quantities of

group velocity and mode interference wavelength will be computed. Note from Eq. 4B-25 that the relative effects of the boundaries and details of the SVP upon the mode quantities may be evaluated individually.

IV-C NORMAL MODE QUANTITIES

The normal mode quantities of interest are the group velocity and mode interference wavelength. To obtain these quantities in the Langer approximation, one begins by taking derivatives of the eigenvalue equation, Eq. 4B-18 or Eq. 4B-23. At first, the derivatives of the factors $\epsilon_n(\omega)$ in Eq. 4B-24 which account for boundary conditions and details of the SVP in Eq. 4B-18 would seem to yield complicated expressions. However, the simple form of the derivative of inverse tangent function, together with the Wronskian of the Airy functions, give expressions for the mode quantities which are amenable to physical interpretation.

To obtain the group velocity, begin with Eq. 4B-24 and take the derivatives of both sides with respect to frequency, holding the mode order constant, to obtain

$$d\epsilon_n/d\omega = \int_{z_U}^{z_L} \left(\frac{\omega}{c^2} - k_n \frac{dk_n}{d\omega}\right)\left(\frac{\omega^2}{c^2} - k_n^2\right)^{-1/2} dz \quad . \quad (4C\text{-}1)$$

Since the integrand vanishes at the end points, there is no contribution from variation of the end points z_U and z_L. From Eq. 4C-1, the group velocity, $\hat{v}_n$,

$$\hat{v}_n = \frac{k_n \int_{z_U}^{z_L} \left(\omega^2/c^2 - k_n^2\right)^{-1/2} dz}{\omega \int_{z_U}^{z_L} c^{-2}\left(\omega^2/c^2 - k_n^2\right)^{-1/2} dz - d\epsilon_n/d\omega} \quad (4C\text{-}2)$$

is obtained.

Similarly, to obtain the mode interference wavelength, take the derivative of Eq. 4B-20 with respect to mode order, holding the frequency constant, to obtain

$$\pi + d\epsilon_n/dn = - \int_{z_U}^{z_L} k_n \frac{dk_n}{dn} \left(\frac{\omega^2}{c^2} - k_n^2 \right)^{-1/2} dz \quad . \qquad (4C\text{-}3)$$

The mode interference wavelength, $\hat{\Lambda}_n$, is then given by

$$\hat{\Lambda}_n(\omega) = \frac{2\pi}{dk_n/dn} = \frac{2\pi k_n \int_{z_U}^{z_L} \left(\omega^2/c^2 - k_n^2 \right)^{-1/2} dz}{\pi + d\epsilon_n/dn} \quad . \qquad (4C\text{-}4)$$

The functions $\epsilon_n(\omega)$ are defined in Eq. 4B-25a, which is repeated here in simplified fashion as

$$\epsilon_n(\omega) = - \delta^U + \sigma^U - \delta^L + \sigma^L \quad . \qquad (4C\text{-}5)$$

Now, the integrals which are in Eq. 4C-2 and Eq. 4C-4 define the ray theory cycle distance and cycle time (Eqs. 2C-13) for a ray having turning point velocity $c_t = \omega/k_n$. Thus, the mode theory group velocity and mode interference distance may be rewritten as

$$\hat{v}_n(\omega) = \frac{\tilde{D}(z_U, z_L;\ \omega/k_n)}{\tilde{T}(z_U, z_L;\ \omega/k_n) - \frac{d\epsilon_n}{d\omega}} \qquad (4C\text{-}6)$$

and

$$\hat{\Lambda}_n(\omega) = \frac{2\pi \tilde{D}(z_U, z_L;\ \omega/k_n)}{\pi + \frac{d\epsilon_n}{dn}} \quad . \qquad (4C\text{-}7)$$

Now, the quantity ϵ_n depends upon both k_n and ω, (there is no explicit dependence upon n), so that

$$\frac{d\epsilon_n}{d\omega} = \frac{\partial\epsilon_n}{\partial\omega} + \frac{\partial\epsilon_n}{\partial k_n}\frac{dk_n}{d\omega}$$

$$= \frac{\partial\epsilon_n}{\partial\omega} + \frac{\partial\epsilon_n}{\partial k_n}\left(v_n(\omega)\right)^{-1}, \qquad (4C\text{-}8)$$

and

$$\frac{d\epsilon_n}{dn} = \frac{\partial\epsilon_n}{\partial k_n}\frac{dk_n}{dn}$$

$$= 2\pi\frac{\partial\epsilon_n}{\partial k_n}\left(\Lambda_n(\omega)\right)^{-1} . \qquad (4C\text{-}9)$$

Thus, by substituting Eqs. 4C-8 and 4C-9 into Eqs. 4C-6 and 4C-7, we get

$$\hat{v}_n(\omega) = \frac{\tilde{D}(z_U, z_L;\ \omega/k_n) - \partial\epsilon_n/\partial k_n}{\tilde{T}(z_U, z_L;\ \omega/k_n) + \partial\epsilon_n/\partial\omega} ,$$

and

$$\Lambda_n(\omega) = 2\tilde{D}(z_U, z_L;\ \omega/k_n) - 2\partial\epsilon_n/\partial k_n .$$

The remainder of this section will be concerned with determining the derivatives of the function ϵ_n, and relating these to physical quantities. The terms which involve the details of the SVP, δ^U and δ^L, and the boundary term σ^U will be treated individually. Also, modes reflecting from the surface must be treated separately, as discussed

AD-A045 346 TEXAS UNIV AT AUSTIN APPLIED RESEARCH LABS F/G 20/1
AN EXTENSION OF LANGER'S ASYMTOTIC SOLUTION WITH APPLICATIONS T--ETC(U)
MAR 77 S K MITCHELL N00014-75-C-0429
UNCLASSIFIED ARL-TR-77-13 NL

2 OF 2
AD
AD45346

END
DATE FILMED
11-77
DDC

in the preceding section, and reflection from the bottom will not be considered.

Effects of Finite Distance between Turning Points and Velocity Minimum

We will first consider the derivatives of δ^U and δ^L, neglecting the effect of σ^U and σ^L. The function δ^U is defined as

$$\delta^U = \arctan\left(\frac{Bi(-\gamma)}{Ai(-\gamma)}\right) + \frac{2}{3}\gamma^{3/2} - \pi/4 \quad , \tag{4C-10}$$

where

$$\gamma = \hat{\gamma}_n^U(z_o) \quad .$$

Taking the derivative of δ^U with respect to ω, one obtains

$$\begin{aligned} d\,\frac{\delta^U}{d\omega} &= d\,\frac{\delta^U}{\partial\gamma}\, d\,\frac{\gamma}{d\omega} \\ &= \left\{\left(1 + \frac{Bi^2(-\gamma)}{Ai^2(-\gamma)}\right)^{-1}\left(\frac{\dot{Bi}(-\gamma)}{Ai(-\gamma)} - \frac{Bi(-\gamma)\dot{Ai}(-\gamma)}{Ai^2(-\gamma)}\right) + \gamma^{1/2}\right\}\frac{d\gamma}{d\omega} \quad , \end{aligned} \tag{4C-11}$$

which simplifies to

$$\frac{d\delta^U}{d\omega} = \left(\gamma^{1/2} - \frac{Ai(-\gamma)\dot{Bi}(-\gamma) - \dot{Ai}(-\gamma)\,Bi(-\gamma)}{Ai^2(-\gamma) + Bi^2(-\gamma)}\right)\frac{d\gamma}{d\omega} \quad . \tag{4C-12}$$

Using the Wronskian relation for the Airy functions (Eq. A13) and using the definition of Eq. 4B-3, Eq. 4C-12 becomes

$$\frac{d\delta^U}{d\omega} = \left\{\gamma^{1/2} - 1/\pi\, M^2(\gamma)\right\}\frac{d\gamma}{d\omega} \quad . \tag{4C-13}$$

Next, the argument γ is

$$\gamma \equiv \left(\frac{3}{2}\int_{z_U}^{z_o}\left(\omega^2/c^2 - k_n^2\right)^{1/2} dz\right)^{2/3} \quad , \tag{4C-14}$$

and its derivative with respect to ω is

$$\frac{d\gamma}{d\omega} = \gamma^{-1/2} \int_{z_U}^{z_o} \left(\frac{\omega^2}{c^2} - k_n^2\right)^{-1/2} \left(\frac{\omega}{c^2} - k_n \frac{dk_n}{d\omega}\right) dz \quad . \quad (4C\text{-}15)$$

Now, the integrals in Eq. 4C-15 may be expressed in terms of the ray theory travel times and travel distances $\tilde{D}$ and $\tilde{T}$ as

$$\frac{d\gamma}{d\omega} = (\gamma)^{-1/2} \left(\tilde{T}\left(z_U, z_o; \frac{k_n}{\omega}\right) - \frac{dk_n}{d\omega} \tilde{D}\left(z_U, z_o; \frac{k_n}{\omega}\right)\right) \quad . \quad (4C\text{-}16)$$

Thus, the derivative of δ^U with respect to ω becomes

$$\frac{d\delta^U}{d\omega} = G(\gamma)\left(\tilde{T}\left(z_U, z_o; \frac{k_n}{\omega}\right) - \frac{dk_n}{d\omega} \tilde{D}\left(z_U, z_o; \frac{k_n}{\omega}\right)\right) \quad , \quad (4C\text{-}17)$$

where the function $G(\gamma)$ is defined by

$$G(\gamma) \equiv \left\{1 - 1/\pi\ \gamma^{1/2}\ M^2(\gamma)\right\} \quad . \quad (4C\text{-}18)$$

A plot of this function is shown in Fig. 4C-1. The derivative of δ^L with respect to frequency is given by

$$\frac{d\delta^L}{d\omega} = G\left(\hat{\gamma}_n^{\,L}(z_o)\right)\left(\tilde{T}\left(z_o, z_L; \frac{k_n}{\omega}\right) - \frac{dk_n}{d\omega} \tilde{D}\left(z_o, z_L; \frac{k_n}{\omega}\right)\right) \quad (4C\text{-}19)$$

In a similar fashion, we may obtain the derivatives with respect to n of the functions δ^U and δ^L; for example, the derivative of δ^U is

$$\begin{aligned} \frac{d\delta^U}{dn} &= \frac{d\delta^U}{d\gamma} \frac{d\gamma}{dn} \\ &= (\gamma^{1/2} - 1/\pi M^2(\gamma))\ d\gamma/dn \quad , \end{aligned} \quad (4C\text{-}20)$$

where $\gamma = \hat{\gamma}_n^{\,U}(z_o)$.

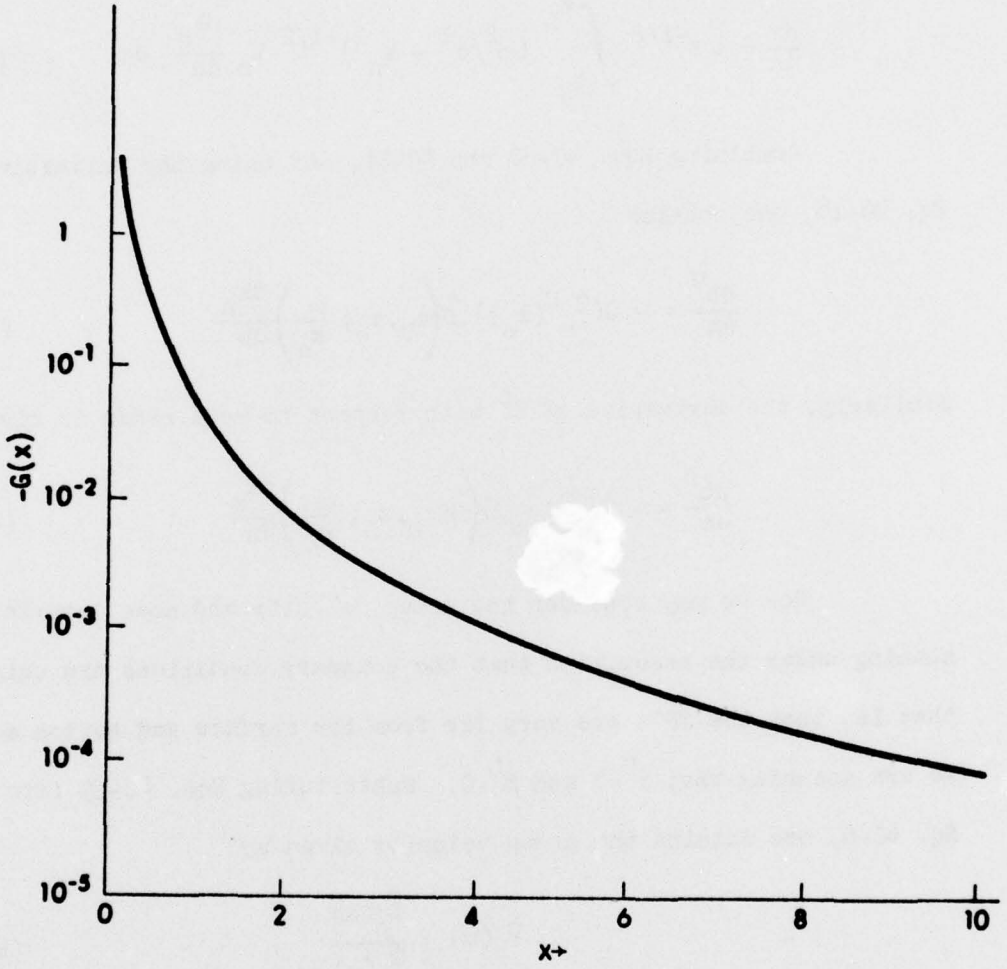

FIGURE 4C-1
THE FUNCTION G(x) (Eq. 4C-18)

$$G(x) = \left(1 - \frac{1}{\pi x^{1/2}[Ai^2(-x) + Bi^2(-x)]}\right)$$

Then, the derivative of γ with respect to mode order is given by

$$\frac{d\gamma}{dn} = -\gamma^{-1/2} \int_{z_U}^{z_L} (\omega^2/c^2 - k_n^2)^{-1/2} \, k_n \frac{dk_n}{dn} \, dz \quad . \qquad (4C\text{-}21)$$

Combining Eqs. 4C-20 and 4C-21, and using the definition of Eq. 4C-18, one obtains

$$\frac{d\delta^U}{dn} = - G(\hat{\gamma}_n^U(z_o)) \, \tilde{D}\left(z_U, z_o; \frac{\omega}{k_n}\right) \frac{dk_n}{dn} \quad . \qquad (4C\text{-}22)$$

Similarly, the derivative of δ^L with respect to mode order is given by

$$\frac{d\delta^L}{dn} = - G(\hat{\gamma}_n(z_o)) \left(\tilde{D}(z_U, z_L; \frac{\omega}{k_n}\right) \frac{dk_n}{dn} \quad . \qquad (4C\text{-}23)$$

Now we may consider the group velocity and mode interference spacing under the assumption that the boundary conditions are unimportant, that is, that the TP's are very far from the surface and bottom so that we are assuming that $\beta^U=0$ and $\beta^L=0$. Substituting Eqs. 4C-19 into Eq. 4C-6, one obtains the group velocity given by

$$\hat{v}_n(\omega) = \frac{\hat{D}_n(\omega)}{\hat{T}_n(\omega)} \quad , \qquad (4C\text{-}24)$$

where the functions $\hat{D}_n(\omega)$ and $\hat{T}_n(\omega)$ are given by

$$\hat{D}_n(\omega) = \tilde{D}\left(z_U, z_o; \frac{\omega}{k_n}\right) + G\left(\hat{\gamma}_n^U(z_o)\right) \tilde{D}\left(z_U, z_o; \frac{k_n}{\omega}\right) + G\left(\hat{\gamma}_n^L(z_U)\right) \tilde{D}\left(z_o, z_L; k_n/\omega\right) \qquad (4C\text{-}25)$$

and

$$\hat{T}_n(\omega) = \tilde{T}_n\left(z_U, z_o; \frac{\omega}{k_n}\right) + G\left(\hat{\gamma}_n^{U}(z_o)\right)\tilde{T}\left(z_U, z_o; \frac{\omega}{k_n}\right) + G\left(\hat{\gamma}_n^{L}(z_o)\right)\tilde{T}\left(z_o, z_L; \frac{\omega}{k_n}\right) \quad . \tag{4C-26}$$

Also, one may substitute Eq. 4C-23 into Eq. 4C-7 to show that $\Lambda_n(\omega) = 2\hat{D}_n(\omega)$.

Equations 4C-23 through 4C-26 are in a form which makes their interpretation straightforward. The functions $\tilde{D}$ and $\tilde{T}$ are the ray theory travel distance and travel times along a ray with TP velocity ω/k_n. The leading terms of $\hat{D}$ or $\hat{T}$ are the distance or the time in going from the upper TP to the lower TP along the ray. The added terms are the distance or time along the ray from, for example, the upper TP to the depth of velocity minimum z_o times the function $G(\hat{\gamma}_n^{U}(z_o))$.

If the SVP is symmetric about z_o, then Eq. 4C-23 predicts that the group velocity v_n depends only upon the phase velocity, k_n/ω. This is so because for a symmetric profile, $\hat{D}(z_U, z_L; c_t) = 2\hat{D}(z_U, z_o; c_t)$ and $\hat{T}(z_U, z_L; c_t) = 2\hat{T}(z_U, z_o; c_t)$. However, Eq. 4C-25 predicts that, even for a symmetric profile, the mode interference spacing Λ_n is not determined solely by the phase velocity. In general, one would expect partial cancellation of the added terms in the numerator and denominator of Eq. 4C-23. That is, the group velocity is very nearly determined by the phase velocity (in accordance with ray theory), as

was seen in Chapter III. However, one can expect a difference between the mode cycle distance of a low order mode at a low frequency and the cycle distance of a high order mode at a high frequency which have the same phase velocity, which is close to $c(z_o)$.

Boundary Effects

Analysis of the terms σ^U and σ^L of Eq. 4B-5 proceeds formally in the same fashion as that of the terms δ^U and δ^L. In this dissertation, the effects of the bottom are not investigated, and only the effect of the pressure release surface is analyzed. The case where the upper TP is beneath the surface, with the boundary interacting only with the diffracted field, is considered first. Then, the problem with reflection from the surface is addressed. It will be shown that only when the phase velocity is close to the sound velocity at the surface are the group velocity and mode cycle distance appreciably different from their ray theory counterparts.

Consider the term σ^U in Eq. 4C-5, which arises from the boundary conditions. For example, from Eq. 4A-21 and Eq. 4B-5, σ^U is given by

$$\sigma^U = -\arctan \mathrm{Ai}\left(-\hat{\gamma}_n^U(0)\right) \Big/ \mathrm{Bi}\left(-\hat{\gamma}_n^U(0)\right) \quad ; \qquad (4C\text{-}27)$$

the derivative of σ^U with respect to frequency is then

$$\frac{d\sigma^U}{d\omega} = -\frac{d\hat{\gamma}_n^U(0)}{d\omega} \Big/ \pi M^2\left(\hat{\gamma}_n^U(0)\right) \quad . \qquad (4C\text{-}28)$$

For the case considered first, with the upper TP below the surface, $\hat{\gamma}_n^{U}(0)$ is given by

$$\hat{\gamma}_n^{U}(0) = -\left(\frac{3}{2}\int_0^{z_U}\left(k_n^2 - \omega^2/c^2\right)^{1/2}\,dz\right)^{2/3} \quad . \qquad (4C\text{-}29)$$

Since the surface is in the geometrically shadowed region above z_o, the sign of k_n^2 in Eq. 4C-29 is positive. The derivative of Eq. 4C-29 with respect to ω of $\gamma_n^{U}(0)$ is given by

$$\frac{d\hat{\gamma}_n^{U}(0)}{d\omega} = -\left(-\hat{\gamma}_n^{U}(0)\right)^{-1/2}\int_0^{z_U}\left(k_n^2 - \frac{\omega^2}{c^2}\right)^{-1/2}\left(k_n\frac{dk_n}{d\omega} - \frac{\omega}{c^2}\right)dz \cdot \qquad (4C\text{-}30)$$

It is now convenient to define the functions $\tilde{D}^*$ and $\tilde{T}^*$, which have the units of distance and time, respectively, by

$$\tilde{D}^*(z_1,z_2;\,c_t) = \int_{z_1}^{z_2}\left(c^2-c_t^2\right)^{-1/2}c(z)\,dz \qquad (4C\text{-}31)$$

and

$$\tilde{T}^*(z_1,z_2;\,c_t) = \int_{z_1}^{z_2}\frac{c_t}{c(z)}\left(c^2-c_t^2\right)^{-1/2}dz \quad . \qquad (4C\text{-}32)$$

The function $\tilde{D}^*$ represents the distance between z_1 and z_2 along a ray of turning velocity c_t in a SVP $c^*(z)$ as sketched in Fig. 4C-2. The function $\tilde{T}^*$ is approximately the travel time along the same ray. In terms of these functions, Eq. 4C-30 becomes

$$\frac{d\hat{\gamma}_n^{U}(0)}{d\omega} = \left(-\hat{\gamma}_n^{U}(0)\right)^{-1/2}\left(\tilde{T}^*\left(0,z_U;\,\frac{k_n}{\omega}\right) - \frac{dk_n}{d\omega}\,\tilde{D}^*\left(0,z_U;\,\frac{k_n}{\omega}\right)\right) \quad . \qquad (4C\text{-}33)$$

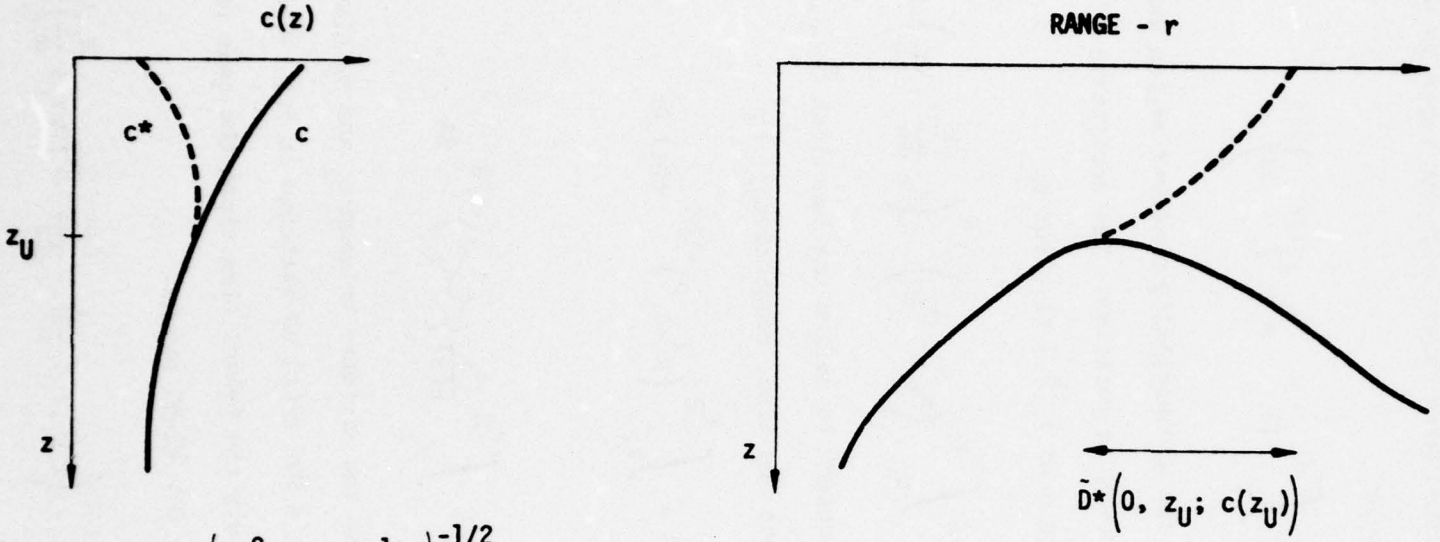

$$c^*(z) = \left(\frac{2}{c^2(z_U)} - \frac{1}{c^2(z)}\right)^{-1/2}$$

FIGURE 4C-2
THE DISTANCE $\tilde{D}^*$ AND THE SOUND VELOCITY c^*
z_U is a TP of a normal mode; $\tilde{D}^*$ and c^* are determined by z_U

Then, with the function F* defined by

$$F^* = \left(\pi M^2 \left(\hat{\gamma}_n^U(0) \right) \left(-\hat{\gamma}_n^U(0) \right)^{1/2} \right)^{-1} \quad , \tag{4C-34}$$

the derivative of σ^U with respect to frequency may be expressed as

$$\frac{d\sigma^U}{d\omega} = -F^* \left(\hat{\gamma}_n^U(0) \right) \left(T^* \left(0, z_U; \frac{k_n}{\omega} \right) - \frac{dk_n}{d\omega} D^* \left(0, z_U; \frac{k_n}{\omega} \right) \right) \quad . \tag{4C-35}$$

A plot of the function F* is given in Fig. 4C-3. The rapid decay of F* means that, except at low frequencies and with the upper TP very near the surface, the presence of the surface does not affect the solutions. The derivative of σ^U with respect to mode number may easily be shown to be given by

$$\frac{d\sigma^U}{dn} = -F^* \left(\hat{\gamma}_n^U(0) \right) \hat{D}^* \left(0, z_U; \frac{\omega}{k_n} \right) \frac{dk_n}{d\omega} \quad . \tag{4C-36}$$

Now, consider the effect of the upper boundary upon the mode quantities, assuming that the TP's are very far from the axis of the SVP, so that the function G of Eq. 4C-18 is effectively zero. Then, $\hat{v}_n$ is given by

$$\hat{v}_n(\omega) = \hat{D}_n(\omega) / \hat{T}_n(\omega) \quad . \tag{4C-37}$$

where $\hat{D}_n$ and $\hat{T}_n$ are given by

$$\hat{D}_n(\omega) = \tilde{D} \left(z_U, z_L; \frac{\omega}{k_n} \right) - F^* \left(\hat{\gamma}_n^U(0) \right) \tilde{D}^* \left(0, z_U; \frac{k_n}{\omega} \right) \tag{4C-38}$$

and

$$\hat{T}_n(\omega) = \hat{T} \left(z_U, z_L; \frac{\omega}{k_n} \right) - F^* \left(\hat{\gamma}_n^U(0) \right) \tilde{T}^* \left(0, z_U; \frac{k_n}{\omega} \right) \quad . \tag{4C-39}$$

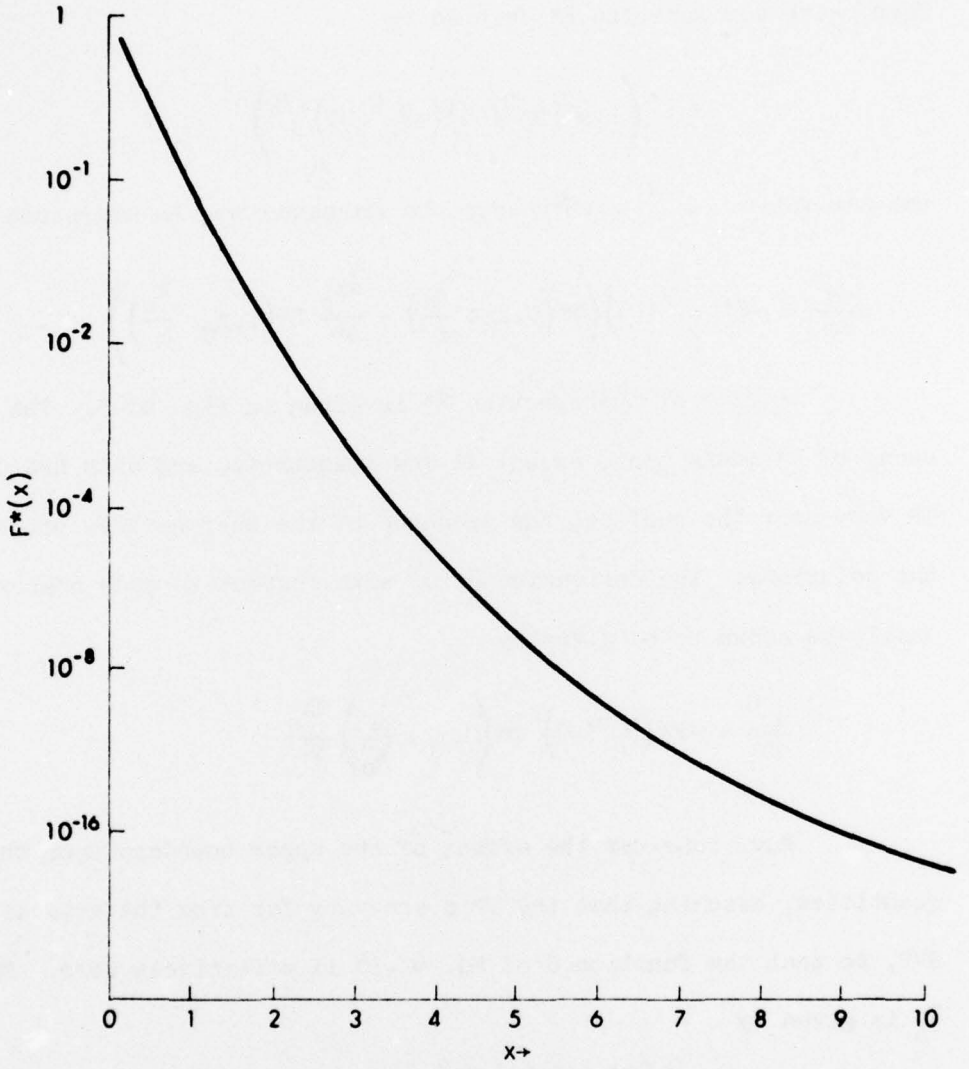

FIGURE 4C-3

THE FUNCTION $F^*(x) = \dfrac{1}{\pi(x)^{1/2}[Ai^2(x) + Bi^2(x)]}$ (Eq. 4C-34)

The ordinate scale is log[log(F*)]

Now, the added terms on the RHS of Eqs. 4D-42 and 4D-43 are largest when the TP is nearest the surface, where a limiting form for these equations is needed. We will assume that $c^{-2}(z)$ is linear near the surface:

$$c^{-2}(z) = c^{-2}(0)(1+\mu z) \quad , \tag{4C-40}$$

so that

$$\hat{\gamma}_n^{\,U}(0) = -\left(\frac{\mu^{1/2}\omega}{c(0)}\right)^{2/3} z_U \quad , \tag{4C-41}$$

$$\tilde{D}^*\left(0, z_U; \frac{\omega}{k_n}\right) \approx 2\left(\frac{z_U}{\mu}\right)^{1/2} \quad , \tag{4C-42}$$

and

$$\tilde{T}^*\left(0, z_U; \frac{\omega}{k_n}\right) \approx \frac{2}{c(0)}\left(\frac{z_U}{\mu}\right)^{1/2} \quad . \tag{4C-43}$$

Thus, as the TP approaches the surface, $\hat{D}_n(\omega)$ and $\hat{T}_n(\omega)$ approach the values:

$$\hat{D}_n(\omega) = \tilde{D}\left(z_U, z_L; \frac{\omega}{k_n}\right) - \left(\frac{c(0)}{\omega\mu^2}\right)^{1/3} \frac{4}{3\pi\, M^2(0)} \quad , \tag{4C-44}$$

$$\hat{T}_n(\omega) = \tilde{T}\left(z_U, z_L; \frac{\omega}{k_n}\right) - \left(\frac{c(0)}{\mu^2\omega}\right)^{1/3} \frac{4}{3\pi c(0)\, M^2(0)} \tag{4C-45}$$

To complete the consideration of boundary effects, reflection from the ocean surface must be taken into account. The modes which reflect from the surface are those whose phase velocities exceed c(0). As we have just seen, when the upper TP is below the surface, the group velocity $\hat{v}_n$ and mode spacing $\hat{D}_n$ are influenced by the presence of the boundary only if the TP is near the surface ($\hat{\gamma}_n^U(0)$ small). Similarly, if there is reflection from the surface, $\hat{D}_n$ and $\hat{v}_n$ differ from their ray theory counterparts only if the phase velocity is close to (in terms of $\hat{\gamma}_n^U(0)$) the sound velocity at the surface, as will be shown.

The situation of surface reflection needs special attention because of the fact that the function $\hat{\gamma}_n^U(z)$ has been defined in terms of an integral from z_U to z; when there is reflection, $z_U=0$, and we need to define the function $\gamma_n^U(z)$ as:

$$\hat{\gamma}_n^U(z) = \left(\frac{3}{2} g_o + \frac{3}{2} \int_o^z q_n^{1/2} \, dz\right)^{2/3} \quad , \qquad (4C\text{-}46)$$

where

$$g_o = \frac{2}{3}\left(\hat{\gamma}_n^U(0)\right)^{3/2} \quad . \qquad (4C\text{-}47)$$

To see that it is not sufficient to set $g_o=0$, consider a situation such as indicated by Fig. 4C-4, where the phase velocity is substantially greater than the c(0). Then, near to the surface, the mode function will be of the form:

$$u_n(z) = \sin(q_n^{1/2}(0)\, z) \quad . \qquad (4C\text{-}48)$$

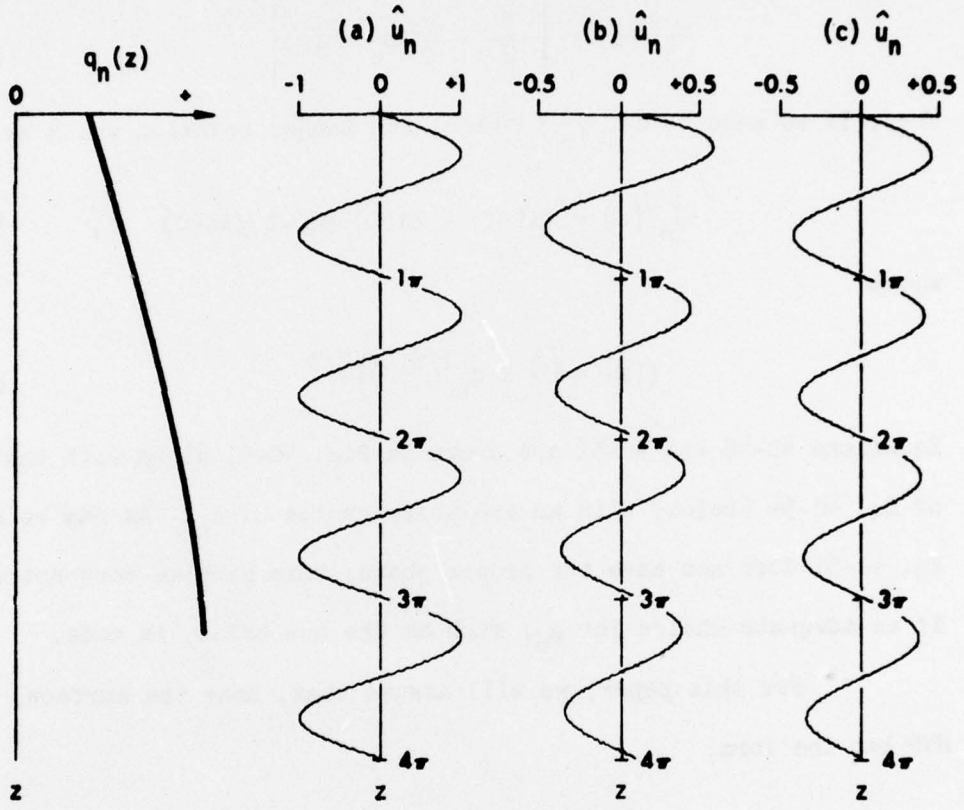

FIGURE 4C-4
MODE FUNCTIONS NEAR THE SURFACE FOR REFLECTION

Left: PROFILE FUNCTION $q_n(z)$ for reflecting mode

Right: Comparison of forms of mode functions for $q_n(0) = 1$

(a) $\hat{u}_n = \sin(z)$ (Eq. 4C-48)

(b) $\hat{u}_n = Ai(-\zeta) - Ai(0)\, Bi(-\zeta)/Bi(0)$ (Eq. 4C-51)

$\zeta = (3\, z/2)^{2/3}$

(c) $\hat{u}_n = Ai(-\zeta') - Ai(-\zeta_1')\, Bi(-\zeta')/Bi(-\zeta_1')$ (Eq. 4C-54)

$\zeta' = [\frac{3}{2}(z + 5)]^{2/3} \qquad \zeta_1' = (15/2)^{2/3}$

The offset of 5 is arbitrary.

Also near the surface, $\hat{\gamma}_n^U$ will be

$$\hat{\gamma}_n^U(z) \approx \left\{ \frac{3g_o}{2} + \frac{3z}{2} q_n^{1/2}(0) \right\}^{2/3} \quad . \tag{4C-49}$$

Thus, if we were to set g_o to zero, the Langer solution would be

$$\hat{u}_n^U(z) = Ai(-\zeta) - Bi(0)\ Bi(-\zeta)/Ai(0) \quad , \tag{4C-50}$$

where

$$\zeta(z) = \left(\frac{3}{2} z\ q_n^{1/2}(0) \right)^{2/3} \quad . \tag{4C-51}$$

Equations 4C-48 and 4C-51 are shown in Fig. 4C-4, along with the form of Eq. 4C-54 (below) with an arbitrary choice of z_n. As may be seen, Eq. 4C-51 does not have the proper phase; this problem does not occur if an adequate choice for g_o, such as the one below, is made.

For this paper, we will assume that, near the surface, the SVP has the form:

$$c^{-2}(z) = c^{-2}(0)(1+\mu z) \quad , \tag{4C-52}$$

so that

$$q_n(z) = \omega^2(1+\mu z)/c^2(0) - k_n^2 \quad . \tag{4C-53}$$

Then, near the surface, u_n will be of the form

$$u_n(z) = Ai\left(-M(z+z_n)\right) - Ai(-Mz_n)\ Bi\left(-M(z+z_n)\right)/Bi(-Mz_n) \quad , \tag{4C-54}$$

where

$$M = \left(\frac{\omega^2 \mu}{c^2(0)} \right)^{1/3} \quad , \tag{4C-55}$$

and

$$z_n = \frac{c^2(0)}{\mu}\left(k_n^{\,2} - \frac{\omega^2}{c^2(0)}\right) \quad . \tag{4C-56}$$

Therefore, when there is reflection from the surface, we need to choose

$$\hat{\gamma}_n^{\,U}(0) = Mz_n \quad , \tag{4C-57}$$

or,

$$\begin{aligned} g_o &= \frac{2}{3}\,(Mz_n)^{3/2} \\ &= \frac{2}{3}\,\frac{\omega}{c(0)}\,\mu^{1/2}\,z_n^{\,3/2} \quad . \end{aligned} \tag{4C-58}$$

To obtain a more familiar form for g_o, note that, if we let Eq. 4C-53 define $q_n(z)$ for negative z, then g_o is equal to

$$g_o = \frac{2}{3}\left(\hat{\gamma}_n^{\,U}(0)\right)^{3/2} = \int_{-z_n}^{o} q_n^{\,1/2}\,dz \quad . \tag{4C-59}$$

Now, we may consider the derivatives of the eigenvalue equation for the case of surface reflection, Eq. 4B-23. Since we are considering only the effect of surface reflection, it is

$$\int_o^{z_L} q_n^{\,1/2}\,dz = (n+1/4)\pi + \delta\left(\hat{\gamma}_n^{\,U}(0)\right) \quad . \tag{4C-60}$$

We will use Eqs. 4C-49 and 4C-59 to specify $\hat{\gamma}_n^{\,U}(0)$. The analysis leading to Eq. 4C-17 dealt with the derivatives of Eq. 4B-18; the form of Eq. 4B-18 differs from that of Eq. 4C-60 only in a factor of $\pi/4$ and the sign of the function $\delta(\cdot)$. Thus, from Eq. 4C-17 we have

$$\frac{d}{d\omega}\,\delta\left(\hat{\gamma}_n^{U}(0)\right) = G\left(\hat{\gamma}_n^{U}(0)\right)\left(\tilde{T}\left(-z_n, 0;\ \frac{k_n}{\omega}\right) - \frac{dk_n}{d\omega}\,\tilde{D}\left(-z_n, 0;\ \frac{k_n}{\omega}\right)\right) \quad , \quad (4C\text{-}61)$$

where $\tilde{T}$ and $\tilde{D}$ are computed using the SVP of Eq. 4C-52 and z_n is given by Eq. 4C-56. Similarly, from Eq. 4C-22, it follows that

$$\frac{d}{dn}\,\delta(\hat{\gamma}_n(0)) = G\left(\hat{\gamma}_n^{U}(z_o)\right)\,\tilde{D}\left(-z_n, 0;\ \frac{\omega}{k_n}\right)\frac{dk_n}{dn} \quad . \quad (4C\text{-}62)$$

Thus, the group velocity for modes reflecting from the surface is

$$\hat{v}_n = \hat{D}_n(\omega)/\hat{T}_n(\omega) \quad , \quad (4C\text{-}63)$$

where

$$\hat{D}_n(\omega) = \tilde{D}\left(z_U, z_L;\ \frac{\omega}{k_n}\right) + G\left(\hat{\gamma}_n^{U}(z_o)\right)\,\tilde{D}\left(-z_n, 0;\ \frac{\omega}{k_n}\right) \quad , \quad (4C\text{-}64)$$

and

$$\hat{T}_n(\omega) = \tilde{T}\left(z_U, z_L;\ \frac{\omega}{k_n}\right) + G\left(\hat{\gamma}_n^{U}(z_U)\right)\,\tilde{D}\left(-z_n, 0;\ \frac{\omega}{k_n 0}\right) \quad . \quad (4C\text{-}65)$$

If the phase velocity is close to c(0), then the limiting forms for $\hat{D}_n$ and $\hat{T}_N$ given by Eqs. 4C-44 and 4C-45 are obtained; this is so because the functions G(x) and -F*(x) approach each other as $x \to 0$.

Summary

By combining the effects of the boundary condition at the surface and the effects of a finite distance from the TP's to the velocity minimum, the group velocity and mode cycle distance may be written as

$$\hat{v}_n(\omega) = \hat{D}_n(\omega)/\hat{T}_n(\omega) \quad (4C\text{-}66)$$

and

$$\hat{\Lambda}_n(\omega) = 2\hat{D}_n(\omega) \quad , \tag{4C-67}$$

where

$$\hat{D}_n(\omega) = \tilde{D}\left(z_U, z_L; \frac{\omega}{k_n}\right) + \Delta_n(\omega) \tag{4C-68}$$

and

$$\hat{T}_n(\omega) = \tilde{T}\left(z_U, z_L; \frac{\omega}{k_n}\right) + \tau_n(\omega) \quad . \tag{4C-69}$$

The quantities $\tilde{D}$ and $\tilde{T}$ are the ray theory travel distance and travel time (Eqs. 2C-13) between TP's of a ray with turning point velocity ω/k_n. The added terms are given by, in the case of modes not reflecting from the surface, combining Eqs. 4C-25 and 4C-38 to obtain $\Delta_n(\omega)$, and by combining Eqs. 4C-26 and 4C-39 to obtain $\tau_n(\omega)$. For the modes which reflect from the surface, combine Eqs. 4C-25 and 4C-64 to obtain $\Delta_n(\omega)$, and Eqs. 4C-26 and 4C-65 to obtain $\tau_n(\omega)$.

IV-D ANALYSIS OF APPROXIMATIONS

Two approximations have been made, the discussion of which has been deferred. It is the purpose of this section to examine them in terms of representative SVP's. In Section IV-A, in order to solve for the argument of the Airy function of Eq. 4A-2, it was assumed that the second term of the RHS of Eq. 4A-9 could be neglected. That is, it was assumed that the solution of Eq. 4A-9 is approximately the same as the solution of Eq. 4A-10. In Section IV-B, it was assumed that, at the depth where the solutions from the upper and lower TP's are matched, Eqs. 4B-7 and 4B-8 are satisfied.

For convenience, we will consider the profile function near, say, the upper TP, and use the variable $\zeta = z - z_U$ as shown in Fig. 4D-1. Also shown are representative sketches for the profile function $q(z)$ and the argument of the Airy function, $\gamma(\zeta)$. We will consider q and γ near the point ζ_o; the quantities a, b, and $\bar{a}$, which are defined in Fig. 4D-1, depend upon the point ζ_o.

First, consider the approximations of Section IV-A. The differential equation of interest, Eq. 4A-9, is rewritten in terms of this section's notation as

$$\gamma\left(\frac{d\gamma}{d\zeta}\right)^2 = q(\zeta) + \frac{1}{W}\frac{d^2W}{d\zeta^2} \quad . \tag{4D-1}$$

To neglect the second term on the RHS of Eq. 4D-1, we assume that

$$\left|\frac{1}{qW}\frac{d^2W}{d\zeta}\right| \ll 1 \quad . \tag{4D-2}$$

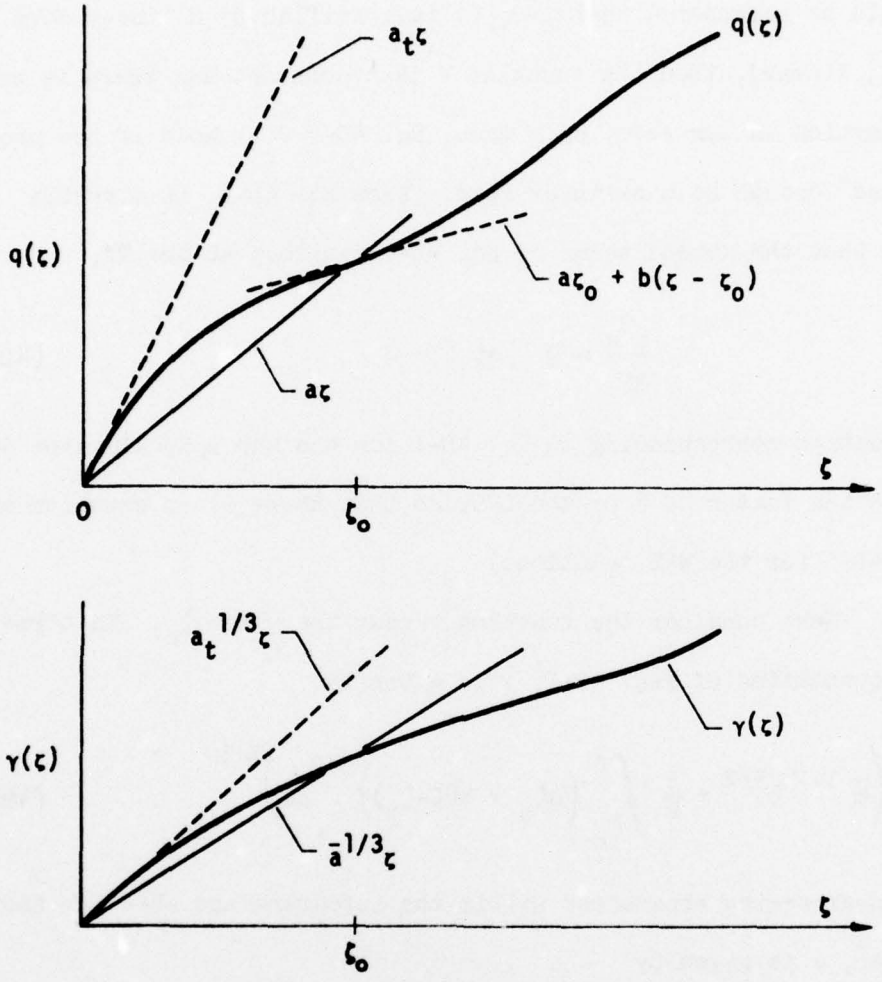

FIGURE 4D-1
SKETCH OF PROFILE FUNCTION $q(\zeta)$ AND OF $\gamma(\zeta)$ BELOW A TP

TOP: PROFILE FUNCTION $q(\zeta)$

$a \equiv q(\zeta_o)/\zeta_o$

$b \equiv dq/d\zeta$ at ζ_o

$a_t = dq/d\zeta$ at $\dot{\zeta} = 0$ (the TP)

BOTTOM: FUNCTION $\gamma(\zeta)$

$\bar{a}^{1/3} \equiv \gamma(\zeta_o)/\zeta_o$

It should be remembered that if $q(\zeta)$ is specified by a linear form ($1/c^2(z)$ linear), then the function W is a constant and there is no approximation in our solution. Thus, Eq. 4D-2 will hold if the profile is "close" enough to a bilinear form. From Eq. 4D-1, it directly follows that the second terms of Eq. 4D-1 vanishes at the TP,

$$\frac{d^2W}{d\zeta^2} = 0 \quad \text{at } \zeta = 0 \quad . \tag{4D-3}$$

(The equation corresponding to Eq. 4D-1 for the WKB approximation does not have the factor of γ on the LHS, so that there is no equation such as Eq. 4D-3 for the WKB solution.)

Next consider the function γ near the point ζ_o. In terms of the quantities of Fig. 4D-1, γ is given by

$$\gamma = \left(\bar{a}^{1/2} \zeta^{3/2} + \frac{3}{2} \int_{\zeta_o}^{\zeta} \left(a\zeta_o + b(\zeta - \zeta_o) \right)^{1/2} dz \right)^{2/3} \quad . \tag{4D-4}$$

Using power series expansions within the integrand and then for the 2/3 power, γ is given by

$$\gamma \approx \bar{a}^{1/3} \zeta_o + \left(1 + \frac{A(\zeta - \zeta_o)}{\zeta_o} + \frac{B(\zeta - \zeta_o)^2}{\zeta_o^2} + \frac{C(\zeta - \zeta_o)^3}{\zeta_o^3} \right) \quad , \tag{4D-5}$$

with the terms A, B, and C given by

$$A = \left(\frac{a}{\bar{a}} \right)^{1/2} \qquad B = \left(\frac{a}{\bar{a}} \right)^{1/2} \left(\frac{b}{4a} - \frac{a}{4\bar{a}} \right) \qquad C = \left(\frac{a}{\bar{a}} \right)^{3/2} \left(\frac{1}{6} - \frac{b}{8a} - \frac{b^2}{24\, a^2} \right). \tag{4D-6}$$

Note that, if q is linear from the TP to ζ, A=1 and B=C=0. Also, if the slope of $q(\zeta)$ at ζ_o is the same as the mean slope from the TP to ζ_o (that is, a=b), then the second derivative of γ vanishes at ζ_o.

Then, neglecting the constant normalizing factor, the amplitude modulation W (Eq. 4A-15) is given by

$$W = \bar{a}^{-1/6} \left(A - \frac{B(\zeta-\zeta_o)}{\zeta_o} - \frac{3C(x-x_o)^2}{\zeta_o^2} \right) , \qquad (4D\text{-}7)$$

so that the desired quantity, W"/qW, is given by

$$\frac{W''}{qW} = \frac{3}{\bar{a}\zeta_o^3} \left(\frac{1}{6} - \frac{b}{8a} - \frac{b^2}{24\,a^2} \right) \quad \text{at } \zeta_o \quad . \qquad (4D\text{-}8)$$

As mentioned above, this vanishes if a=b; when this happens, W" will change sign. Therefore, along a profile such as shown by Fig. 4D-2, even though the magnitude of W"/W might become large, it will oscillate and be negligible, after integration, in comparison with $q(\zeta)$.

Equation 4D-8 may be used to estimate whether or not a solution will hold across a break in the SVP. For example, Fig. 4D-3 illustrates a profile with one break - at the axis. Using the values of a, b, and $\bar{a}$ in Fig. 4D-3, Eq. 4D-2 becomes

$$\frac{10}{f^2} \ll 1 \quad . \qquad (4D\text{-}9)$$

That is, at frequencies above, say, 20 Hz, a solution about the upper TP should be valid even across the large jump in the slope of the SVP shown. (In practice, one would use the solution developed about the lower TP below z_o.) However, at lower frequencies this would not be the case. This is illustrated by Fig. 4D-3, which shows the functions

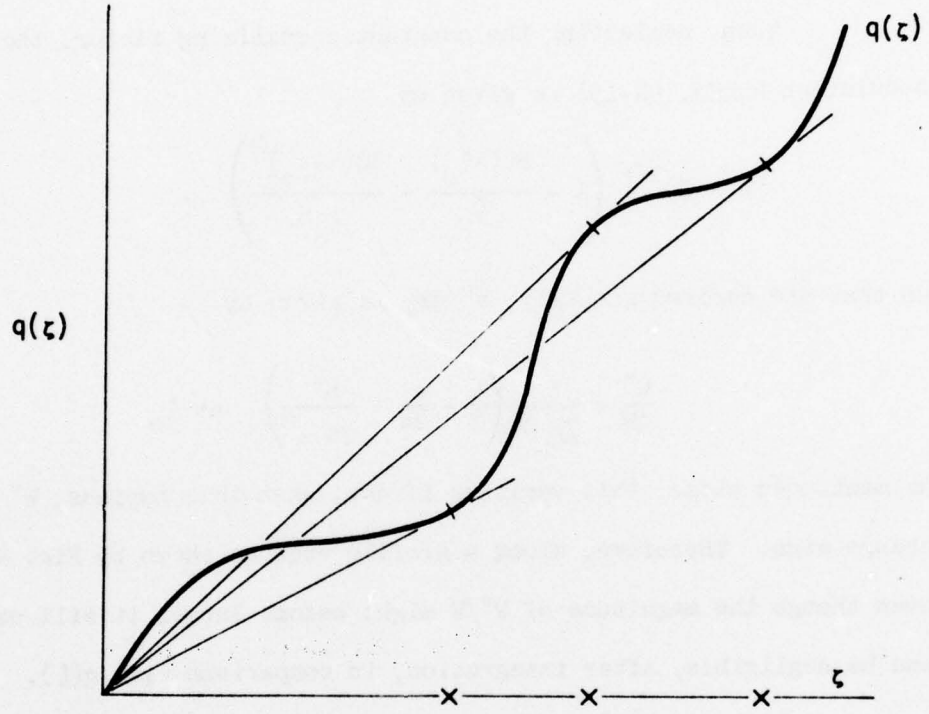

FIGURE 4D-2
PROFILE FUNCTION $q(\zeta)$ WHICH OSCILLATES ABOUT A LINEAR FORM

At the depths marked X on the abscissa, $\frac{dq}{d\zeta} = \frac{q}{\zeta}$, so that $W'' = 0$

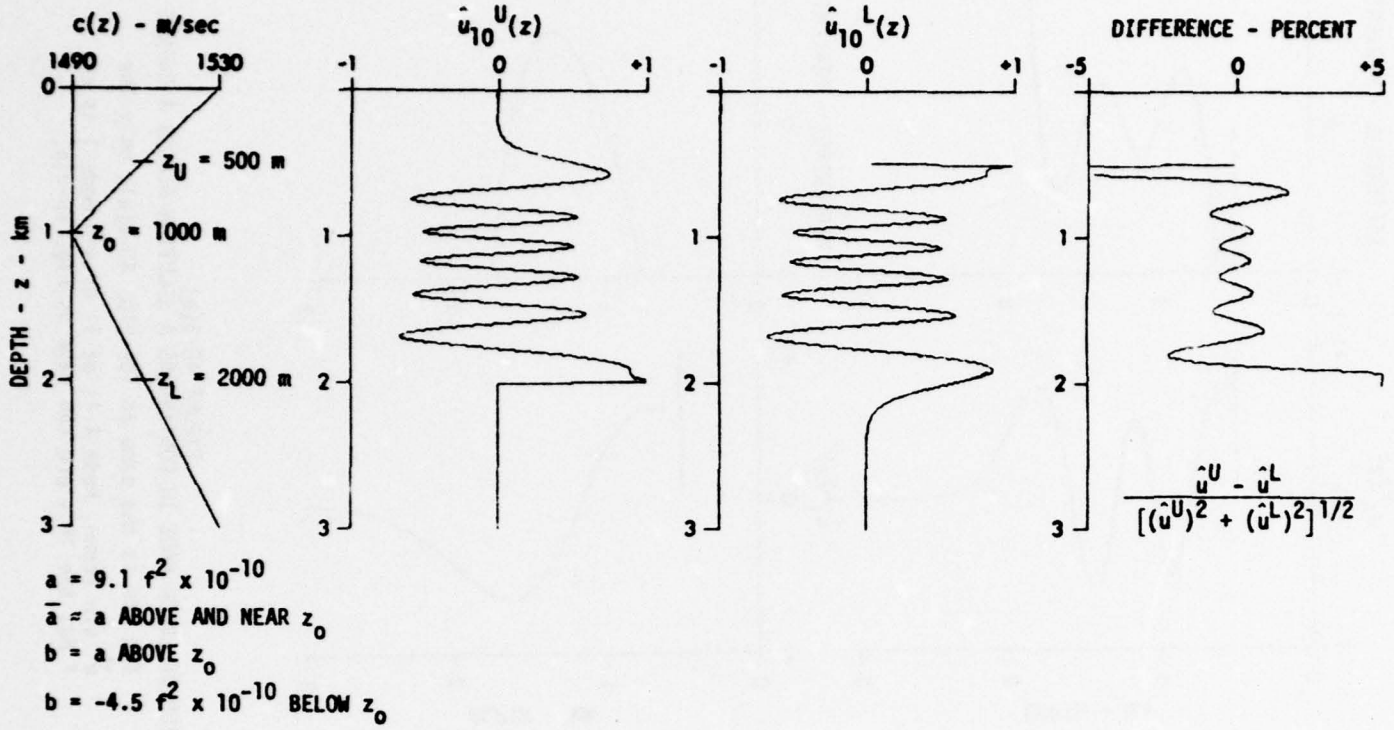

$a = 9.1\ f^2 \times 10^{-10}$

$\bar{a}$ = a ABOVE AND NEAR z_o

b = a ABOVE z_o

$b = -4.5\ f^2 \times 10^{-10}$ BELOW z_o

FIGURE 4D-3(a)
ILLUSTRATION OF ERROR MADE IN CONTINUING A SOLUTION ACROSS A CHANGE IN dc/dz

Mode 10 at 49 Hz for the SVP on the left. In application, $\hat{u}^U$ would be used above z_o and $\hat{u}^L$ below; thus, the difference represents the error made by, for example, using $\hat{u}^U$ below z_o. The quantities a, $\bar{a}$, b, defined in Fig. 4D-1, are referenced to z_U. Mode amplitude is arbitrary. f is frequency.

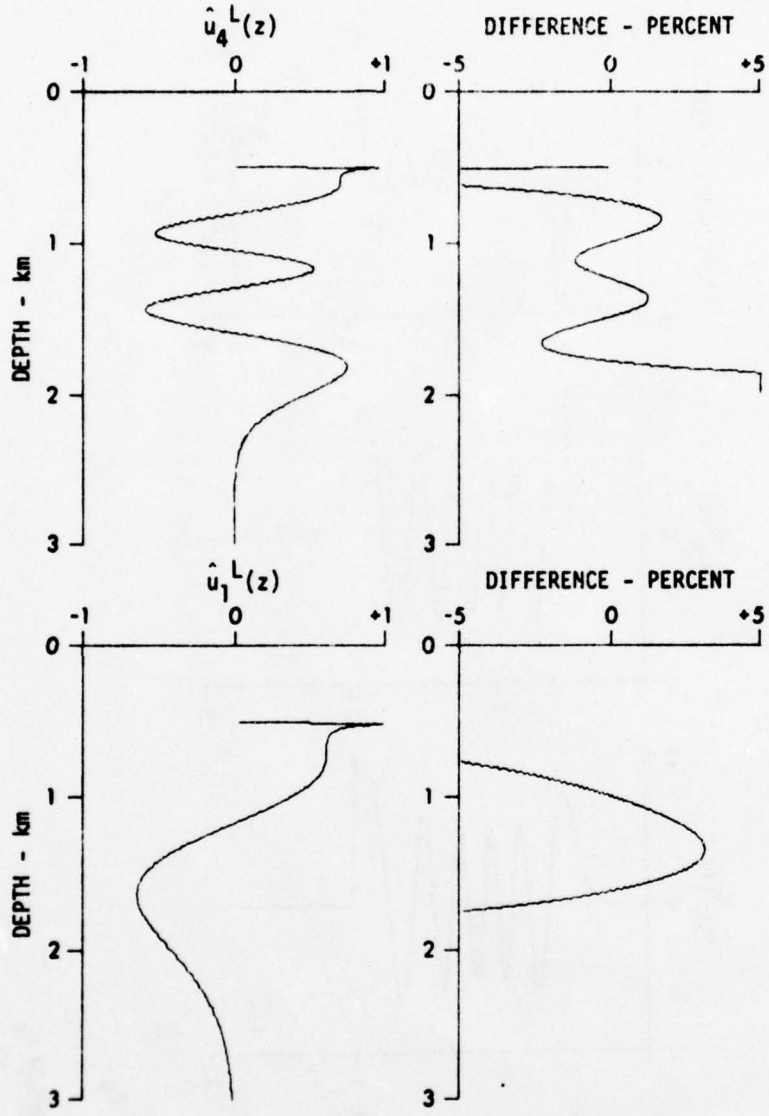

FIGURE 4D-3(b)
ILLUSTRATION OF ERROR MADE IN CONTINUING A SOLUTION ACROSS A CHANGE IN dc/dz

The SVP is the same as for Fig. 4D-3(a); only the $\hat{u}^L$ are shown. Mode 4 is at 11 Hz and mode 1 is at 7 Hz; the TP's are the same as Fig. 4D-3(a).

$\hat{u}_n^U(z)$ and $\hat{u}_n^L(z)$ at 49, 11, and 7 Hz, which have the same TP's. Note that, at the higher frequency, very little error is made by continuing across the break in the SVP, as predicted by Eq. 4D-9.

Next, consider the approximations of Sections IV-B. Again, it will be convenient to express the derivative of θ as

$$\frac{d\theta}{dz} = \frac{1}{\pi M^2} \frac{d\gamma}{dz} \quad . \tag{4D-10}$$

Using Eq. 4D-10, Eq. 4B-8 becomes

$$\frac{1}{2} \left| \frac{d}{d\gamma} M^2(\gamma) \right| \ll \pi^{-1} \quad . \tag{4D-11}$$

That this will be satisfied very close to the TP is shown by Fig. 4D-4.

Lastly, for Eq. 4B-7, we will use the form of W(z) given by

$$W = \left| \frac{\gamma}{q} \right|^{1/4}$$

$$W' = \frac{1}{4} \left| \frac{\gamma}{q} \right|^{-3/4} \left(\frac{\gamma'}{q} - \frac{\gamma q'}{q^2} \right) \quad . \tag{4D-12}$$

At the axis of the SVP, where we wish to match solutions, q'=0 so that W'/W is given by

$$W'/W = \gamma'/4\gamma \quad (\text{when } q' = 0) \quad . \tag{4D-13}$$

If Eq. 4D-13 and 4D-10 are substituted into Eq. 4B-9, the requirement of Eq. 4D-14 is obtained

$$\frac{M^2(\gamma)}{4\gamma} \ll \pi^{-1} \quad . \tag{4D-14}$$

The LHS of Eq. 4D-14 is also plotted in Fig. 4D-4.

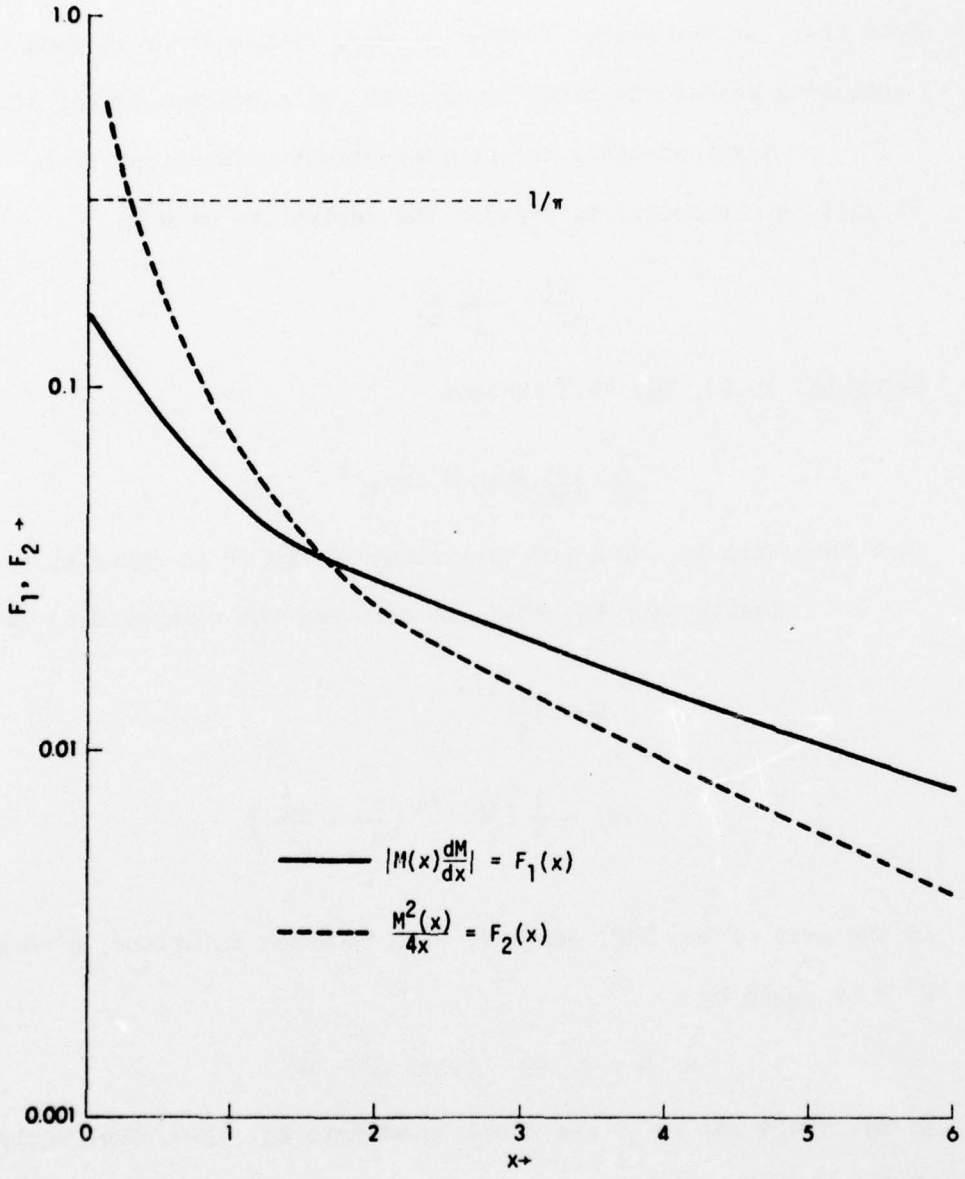

FIGURE 4D-4
THE FUNCTIONS OF Eqs. 4D-11 AND 4D-14

V. EXAMPLE APPLICATIONS

To illustrate the Langer solution, the formulae developed in Chapter IV will be applied to compute normal mode quantities for specific examples. First, in Section V-A, a series of profiles constructed from a few linear segments will be considered. These examples will illustrate that the predictions of ray theory and normal mode theory differ significantly when the turning points are near to a boundary. Then, in Section V-B, normal mode functions and quantities for illustrative experimental profiles will be presented.

V-A SIMPLE LINEAR SEGMENT PROFILES

In this section, we present plots of the group velocity, $\hat{v}_n(\omega)$ and mode cycle distance, $\hat{\Lambda}_n(\omega)$ for a series of SVP's constructed from a few linear segments. This will illustrate the conditions under which these mode theory quantities differ significantly from their ray theory counterparts, and therefore there is a significant frequency dependence of the mode theory quantities. The condition under which the $\hat{v}_n(\omega)$ versus $c_n(\omega)$ plots have the greatest frequency dependence is when the upper TP is slightly below the surface or when $c_n(\omega)$ is slightly greater than $c(0)$. When this happens, the boundary value at the surface is an important factor determining the normal mode function at low frequencies, whereas the boundary condition has no counterpart in ray theory. The Langer solution developed in Chapter IV was used to compute the figures presented here. As stated previously, the Langer solution is well suited to the problem with TP's near to a boundary.

The profiles designated A1000, A500, A200, and A100 are shown in Figs. 5A-1, 5A-2, 5A-3, and 5A-4, respectively. The group velocity $\hat{v}_n$ versus phase velocity c_n for each profile at 20, 50, and 150 Hz is also shown. In Fig. 5A-1, the ray theory signal speed $(\tilde{D}/\tilde{T})$, and $\hat{v}_n$ at 10 Hz also are shown. The ray theory signal speed is not distinguishable from $\hat{v}_n$ at 150 Hz, except at the phase velocity of surface reflection. Therefore, the ray theory quantities are not shown in the other figures of this section. The most prominent feature of these figures is the frequency dependence of the $\hat{v}_n$ versus c_n curve near $c_n = 1540$ m/sec, the sound velocity at the surface. As indicated by Eq. 4C-44, this

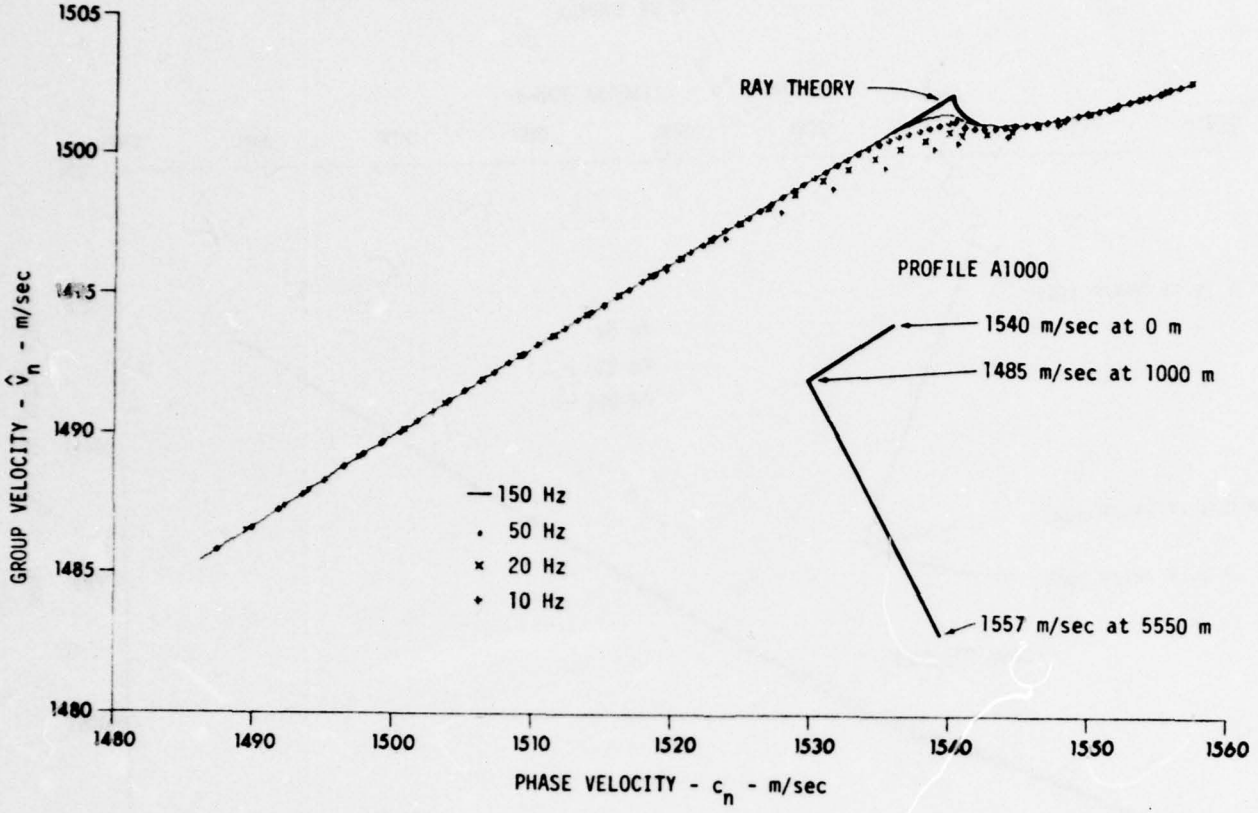

FIGURE 5A-1
GROUP VELOCITY VERSUS PHASE VELOCITY FOR PROFILE A1000

The c_n and $\hat{v}_n$ for the modes at 150 Hz are so closely spaced that they are plotted as a continuous curve. The ray theory signal velocity for this profile is also shown.

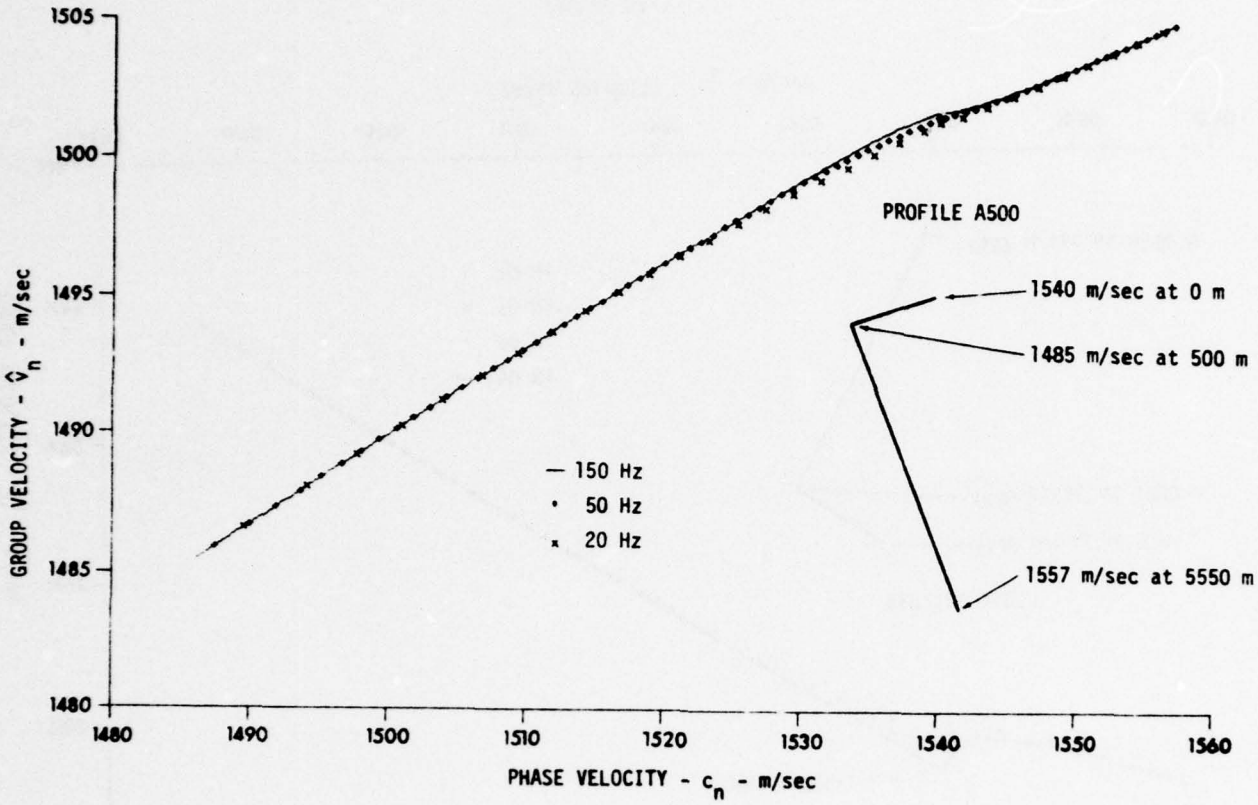

FIGURE 5A-2
GROUP VELOCITY VERSUS PHASE VELOCITY FOR PROFILE A500
The c_n and $\hat{v}_n$ for the modes at 150 Hz are so closely spaced that they are plotted as a continuous curve.

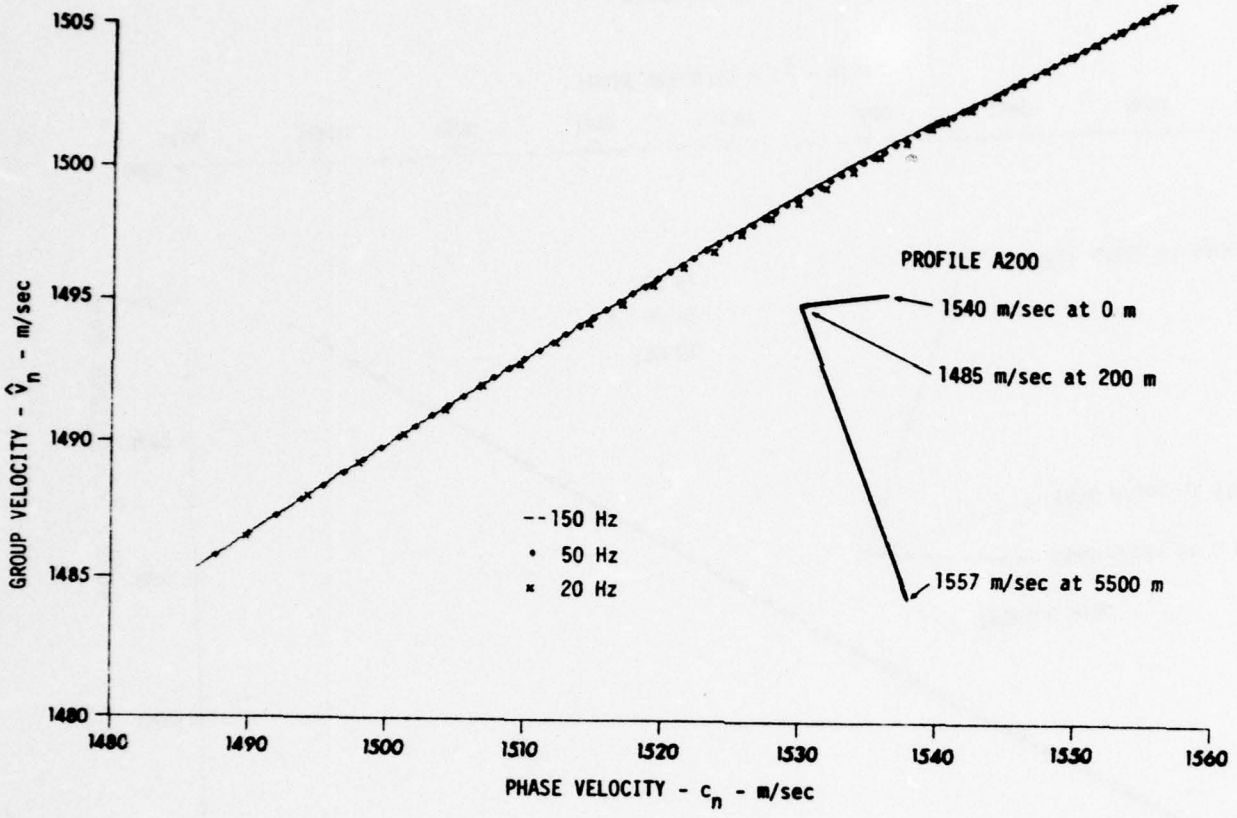

FIGURE 5A-3
GROUP VELOCITY VERSUS PHASE VELOCITY FOR PROFILE A200
The c_n and $\hat{v}_n$ for the modes at 150 Hz are so closely spaced that they are plotted as a continuous curve.

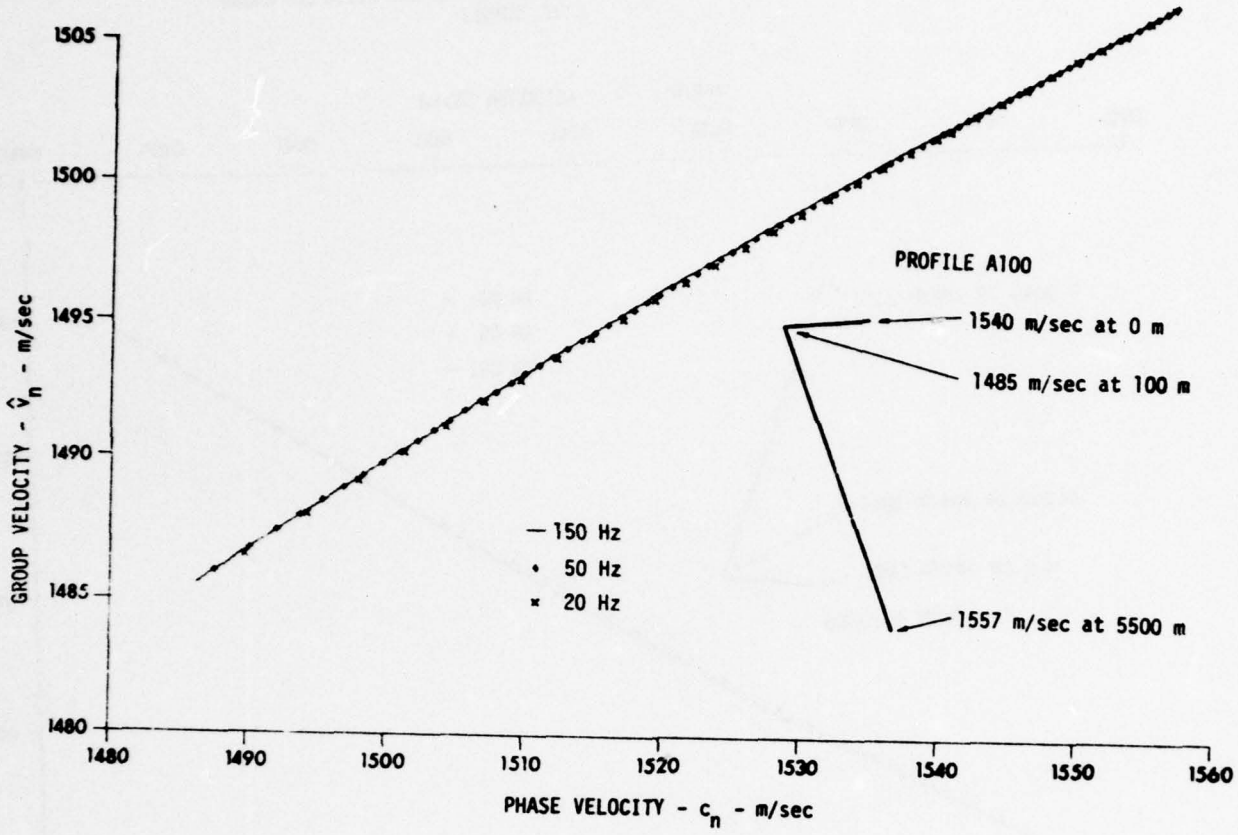

FIGURE 5A-4
GROUP VELOCITY VERSUS PHASE VELOCITY FOR PROFILE A100
The c_n and $\hat{v}_n$ for the modes at 150 Hz are so closely spaced that they are plotted as a continuous curve.

frequency dependence (or departure from ray theory) is greater, the less the slope of the layer near the surface. Figures 5A-1 through 5A-4 illustrate the amount of frequency dependence to be expected for these four nominal SVP's. The mode cycle distance, $\hat{\Lambda}_n$, versus c_n at 20 Hz, 50 Hz, and 150 Hz for profiles A1000 and A100 are shown in Figs. 5A-5 and 5A-6, respectively. Profile A1000 is similar to the one used by A. Guthrie [1974] to explain the frequency dependence of experimental convergence zone spacings, and the mode cycle distances shown in Fig. 5A-5 are approximately equal to the ones presented by Guthrie.

We will consider next the effect of the presence of a layer in which the gradient of the SVP is relatively small in comparison with the average gradient at nearby depths. From the point of view of ray theory, those rays which have a TP within such a layer will have an anomalous increase in $\tilde{D}$ and $\tilde{D}/\tilde{T}$, because of the relatively large curvature of rays within the layer. The examples examined show that, when the anomalous layer is far from the boundary, the normal mode quantities (plotted versus c_n) do not have significant frequency dependence as far as the effects of the layer are concerned. However, if the layer is near the surface (as is often the case in the ocean environment) then the effect of the layer is very frequency dependent.

Figures 5A-7 and 5A-8 show $\hat{v}_n$ versus c_n for the profiles named B500 and B501, respectively. These are similar to the profile designated A1000 (Fig. 5A-1), except that, starting at 500 m depth, there is a layer in which $|dc/dz|$ is only 0.010 sec^{-1} rather than 0.055 sec^{-1}. The layer is 100 m thick in B500 and only 10 m thick in B501. A plot of the ray theory signal speed would be indistinguishable

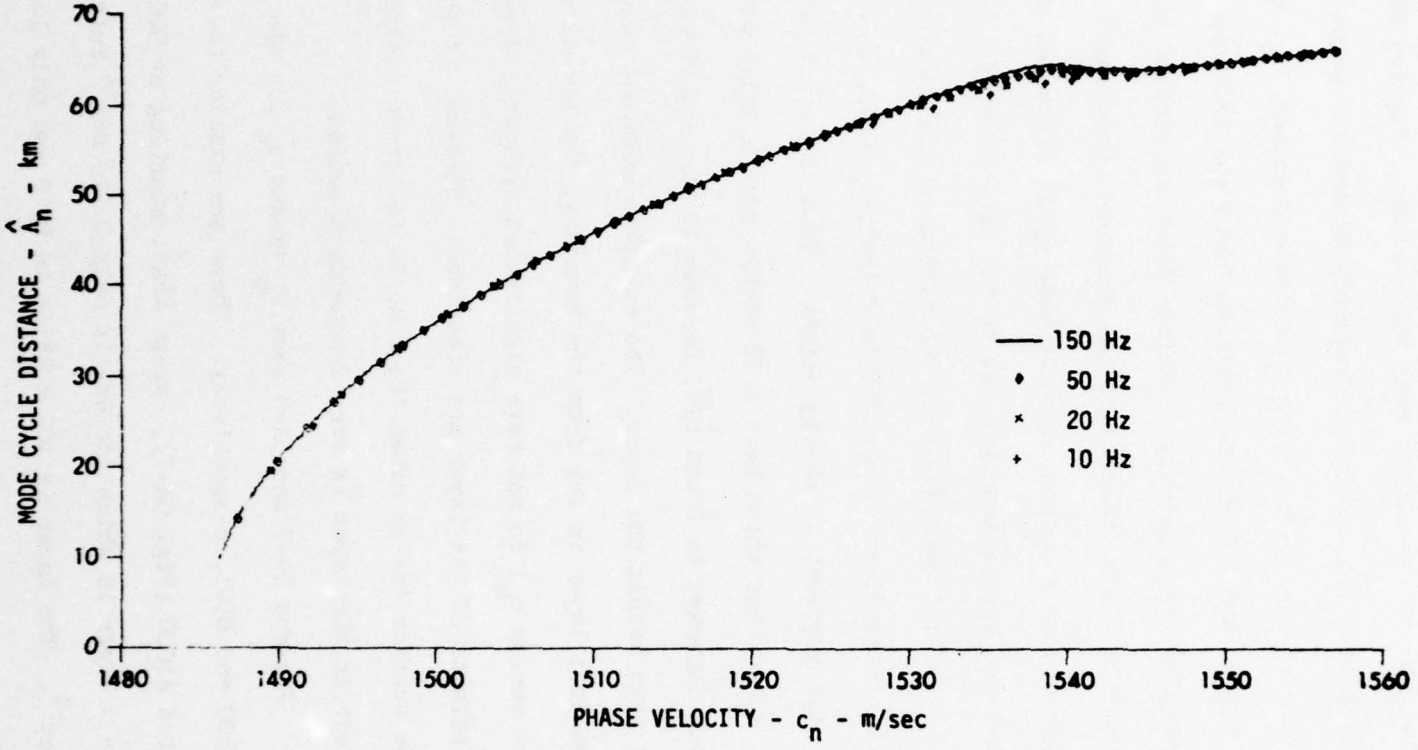

FIGURE 5A-5
MODE CYCLE DISTANCE VERSUS PHASE VELOCITY FOR PROFILE A1000

This profile is shown in Figure 5B-1. The points for the modes at 150 Hz are so closely spaced that they are plotted as a continuous curve.

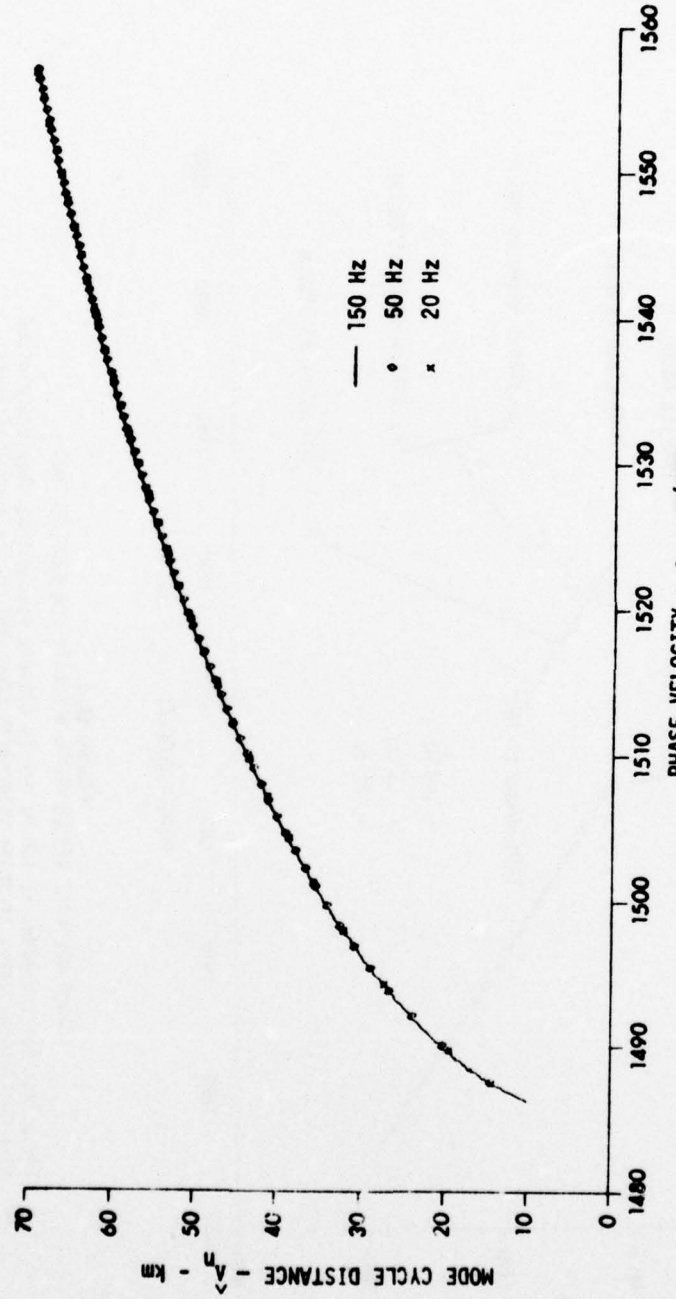

FIGURE 5A-6
MODE CYCLE DISTANCE VERSUS PHASE VELOCITY FOR PROFILE A100
This profile is shown in Figure 5B-4. The points for the modes at 150 Hz are so closely spaced that they are plotted as a continuous curve.

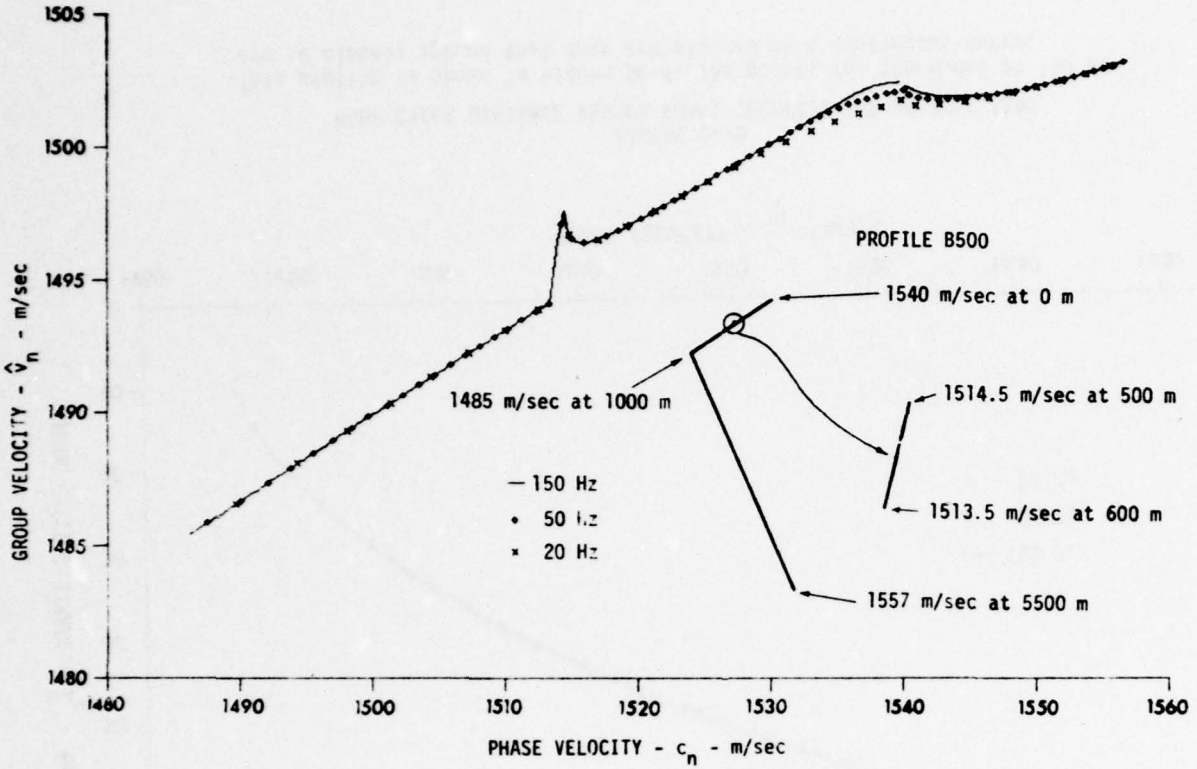

FIGURE 5A-7
GROUP VELOCITY VERSUS PHASE VELOCITY FOR PROFILE B500

The points for the modes at 150 Hz are so closely spaced that they are plotted as a continuous curve. At phase velocities near that of the anomolous layer which is far from the surface, there is little frequency dependence.

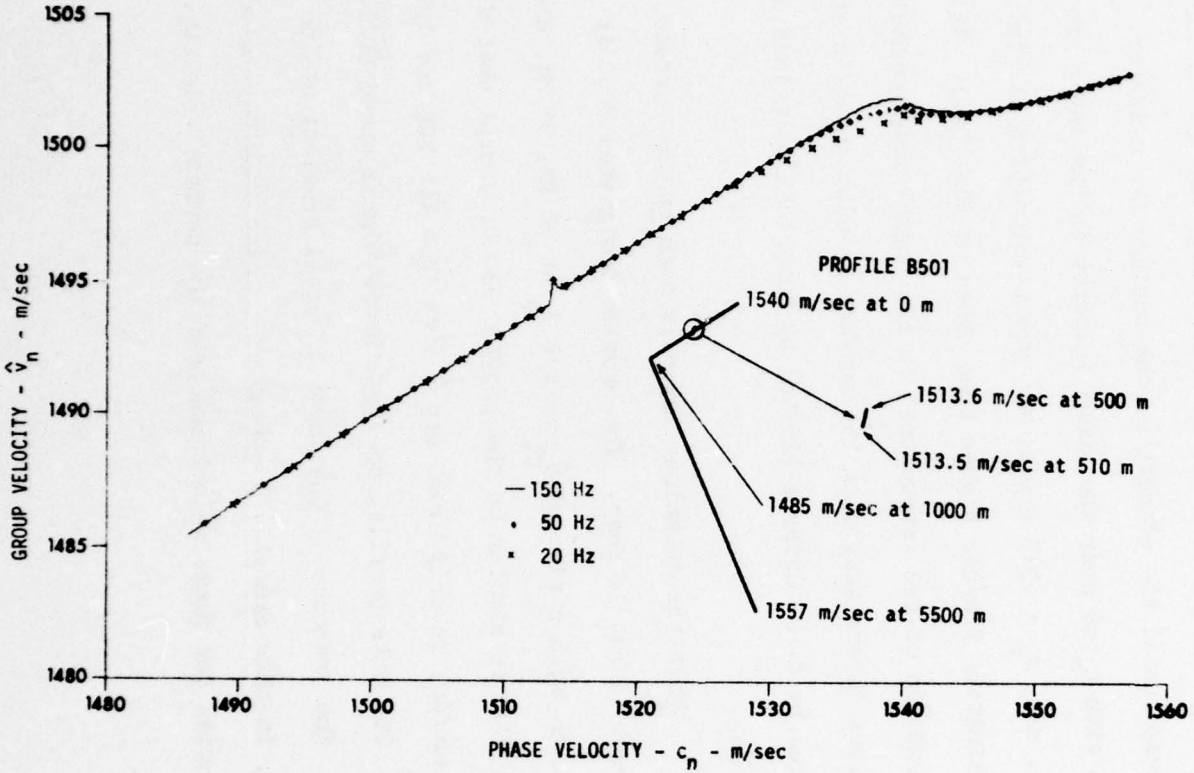

FIGURE 5A-8
GROUP VELOCITY VERSUS PHASE VELOCITY FOR PROFILE B501

The points for the modes at 150 Hz are so closely spaced that they are plotted as a continuous curve. At phase velocities near that of the anomolous layer which is far from the surface, there is little frequency dependence.

from the 150 Hz curve except for the effects of the surface, near c_n = 1540 m/sec. In particular, the cusp near c_n = 1513.5 m/sec is the anomalous increase in $\tilde{D}/\tilde{T}$ predicted by ray theory. The $\hat{v}_n(\omega)$ at 20 Hz and 50 Hz in Figs. 5A-7 and 5A-8 lie along the 150 Hz curve, including the cusp, until the effects of the surface are a factor. Not only the modes with $c_n(\omega)$ near the sound velocity in the layer are affected; above, say, c_n = 1515 m/sec, the group velocities of Fig. 5A-7 are approximately 2 m/sec higher than those of Fig. 5A-1. This frequency independence of the "structure" in the normal mode quantities caused by anomalous layers away from the surface is also shown in similar curves computed by K. M. Guthrie [1974a] by numerical solutions of the depth equation.

When the anomalous layer is near to the surface, a very different effect is seen. The profile designated B000 is shown in Fig. 5A-9, with a plot of $\hat{v}_n$ versus c_n at 20 Hz, 50 Hz, and 150 Hz. Again, B000 is similar to the profile A1000, except that a layer in which $|dc/dz|$ is only 0.010 sec^{-1} lies from the surface down to 100 m depth. For this profile, the ray theory signal speed ($\tilde{D}/\tilde{T}$) is also shown. The presence of the layer of small gradient at the surface causes, in this example, a spread of 5 m/sec in group velocity at these frequencies for phase velocities near the surface velocity.

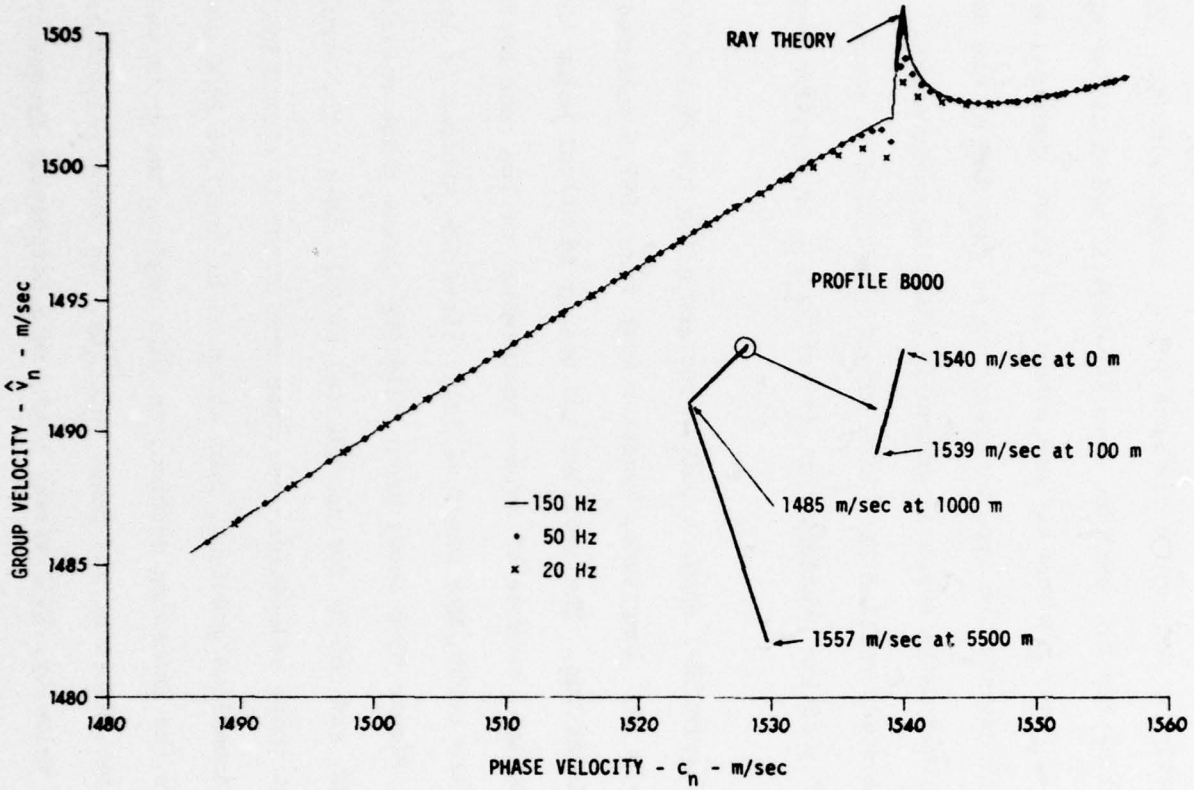

FIGURE 5A-9
GROUP VELOCITY VERSUS PHASE VELOCITY FOR PROFILE B000

The points for the modes at 150 Hz are so closely spaced that they are plotted as a continuous curve. At phase velocities near that of the anomolous layer at the surface, there is a strong frequency dependence.

V-B EXAMPLE EXPERIMENTAL PROFILES

Normal mode quantities and mode functions have been computed for SVP's from two areas. The profiles from the two areas are of a very different nature; this results in a marked difference in the curves of group velocity or mode cycle distance versus phase velocity. The normal mode functions for two profiles from the Pacific which differ at depths above the velocity minimum but are otherwise almost identical are presented to illustrate the type of change to be expected of the mode functions along paths across a gradually changing environment. Some of the experimental profiles have been slightly modified to remove small segments of positive gradients of $c(z)$ above z_o, or negative segments below.

Figure 5B-1 shows a bottom section along the Pacific Ocean at approximately 143° longitude, together with three SVP's measured at different locations. The profiles are nearly identical below the velocity minimum, but, because of colder temperature of the near surface portion to the north, the sound velocity above the minimum is less to the north. Figure 5B-2 shows group velocity versus phase velocity at 15 Hz, 50 Hz, and 160 Hz for profile (a) of Fig. 5B-2. The structure in the plots at phase velocities less than 1500 m/sec is caused by layers of locally anomalous gradient, such as those of profiles B500 and B501 discussed in the preceding section; in this region, the group velocity is largely determined by the phase velocity. At phase velocities near the surface velocity, 1532 m/sec, there is a noticeable frequency dependence of group velocity at a given phase velocity.

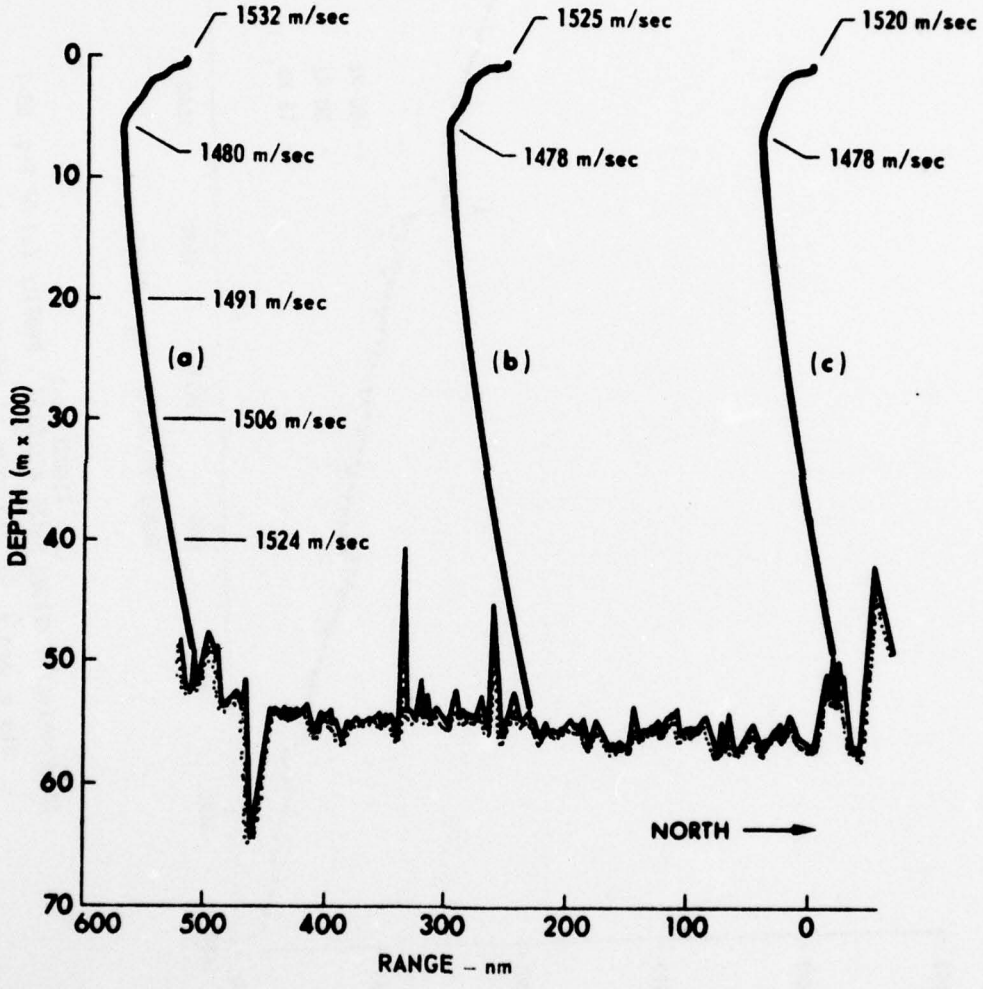

FIGURE 5B-1
BATHYMETRY AND SOUND VELOCITY PROFILES
NE PACIFIC
Below 2000 m, the three profiles
are nearly identical

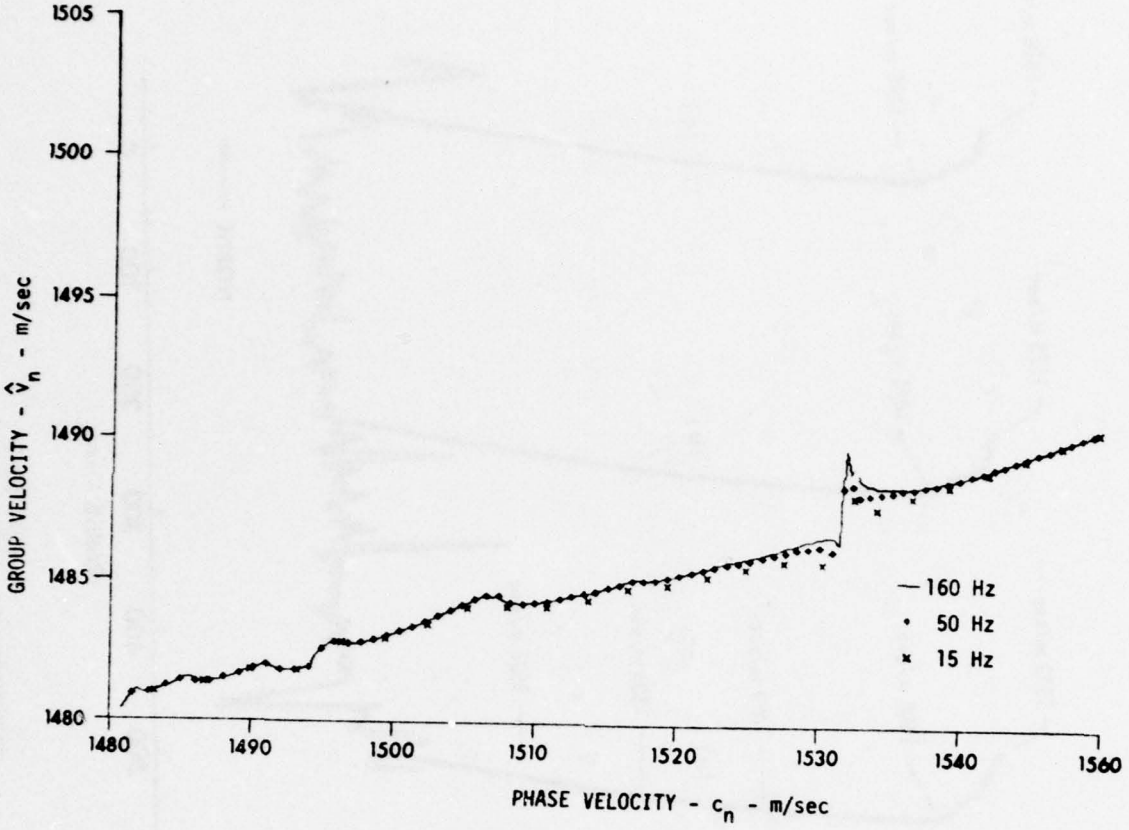

FIGURE 5B-2
GROUP VELOCITY VERSUS PHASE VELOCITY - PROFILE (a) OF Fig. 5B-1
The c_n and $\hat{v}_n$ for the modes at 160 Hz are so closely spaced that they are plotted as a continuous curve.

Figure 5B-3 shows an SVP from the North Atlantic and a plot of $\hat{v}_n(\omega)$ versus $c_n(\omega)$, again at 20 Hz, 50 Hz, and 160 Hz. This profile differs from that of Fig. 5B-1 in that the span of c(z) is only 25 m/sec, and the profile shapes differ. In Fig. 5B-3, the sound velocity decreases steadily in the first 50 m, and then varies about a constant value down to approximately 1000 m depth. This structure is caused by the presence of different water masses flowing at different depths. Because of the several velocity minimae in the SVP of Fig. 5B-3, only modes with phase velocities greater than 1485 m/sec were computed. The group velocity curve of Fig. 5B-3 is also different from that of Fig. 5B-2. In particular, at phase velocities near the surface velocity, there is little difference among the group velocities at different frequencies. This lack of frequency dependence arises from the large gradient in c(z) at the surface, where the SVP is similar to profile A200 (Fig. 5A-3).

As a final example, normal mode functions for profiles (a) and (c) of Fig. 5B-1 have been computed. The propagation along such a "slowly varying" propagation path is analyzed by Mildner [1969], who shows that, at sufficiently low frequencies, individual mode excitations propagate adiabatically, that is, without intermode coupling. Figure 5B-4 shows the sixth order mode function at 15 Hz for profiles (a) and (c) of Fig. 5B-1, computed with the Langer solution; at this frequency, propagation is adiabatic by Mildner's formulae.

The phase velocity, group velocity, and upper TP depth for the two mode functions are also given. Notice that, above the upper TP for the mode function of profile (a), the function shows a definite

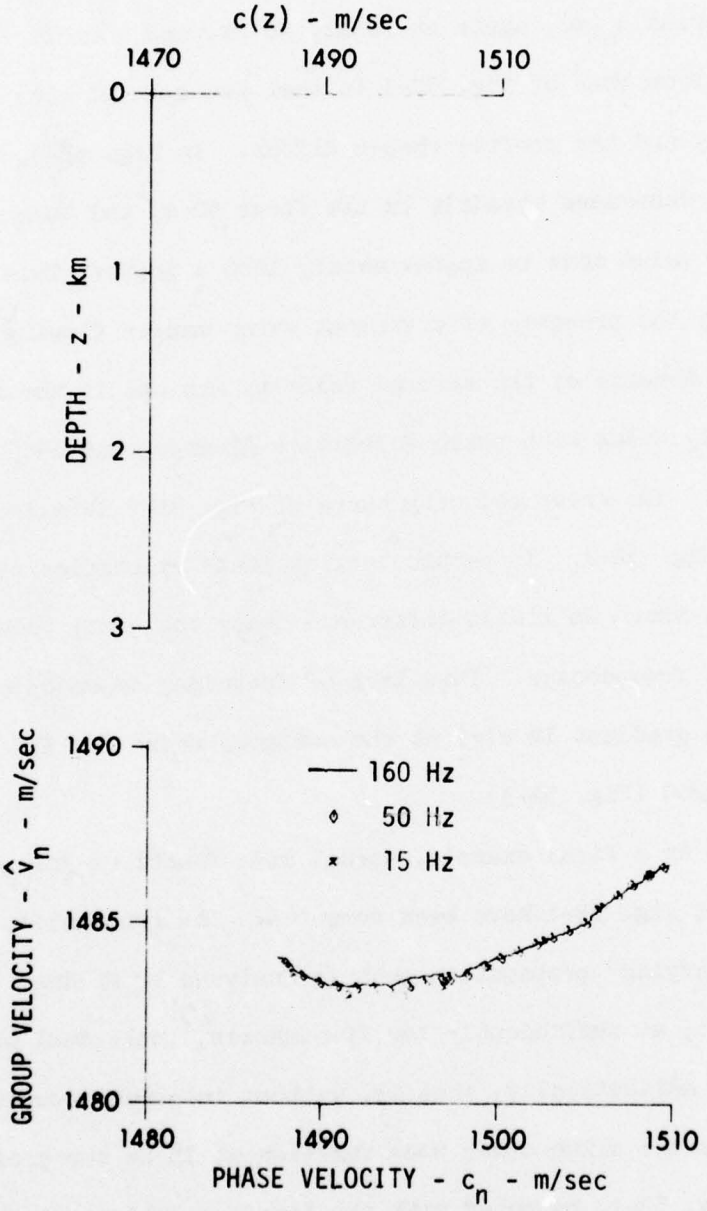

FIGURE 5B-3
GROUP VELOCITY VERSUS PHASE VELOCITY - PROFILE FROM NE ATLANTIC
The c_n and $\hat{v}_n$ for the modes at 160 Hz are so closely spaced that they are plotted as a continuous curve.

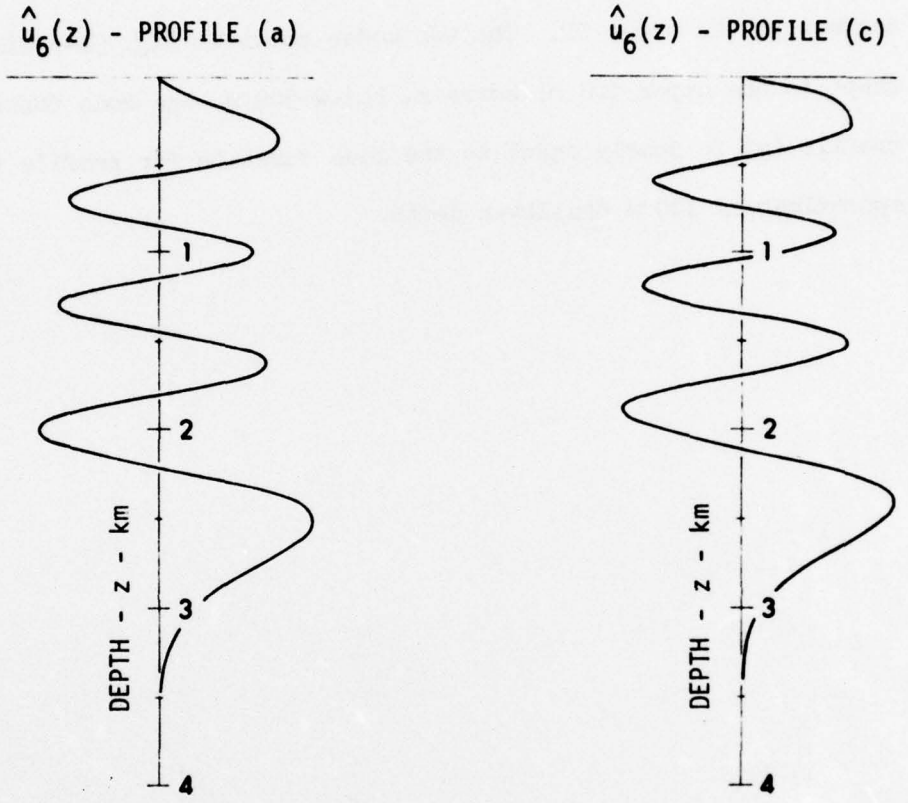

FIGURE 5B-4
SIXTH ORDER MODE FUNCTIONS AT 15 Hz
The profiles are (a) and (c) of Fig. 5B-1.
The mode amplitudes are arbitrary

decay towards the surface. In contrast, the mode for profile (c), which has its upper TP closer to the surface, is nearly linear from the surface to the upper TP. The two modes shown in Fig. 5B-4 differ in shape in the upper 500 m; however, below 500 m, the mode function for profile (a) is nearly equal to the mode function for profile (c) at approximately 100 m shallower depth.

VI. SUMMARY AND EXTENSIONS

In this dissertation, Langer's asymptotic solution has been applied to the problem of acoustical propagation in the ocean. It is shown that the eigenvalue equations for the normal modes of propagation may be given in the form:

$$\int_{z_U}^{z_L} \left(\frac{\omega^2}{c^2(z)} - k_n^2 \right)^{1/2} dz = (n + 1/2)\, \pi + \epsilon_n(\omega) \quad .$$

The quantities $\epsilon_n(\omega)$ arise from the Langer solution; in addition to mode order and frequency, the $\epsilon_n(\omega)$ depend upon boundary values and upon the distance from turning points to the depth of minimum velocity. From the eigenvalue equation, formulae for the normal mode quantities of group velocity and mode cycle distance were derived. These were expressed in terms of a characteristic distance, $\hat{D}_n(\omega)$, and period, $\hat{T}_n(\omega)$. It was shown that

$$\hat{D}_n(\omega) = \tilde{D}\left(z_U, z_L; \frac{\omega}{k_n}\right) + \Delta_n(\omega) \quad ,$$

and

$$\hat{T}_n(\omega) = \tilde{T}\left(z_U, z_L; \frac{\omega}{k_n}\right) + \tau_n(\omega) \quad .$$

The terms $\tilde{D}$ and $\tilde{T}$ are the ray theory horizontal distance and travel time between the turning points of a ray with turning point velocity equal to the phase velocity of mode n. The additional terms, Δ_n and τ_n, depend

upon boundary values and upon c(z) between the turning points and the boundaries, and c(z) between turning points and the depth of velocity minimum. For representative sound velocity profiles, normal mode quantities were computed using the formulae developed in this work to illustrate the effects of the ocean surface and of anomalies within the SVP upon the group velocity and mode cycle distance.

There are several areas in ocean acoustics for future work with the Langer solution. First, the solution (Eq. 4A-20) may be incorporated in a computerized model for computation of the acoustic field from a source (Eq. 2D-25), or propagation loss (Eq. 3-1); the Langer solution for the normal modes may be incorporated in existing computer programs. A second, and more interesting, area is the use of more realistic boundary conditions for the ocean bottom (Williams [1976]). It was shown in this work (Fig. 5A-1, for example) that the normal mode quantities (versus phase velocity) are most dependent upon frequency for the mode whose phase velocities are close to the sound velocity at the surface. A similar effect will occur at the ocean bottom, with additional features due to the acoustic properties of the bottom.

APPENDIX A

RELEVANT PROPERTIES OF AIRY FUNCTIONS

The purpose of this appendix is to record the properties of Airy functions which are used in this work; only functions of real argument are considered. A thorough discussion of the solutions to Stokes' equation, including historical background, is given by Miller [1946]; additional references are Antosiewicz [1964] and Erdelyi [1956].

The Airy functions are solutions to Stokes' equation,

$$w'' - zw = 0 \quad . \tag{A-1}$$

The two solutions to Eq. A-1 are the functions Ai(z) and Bi(z), so that, letting α and β be arbitrary constants,

$$w(z) = \alpha \, Ai(z) + \beta \, Bi(z) \quad . \tag{A-2}$$

The functions Ai(z) and Bi(z) are shown in Fig. A-1; ascending series expansions about z=0 are given in the references. The asymptotic expansions for Ai(z) and Bi(z) use the auxiliary variable,

$$\zeta = \frac{2}{3} z^{3/2} \quad . \tag{A-3}$$

For positive real argument,

$$Ai(z) \sim \frac{1}{2} \pi^{-1/2} z^{-1/4} e^{-\zeta} \tag{A-4}$$

$$Bi(z) \sim \pi^{-1/2} z^{-1/4} e^{\zeta} \tag{A-5}$$

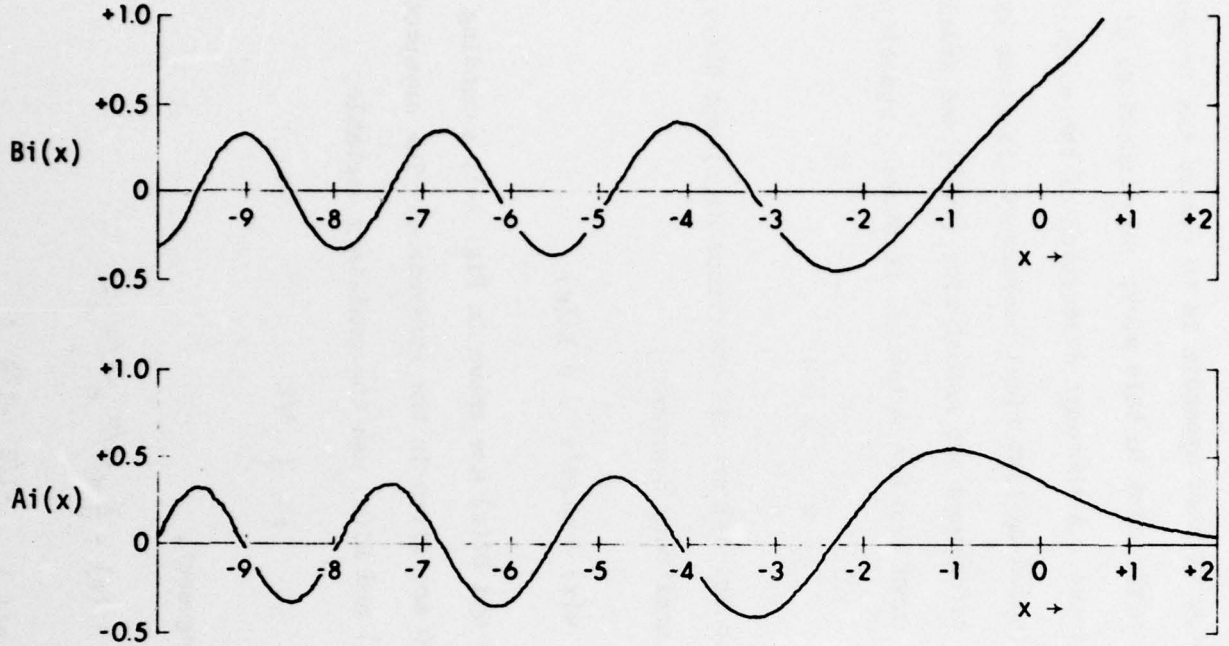

FIGURE A-1
THE AIRY FUNCTIONS Ai(x) AND Bi(x)

whereas for negative argument, as may be seen in Fig. A-1, the functions oscillate. For negative argument, it is convenient to introduce the amplitude and phase functions, $M(z)$ and $\theta(z)$, defined by

$$Ai(-z) = M(z) \cos \theta(z) \tag{A-6}$$

$$Bi(-z) = M(z) \sin \theta(z) \tag{A-7}$$

$$M^2(z) = Ai^2(-z) + Bi^2(-z) \tag{A-8}$$

$$\theta(z) = \text{arc tan}[Bi(-z)/Ai(-z)] \quad . \tag{A-9}$$

Then, the asymptotic form of the amplitude function is given by

$$M^2(z) \sim 1/(\pi z^{1/2}) \quad , \tag{A-10}$$

and the asymptotic form of the phase function is

$$\theta(z) \sim \pi/4 - 2z^{3/2}/3 \quad . \tag{A-11}$$

An exact equation for the derivative of the phase function is

$$\theta'(z) = -1/\pi \, M^2(z) \quad . \tag{A-12}$$

The Wronskian of the functions $Ai(z)$, $Bi(z)$ is

$$Ai(z) \, Bi'(z) - Ai'(z) \, Bi(z) = \pi^{-1} \quad . \tag{A-13}$$

BIBLIOGRAPHY

Antosiewicz, H. A., 1970. "Bessel Functions of Fractional Order" in M. Abromowitz and I. Stegun, ed., Handbook of Mathematical Functions (National Bureau of Standards, Washington, D.C.), Chpt. 10.

Bellman, R., 1964. Perturbation Techniques in Mathematics, Physics and Engineering (Holt, Rinehart, and Winston, Inc., New York).

Bergmann, P., 1946. "The Wave Equation in a Medium with a Variable Index of Refraction," J. Acoust. Soc. Am. 17, 329-333.

Brekhovskikh, L. M., 1960. Waves in Layered Media (Academic Press, New York).

Bucker, H. P., 1970. "Sound Propagation in a Channel with Lossy Boundaries," J. Acoust. Soc. Am. 48, 1187-1190.

Cherry, T. M., 1950. Trans. Amer. Math. Soc. 24, 121-130.

Cole, R. H., 1948. Underwater Explosions (Princeton University Press, Princeton).

Copson, E. T., 1967. Asymptotic Expansions (The University Press, Cambridge).

Dingle, R. B., 1956. "The Method of Comparison Equations is the Solution of Linear Second-Order Differential Equations (Generalized W.K.B. Method)," Appl. Sci. Res. B5.

Erdelyi, A., 1956. Asymptotic Expansions (Dover Publications, Inc., New York).

Ewing, W. M., and J. L. Wortzel, 1948. "Long Range Sound Propagation," Geol. Soc. Am., Mem 27.

Fitzgerald, R. M., A. N. Guthrie, D. A. Nutile, and J. D. Shaffer, 1974. "Influence of the Subsurface Sound Channel on Long-Range Propagation Paths and Travel Times," J. Acoust. Soc. Am. 55, 47-53.

Guthrie, A. N., R. M. Fitzgerald, D. A. Nutile, and J. D. Shaffer, 1974. "Long-Range Low-Frequency CW Propagation in the Deep Ocean: Angigua-Newfoundland," J. Acoust. Soc. Am. 56, 58-69.

Guthrie, K. M., 1974a. "The Propagation of SOFAR Signals," Ph.D. Thesis, The University of Auckland, Auckland, New Zealand.

Guthrie, K. M., 1974b. "Wave Theory of SOFAR Signal Shape," J. Acoust. Soc. Am. 56, 826-833.

Hampton, L. D. (ed.), 1974. Physics of Sound in Marine Sediments, (Plenum Press, New York).

Hirsch, P., and A. H. Carter, 1965. "Mathematical Models for the Prediction of SOFAR Propagation Effects," J. Acoust. Soc. Am. 37, 90-94.

Hirsch, P., 1965. "Acoustic Field of a Pulsed Source in the Underwater Sound Channel," J. Acoust. Soc. Am. 38, 1018-1030.

Kibblewhite, A. C., R. N. Denham, and R. H. Barker, 1965. "Long Range Sound Propagation Study in the Southern Ocean - Project Neptune," J. Acoust. Soc. Am. 38, 629-643.

Kibblewhite, A. C., 1974. "The Interaction of Underwater Acoustics and Marine Geophysics," in Physics of Sound in Marine Sediments, L. D. Hampton (ed.) (Plenum Press, New York).

Kemble, Edwin C., 1958. The Fundamental Principles of Quantum Mechanics (Dover Publications, Inc., New York).

Langer, R. E., 1931. "On the Asymptotic Solutions of Ordinary Differential Equations," Trans. Am. Math. Soc. 33, 23-64.

Langer, R. E., 1935. "On the Asymptotic Solutions of Ordinary Differential Equations, with Reference to Stokes' Phenomenon About a Singular Point," Trans. Am. Math. Soc. 37, 397-416.

Langer, R. E., 1937. "On the Connection Formulae and the Solutions of the Wave Equation," Phys. Rev. 51, 669-676.

Lindsay, R. B., 1960. Mechanical Radiation (McGraw Hill Book Company, Inc., New York).

Luke, V. L., 1970. "Integrals of Bessel Functions," in M. Abramowitz and I. Stegun (ed.), Handbook of Mathematical Functions (National Bureau of Standards, Washington, D.C.), Chpt. 11.

Mildner, D. M., 1969. "Ray and Wave Invariants for SOFAR Channel Propagation," J. Acoust. Soc. Am. 46, 1259-1263.

Miller, J. C. P., 1946. The Airy Integral, Mathematical Tables Part-Volume B, British Association for the Advancement of Science (The University Press, Cambridge).

Mitchell, S. K., and N. R. Bedford, 1975. "Long Range Sensing of Explosive Source Depths Using Cepstrum," J. Acoust. Soc. Am. 58, S20 (A).

Mitchell, S. K., and L. D. Hampton, 1975. "Signal Travel Time in Long Range Propagation," J. Acoust. Soc. Am. 58, S49(A).

Morse, P. M., and H. Feshbach, 1953. Methods of Mathematical Physics (McGraw-Hill Book Company, Inc., New York).

Nomady, V. G., and H. Uberall, 1975. "Sound Propagation and Attenuation in the Deep Ocean at Very Long Ranges," J. Acoust. Soc. Am. 57, 320-330.

Officer, C. B., 1958. Introduction to the Theory of Sound Transmission (McGraw-Hill Book Company, Inc., New York).

Olver, F. W. J., 1954a. "The Asymptotic Solution of Linear Differential Equations of Second Order for Large Values of a Parameter," Philos. Trans. Roy. Soc. London[A] 247, 307-327.

Olver, F. W. J., 1954b. "The Asymptotic Expansion of Bessel Functions of Large Order," Philos. Trans. Roy. Soc. London[A] 247, 328-368.

Pekeris, C. L., 1948. "Theory of Propagation of Explosive Sound in Shallow Water," Geol. Soc. Am., Mem. 27.

Porter, R. P., 1973. "Dispersion of Axial SOFAR Propagation in the Western Mediterranean," J. Acoust. Soc. Am. 53, 181-191.

Schiff, L. I., 1955. Quantum Mechanics (McGraw-Hill Book Company, Inc., New York).

Titchmarsh, E. C., 1962. Eigenfunction Expansions (Oxford University Press, London).

Tindle, C. T., and K. M. Guthrie, 1974. "Rays as Interfering Modes in Underwater Acoustics," J. Sound Vib. 34, 291-295.

Tolstoy, Ivan, 1973. Wave Propagation (McGraw-Hill Book Company, Inc., New York).

Tolstoy, Ivan, and C. S. Clay, 1966. Ocean Acoustics (McGraw-Hill Book Company, Inc., New York).

Urick, R. J., 1963. "Low Frequency Sound Attenuation in the Deep Ocean," J. Acoust. Soc. Am. 29, 1413-1423.

Urick, R. J., 1966. "Long Range Deep Sea Attenuation Measurement," J. Acoust. Soc. Am. 39, 904-906.

Weinberg, H., 1975. "Application of Ray Theory to Acoustic Propagation in Horizontally Stratified Oceans," J. Acoust. Soc. Am. 58, 97-109.

Weston, D. E., 1968. "Sound Focusing and Beaming in the Interference Field Due to Several Shallow-Water Modes," J. Acoust. Soc. Am. 44, 1706-1712.

Williams, A. O., Jr., 1970. "Normal Mode Underwater Sound" in Underwater Acoustics, R. W. B. Stephens (ed.) (Wiley-Interscience, London).

Williams, A. O., Jr., 1976. "Acoustic Reflection from a Structured Sea Bottom," J. Acoust. Soc. Am. 59, 62-68.

Wilson, W. D., 1960. J. Acoust. Soc. Am. 32, 641-644.

Wood, A. B., 1963. In Underwater Acoustics, V. M. Albers (ed.) (Plenum Press, New York).

1 March 1977

DISTRIBUTION LIST FOR
ARL-TR-77-13
UNDER CONTRACT N00014-75-C-0429
UNCLASSIFIED

Copy No.

Commanding Officer
Naval Ocean Research and Development Activity
NSTL Station
Bay St. Louis, MS 39529

1 Attn: R. R. Goodman (Code 110)
2 R. D. Gaul (Code 600)
3 A. L. Anderson (Code 320)
4 Samuel Marshall (Code 340)
5 Herbert Eppert (Code 360)
6 Thomas Pyle (Code 430)
7 Hugo Bezdek (Code 460)
8 G. J. Ranes (Code 500)
9 J. Paquin (Code 600)
10 K. V. Mackenzie

Commanding Officer
Naval Electronic Systems Command
Department of the Navy
Washington, DC 20362

11 Attn: J. Sinsky
12 W. Kamminga (Code 320)
13 Jesse Reeves (Code PME 124-34)

Commander
Naval Sea Systems Command
Department of the Navy
Washington, DC 20362

14 Attn: A. P. Franceschetti

Commanding Officer
Office of Naval Research
Arlington, VA 22217

15 Attn: J. B. Hersey (Code 102-OS)
16 Al Sykes

Dist. List for ARL-TR-77-13 under Contract N00014-75-C-0429 (Cont'd)

Copy No.

Commander
Naval Ocean Systems Center
Department of the Navy
San Diego, CA 92132
17 Attn: M. A. Pedersen (Code 307)
18 R. R. Gardner (Code 40)
19 Edwin L. Hamilton
20 Homer P. Bucker (Code 409)
21 H. Morris
22 O. D. Grace
23 G. Mohnkern

Director
Naval Research Laboratory
Department of the Navy
Washington, DC 20375
24 Attn: B. G. Hurdle
25 R. H. Ferris

Naval Oceanographic Office
Department of the Navy
Washington, DC 02373
26 Attn: W. H. Geddes

27 Commanding Officer
Naval Ocean Research and Development Activity
Liaison Office
Arlington, VA 22217
Attn: R. S. Winokur

Commander
Naval Air Development Center
Department of the Navy
Warminster, PA 18974
28 Attn: C. L. Bartberger
29 P. Haas

Commander
New London Laboratory
Naval Underwater Systems Center
Department of the Navy
New London, CT 06320
30 Attn: F. R. DiNapoli
31 R. L. Deavenport
32 H. Weinberg
33 P. Herstein

Dist. List for ARL-TR-77-13 under Contract N00014-75-C-0429 (Cont'd)

Copy No.

34 Commanding Officer
Naval Coastal Systems Laboratory
Panama City, FL 32401
Attn: E. G. McLeroy, Jr.

35 Superintendent
Naval Postgraduate School
Monterey, CA 93940
Attn: H. Medwin

DARPA Acoustic Research Center
Unit 1
Moffett Field, CA 94035
36 Attn: T. Kooij
37 R. Smith

38 Defense Advanced Research Projects Agency
1400 Wilson Blvd.
Arlington, VA 22209
Attn: CAPT Harry Cox

39 - 50 Commanding Officer and Director
Defense Documentation Center
Defense Services Administration
Cameron Station, Building 5
5010 Duke Street
Alexandria, VA 22314

Woods Hole Oceanographic Institution
Woods Hole, MA 02543
51 Attn: E. Hayes
52 R. Porter
53 R. Spindel

54 Morris Schulkin, Consultant
9325 Orchard Brook Drive
Potomac, MD 20854

55 Bolt, Beranek, and Newman, Inc.
50 Moulton Street
Cambridge, MA 02138
Attn: Preston W. Smith, Jr.

Science Applications, Inc.
1651 Old Meadow Road
McLean, VA 22101
56 Attn: John Hanna
57 C. Spofford

Dist. List for ARL-TR-77-13 under Contract N00014-75-C-0429 (Cont'd)

Copy No.

Applied Research Laboratory
Pennsylvania State University
P.O. Box 30
State College, PA 16801
58 Attn: D. C. Stickler
59 S. T. McDaniel

60 Underwater Systems, Inc.
3121 Georgia Avenue
Silver Spring, MD 20910
Attn: Marvin S. Weinstein

61 Geophysics Laboratory
Marine Science Institute
The University of Texas
700 The Strand
Galveston, TX 77550

TRACOR, Inc.
1601 Research Boulevard
Rockville, MD 20850
62 Attn: R. J. Urick
63 A. F. Wittenborn

64 The Catholic University of America
6220 Michigan Avenue, NE
Washington, DC 20017
Attn: H. M. Uberall

Lamont-Doherty Geological Observatory
Palisades, NY 10964
65 Attn: Henry R. Kutschale
66 John E. Nafe

67 Brown University
Providence, RI 02912
Attn: A. O. Williams, Jr.

The University of Auckland
Physics Department
Auckland, New Zealand
68 Attn: Alick Kibblewhite
69 Kris Tindle

Copy No.

Defence Scientific Establishment
HMNZ Dockyard
Devonport, Auckland
New Zealand
70 Attn: Michael Guthrie
71 R. N. Denham

72 Applied Physics Laboratory
The University of Washington
1013 Northeast Fortieth Street
Seattle, WA 98195
Attn: Terry D. Plemons

73 The University of Colorado
Boulder, CO 80302
Attn: Petr Beckmann

The University of Michigan
Ann Arbor, MI 48104
74 Attn: C. S. Clay
75 T. Birdsall

76 Renseller Polytechnic Institute
Troy, NY 12181
Attn: M. J. Jacobson

Lockheed Ocean Laboratory
3380 N. Harbor Drive
San Diego, CA 92101
77 Attn: J. M. McKissick
78 B. P. Hamm

79 Admiralty Research Laboratory
Teddington, Middlesex
England
Attn: D. E. Weston

Institute for Acoustical Research, Miami Division
Palisades Geophysical Institute
Miami, FL 33130
80 Attn: J. G. Clark
81 R. P. Flanagan

82 The University of Miami
School of Engineering
Coral Gables, FL 33124
Attn: N. L. Weinberg

Distribution List for ARL-TR-77-13 under Contract N00014-75-C-0429 (Cont'd)

Copy No.

83 Defense Research Establishment Pacific
CF Dockyard
Victoria, B. C., Canada

84 Defense Research Establishment Atlantic
Grove St.
Dartmouth, N. S., Canada

85 SACLANT ASW Research Centre
APO 09019
New York, N.Y.
Attn: Giancarlo Vettori

86 Department of Electronics and Electrical Engineering
The University of Birmingham
P.O. Box 363
Birmingham, United Kingdom
Attn: H. Orhan Berktay

A. D. Little, Inc.
35 Acorn Park
Cambridge, MA 02138
87 Attn: D. L. Sullivan
88 G. Raisbeck

XONICS, Inc.
6849 Hayvenhurst Avenue
Van Nuys, CA 91406
89 Attn: J. Wilson
90 N. Moise

91 The University of California
Santa Cruz, CA 95064
Attn: S. M. Flatte

92 Courant Institute of Mathematical Sciences
New York University, NY 10012
Attn: F. D. Tappert

93 Florida State University
Tallahassee, FL 32306
Attn: I. Tolstoy

Orincon Corporation
2223 Avenida De La Playa
Suite 151
La Jolla, CA 92037
94 Attn: D. L. Alspach
95 R. L. Himbarger

Distribution List for ARL-TR-77-13 under Contract N00014-75-C-0429 (Cont'd)

Copy No.

Institute of Geophysics and Planetary Physics
Scripps Institution of Oceanography
La Jolla, CA 92093
96 Attn: Walter Munk

Bell Telephone Labs
Whippany, NJ 07981
97 Attn: F. M. Labianca
98 E. Y. Harper

99 Royal Australian Naval Research Laboratory
Garden Island, New South Wales 2000
Australia
Attn: Bill Hunter

100 Office of Naval Research
Resident Representative
Room No. 582
Federal Building
Austin, TX 78701

101 Environmental Sciences Division, ARL/UT

102 Dudley D. Baker, ARL/UT

103 Garland R. Barnard, ARL/UT

104 Nancy R. Bedford, ARL/UT

105 David T. Blackstock, ARL/UT

106 Larry M. Deuser, ARL/UT

107 Glen E. Ellis, ARL/UT

108 Karl C. Focke, ARL/UT

109 Terry L. Foreman, ARL/UT

110 Harlan G. Frey, ARL/UT

111 Ruth Gonzalez, ARL/UT

112 Loyd D. Hampton, ARL/UT

113 Kenneth E. Hawker, ARL/UT

Distribution List for ARL-TR-77-13 under Contract N00014-75-C-0429 (Cont'd)

Copy No.	
114	C. W. Horton, ARL/UT
115	Chester M. McKinney, ARL/UT
116	Max K. Miller, ARL/UT
117	Stephen K. Mitchell, ARL/UT
118	Thomas G. Muir, ARL/UT
119	K. Russell Peterman, ARL/UT
120	S. Patrick Pitt, ARL/UT
121	Jack A. Shooter, ARL/UT
122	Reuben H. Wallace, ARL/UT
123	Steven Watkins, ARL/UT
124	Joseph F. Willman, ARL/UT
125	Charles L. Wood, ARL/UT
126	Library, ARL/UT
127-136	Reserve, ARL/UT